Low-friction coatings based on lubricious vanadium oxides

Dipl.-Ing. Nazanin Fateh

being a thesis in partial fulfilment of the requirements for the degree of a

Doctor of Montanistic Sciences (Dr. mont.)

at the University of Leoben

Leoben, February, 2008

This thesis was supported by the Austrian NANO Initiative via a grant from the Austrian Science Fund FWF within the project “LowFrictionCoatings”.

Affidavit

I declare in lieu of oath that I did the PhD thesis by myself using only literature cited in this volume.

Leoben, February 2008

Nazanin Fateh

Acknowledgements

I would like to express my great appreciation to my supervisor Christian, head of the Thin Film Group at the Department of Physical Metallurgy and Material Testing, for giving me the opportunity to carry out this work and for his support and guidance throughout this project. Working in your group was a great pleasure and a wonderful experience.

I am also very grateful to my scientific supervisor and friend Gerardo who was always beside me with his advice, patience and encouragement. Thank you not only for your support throughout this work, but also for your friendship over the last ten years.

I also extend my appreciation to Christian Teichert, head of Scanning Probe Microscopy Group at the Institute of Physics in Leoben as well as to Gregor and Thomas for their contribution to this project.

Special thanks to all the people from the Thin Film Group, past and present, including Anna, Christian T., Claudia, David, Florian, Gert, Hannes, Harald, Herbert, Joe, Jörg N., Jörg P., Kerstin, Marisa, Markus, Martin M., Martin P., Paul, Robert, Rostislav, Thomas and Vicky, for their support and more importantly, the casual chats during the innumerable coffee and tea breaks that kept me sane.

I am very thankful to the stuff and all the friends at the Department of Physical Metallurgy and Material Testing for their support.

To everybody out there who supported me with their love and understanding and made every chapter of my private life so much easier and enjoyable, thank you so much for reminding me that we are all travellers in this world. You will always be in my heart wherever you are.

Inexpressible thanks to my parents Marzieh and Jahangir for not only believing in me and encouraging me, but much more for their love and endurance through what became a long distance relationship during my studies in Austria. In equal measure I would like to thank my family Negin, Nesam, Moluk, Franz, Ebi, Gabi, Neda and Bianca for their endless love and trust. My special thanks goes to Ata for loving me the way I am and for always being on my side. I love you all.

Contents

1. Introduction 1
2. Material selection 3
2.1. Lubricious oxides 3
2.2. Nitride coatings containing vanadium 5
2.3. Vanadium pentoxide – V_2O_5 6
3. Thin film synthesis 9
3.1. Physical Vapour Deposition 9
3.2. Magnetron sputtering 9
3.3. Pulsed dc magnetron sputtering 12
3.4. Coatings deposition 13
4. Nucleation and thin film growth 15
4.1. Structure evolution mechanisms 15
4.2. Structure zone models 17
5. Tribology 21
5.1. Theories of friction and wear 21
5.2. Tribological coatings: contact mechanisms 25
6. Coating characterisation 28
6.1. High temperature tribotesting 28
6.2. Raman spectroscopy 29
6.3. Transmission electron microscopy (TEM) 31
7. Summary and conclusions 34
8. References 37
9. Publications 44
9.1. List of included publications 44
9.2. Publications related to this work 44
9.3. My contribution to the included publications 45
Publication I 46
Publication II 61
Publication III 75
Publication IV 86
Publication V 97

1. Introduction

High performance manufacturing processes such as dry machining or other high temperature applications require new properly designed components. The demand on advanced materials to reduce or control economic losses generated by friction and wear in order to extend machinery lifetime drives the development of thin film technology. Coated materials allow the combination of beneficial bulk properties like high toughness and strength with excellent film properties like hardness, wear and corrosion resistance [1-3]. In this way, the surface properties of bulk materials are usefully changed according to the diverse application requirements.

Within the last decades, plasma-assisted methods have stimulated the development of advanced hard coatings where material limitations have been overcome. First generation hard coatings based on transition metal nitrides and carbides showed success in reducing wear and corrosion of tools and increasing lifetime, combined with the drawback of unfavourable high friction, limiting their ability in dry machining. Due to the high performance requirements, the major trend of synthesizing multi-component and multi-phased structures has gained considerable interest [2-5]. Well-established in cutting tool industry are metastable coatings in the Ti-Al-N system due to their high hardness and good wear resistance combined with superior oxidation resistance up to 700°C [2,4]. Since these coatings reveal a rather high coefficient of friction at elevated temperatures, one trend in the development of next generation coatings follows the strategy of adding new elements to the matrix to achieve enhanced friction behaviour at high temperatures.

A lot of effort has been made to develop the so-called low-friction protective coatings, which act as solid lubricants, to replace the commonly used external fluid or lubricants. Low friction due to the lubricating action of such coatings can effectively reduce contact heating during sliding and thus improve the tribological behaviour in high speed and dry machining applications. Developments of nanocomposite coatings that consist of solid lubricants (such as diamond like carbon (DLC), MoS_2 or WS_2) and a hard metal nitride or carbide (i.e., TiN, TiC, WC) have greatly improved the tribological properties [6-8]. However, these intrinsic solid lubricants often begin to fail in their tribological effectiveness due to degradation at elevated temperatures.

In recent years, oxide materials have become more interesting due to their low adhesion tendency and high oxidation stability. The so-called lubricious oxides with easy

crystallographic shear planes can serve as lubricants at elevated temperatures. They are found among the oxides of V, Mo, W and Ti [9-12], which form oxygen deficient homologous series with a variety of phases. Such lubricious oxides can accommodate the velocity between two surfaces in relative motion by shearing, and due to their crystallographic easy shear planes, provide low friction and also even prevent wear damage [13]. Several researchers have explored the feasibility of incorporating lubricious oxides and/or oxide forming elements that can potentially result in lubricious oxide phases during machining or other sliding operations [6,13]. A major progress in terms of improving the tribological performance at elevated temperatures has been achieved by the addition of V into a hard matrix, like TiAlN/VN superlattices and AlCrVN coatings. The improvement of the tribological properties of these coatings at high temperatures is connected to vanadium oxide formation, in particular vanadium pentoxide (V_2O_5), which is known to act as solid and liquid lubricant at elevated temperatures [14,15].

The contribution of the present work is focused on the design of a new class of low-friction coatings based on lubricious vanadium oxides. The main approach is to fill the gap between room temperature low-friction coatings (e.g. DLC or MoS_2) and high temperature low-friction coatings such as the previously developed TiAlVN [14] or AlCrVN [15]. In the first step of this work, TiN, VN and V coatings prepared by unbalanced magnetron sputtering were characterized with respect to their oxidation behaviour to verify the concept of solid/liquid oxide lubrication. The corresponding and eventually lubricious oxides within the system Ti-O and V-O are expected to be formed during tribological testing at elevated temperatures. Next step concentrated on the establishment of interrelationships between growth parameters and the structure evolution of lubricious V_2O_5 thin films. Subsequently, the correlation of V_2O_5 film structure and properties with its tribological performance was characterized by deposition of V_2O_5 as single-layer and bi-layer coatings. The outline of this thesis starts with a general overview of material selection, i.e. vanadium containing nitride coatings and lubricious oxides, in particular V_2O_5, by reviewing the published literature. The following chapters in this thesis outline the thin film synthesis, the tribology of films as well as some experimental aspects of the coating characterization, particularly with regard to the investigated films. Subsequent to a short summary of the main findings, the major experimental research is given in five scientific publications, where the obtained results are comprehensively discussed.

2. Material selection

Within this chapter, the general concept of lubricious oxides for high-temperature lubrication and an overview of available literature and recent scientific findings designing low-friction coatings are provided. Furthermore, the crystal structure of V_2O_5 is introduced.

2.1. Lubricious oxides

Lubrication is defined as any means capable of controlling friction and wear of interacting surfaces in relative motion under load [13]. A wide variety of materials, gases, liquids or solids have been used as lubricants to reduce the frictional force between surfaces. However, at very low or high temperatures, in vacuum or extreme contact pressures, often the only way to control friction is to use solid lubricants such as MoS_2, DLC or WS_2 [2]. Nevertheless, in modern industrial operations like metal cutting, most of these solid lubricants begin to fail due to their limited thermal stability and loose their tribological effectiveness. As a result, they oxidise under ambient atmosphere, thus, friction and wear are subsequently dominated by the formed oxide film. On the contrary, soft, stable and adherent oxides with low shear strength can serve as lubricants at different temperatures and are, therefore, referred to as lubricious oxides. First investigations on oxidised TiN and TiC coatings by Gardos revealed low friction coefficients in air due to the formation of rutile layer TiO_2 [10,11]. Gardos et al. demonstrated that oxygen vacancies in rutile TiO_2 significantly change the shear strength in the surface region [11]. Further work by Gardos revealed the correlation between oxygen deficient structure of rutile (TiO_{2-x}), shear strength and the tribological behaviour in detail [12].

In 1953, Magnéli first investigated the crystal structure of substoichiometric oxides of Mo and W with planar faults belonging to homologous series. They can be described generally by the formulas Me_nO_{3n-1} or Me_nO_{3n-2}, and consist of a crystalline structure based on rutile [16]. Andersson first reported on the existence of a homologous series of vanadium oxides corresponding to the formula V_nO_{2n-1} with $n \geq 4$ [17]. Generally, these sequences of oxides exhibit a high concentration of vacancies and different stoichiometries, leading to reduced binding strength and easy crystallographic shear planes. Such oxides are referred to as Magnéli phases.

To predict the lubricity of oxides or oxide mixtures for designing advanced low friction coatings, a new crystal-chemical approach was presented by Erdemir [6,18]. Specific selection and incorporation of such oxides may have significant beneficial effects on the

tribological behaviour. The crystal-chemical parameter is based on the ionic potential $\varphi=Z/r$, defined as the ratio between the cationic charge Z and the radius of the cation r [19]. Ionic potential controls several physical and chemical phenomena in oxides. Specifically, it is possible to establish a correlation between ionic potential of an oxide and its shear rheology, and hence, with its lubricity. In general, the higher the ionic potential is, the greater is the extent of screening of a cation by surrounding anions, as illustrated in Figure 2.1.

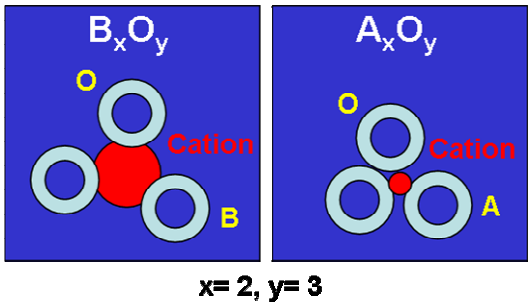

Oxide case	Cationic charge	Cation radius (Å)	Ionic potential
B_xO_y	3	0.5	6
A_xO_y	3	0.2	15

Figure 2.1: A schematic illustration of the concept for ionic potentials of two oxides having the same cationic charge but different cation radius [18].

Oxides with highly screened cations (such as V_2O_5, WO_3 and Re_2O_7) are normally soft, shear rather easily and their melting point is low. Their cations are well-separated and completely screened by the oxygen atoms. As a result, their chemical interaction with other cations is greatly hindered and most of their bonding is with surrounding oxygen anions. They also can act as liquid lubricant due to their low melting points at elevated temperatures. On the other hand, oxides with lower ionic potentials (such as Al_2O_3, ZrO_2, Fe_2O_3 and MgO) are very strong and stiff. Their cations are free to interact with each other and form strong covalent or ionic bonds which make them very strong and hard to shear even at high temperatures [18].

Figure 2.2 presents the correlation between the ionic potential and the frictional performance of some oxides. It can be noticed that oxides with higher ionic potentials appear to provide lower friction coefficients. V_2O_5 with a high ionic potential of $\varphi=10.2$ provides excellent lubricity and reveals a friction coefficient of ~ 0.2. Several promising investigations have been published in which the existence of lubricious oxides, in particular V_2O_5, has improved the tribological behaviour of VN and VN/TiAlN coatings [5,9,16,20,21]. Thus, the incorporation of V into a hard matrix to produce V_2O_5 on sliding surfaces has attracted significant research activities in the last years and is in part also the scope of this work. Most

of these observed lubricious effects are attributed to the structure of V_2O_5 which is described in more detail in section 2.3.

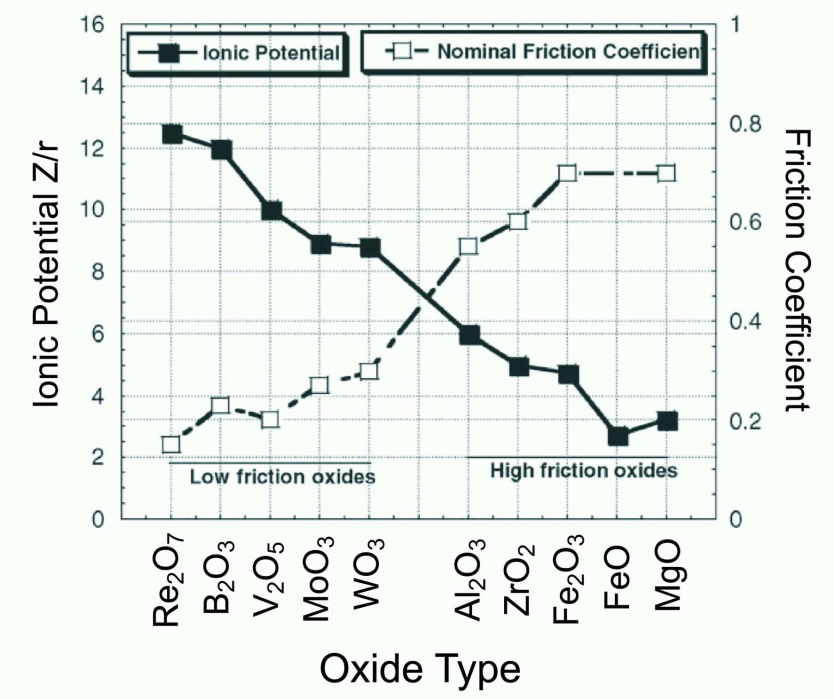

Figure 2.2: Relationship between ionic potentials and averaged friction coefficients of various oxides [18].

2.2. Nitride coatings containing vanadium

As already mentioned, several researchers have presented promising strategies where the addition of vanadium to hard coatings improves the tribological performance during dry machining, mainly due to the formation of an oxide film containing V_2O_5 in the frictional contact. TiAlN/VN coatings have proven to have excellent wear resistance and low friction coefficient under dry sliding conditions at elevated temperatures due to the detected surface oxide V_2O_5 [5,20-25]. Münz et al. [23] and Hovsepian et al. [25] have reported on the excellent wear behaviour and low friction coefficient of TiAlN/VN multilayer coatings synthesised by a combined cathodic arc/unbalanced sputtering technique. Concerning the friction mechanism operating in the TiAlN/VN multilayer coatings, the oxidation and the tribological behaviour of TiAlN/VN at elevated temperature have been studied extensively [27,28]. According to their observations, the achieved low coefficient of friction and wear rates are attributed to the formation of a tribo-oxide film in the wear track during sliding, which contains lubricious V_2O_5. Mayrhofer et al. investigated TiAlN/VN superlattice coatings, where by the incorporation of vanadium into the hard coating efficient lubrication

with a friction coefficient as low as 0.18 at 700°C was achieved [14]. The observed low friction effect at 700°C compared to the room temperature values of approximately 0.6-0.8 was attributed to the formation and melting of V_2O_5 on the coating surface. However, the V_2O_5 undergoes a transition to lower oxidised VO_2 [29], which is responsible for the loss of the liquid oxide lubrication effect and a rise of the friction coefficient with annealing time. Further work by Gassner et al. on VN and by Kutschej et al. on vanadium containing TiAlN coatings has also confirmed the formation of lubricious oxides on the coating surface at elevated temperatures [30,31]. Franz et al. have reported the tribological behaviour of arc evaporated AlCrVN coatings from room temperature up to 700°C for different V contents. The best friction performance was observed at 700°C for higher V concentration in the coating. Due to the formation and melting of V_2O_5 on the coating surface, the coefficient of friction could be reduced from 0.7 at room temperature to 0.2 at 700°C [15].

Publication I and II present the influence of oxide phase formation on the high temperature tribological performance of VN and V coatings. Differential scanning calorimetry (DSC) measurements revealed that the onset of oxidation for V and VN coatings occurs in a range between 400 and 450°C, whereas the oxidation processes of these coatings seem to be different. For both coatings, a significant decrease in friction coefficient at temperatures above 400°C was observed reaching a value of 0.25-0.27 at 700°C. The formation of V_2O_5 gives rise to solid lubrication while the subsequent melting of this phase at temperatures above 600°C leads to liquid lubrication.

2.3. Vanadium pentoxide – V_2O_5

In recent years V_2O_5 has been the subject of a number of studies due to its material characteristics, and has been sucessfully integrated into various applications. This oxide corresponds to the V_nO_{2n+1} series, with n=2, 3, 6, which can be considered as oxygen deficient (face-centre-cubic) fcc structures. It is deduced from the cubic structure by introducing different ordered vacancies in the oxygen close-packing array. There are some polymorphs of V_2O_5 which are identified in the literature as α-V_2O_5 (orthorhombic), β-V_2O_5 (monoclinic or tetragonal) and δ-V_2O_5 (a modification of β-V_2O_5) [32]. The most stable crystal structure is orthorhombic α-V_2O_5 which belongs to the space group Pmmn (59) with lattice parameters defined as a=11.512, b=3.564 and c=4.368 Å [32,33]. The crystal structure of α-V_2O_5, determined by Byström et al. [34] has been refined by Bachmann et al. [35] and Enjalbert [33]. Galy et al. reported a general expansion of the lattice constants with increasing

temperature but no phase transition could be noticed [36]. The V_2O_5 structure is characterized by periodic arrangements of distorted VO_5 square pyramids, which share corner and edges, as shown in Figure 2.3.

The vanadium atoms form five bonds with oxygen with V-O bond lengths varying between 1.585 and 2.021 Å. There are three structurally different oxygen atoms, terminal (vanadyl) oxygen O_1 coordinated to one vanadium atom through the shortest bond (1.585 Å) and bridging oxygen O_2/O_3 coordinated to two or three vanadium atoms with V-O distances ranging between 1.78 and 2.021 Å. The result is a series of V_2O_5 layers parallel to the (001) plane and stacked along [001]. The layers so formed are held together by weak vanadium-oxygen interactions with a distance as large as 2.79 Å. The interaction between the V_2O_5 layers is so weak (van der Waals type) that the crystals cleave easily along the (001) plane, as described in detail by Ramana et al. [37].

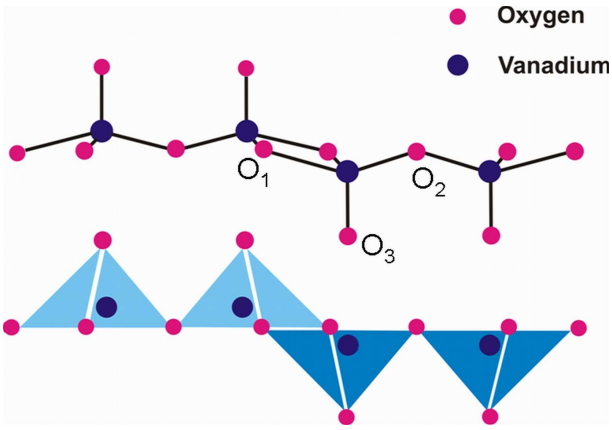

Figure 2.3: Perspective view of orthorhombic V_2O_5 crystal lattice [36].

This specific structure with easy crystallographic shear planes along (001) determines the potential of V_2O_5 as solid lubricant. Several research works have been focused on the structure characterisation and optical properties of V_2O_5 thin films. Different deposition techniques have been used to synthesize V_2O_5 thin films, such as, sol-gel method, magnetron sputtering, pulsed laser deposition and thermal evaporation [37-41]. The crystallinity and properties of V_2O_5 films are mainly dependent on the deposition technique and the deposition conditions. The synthesis of (001) textured crystalline V_2O_5 films by sputtering a V_2O_5 target in the presence of oxygen was reported by Benmoussa et al. [42]. Ramana et al. investigated V_2O_5 thin films synthesized in a wide temperature range using pulsed laser deposition [43]. They reported an onset of crystallization at 200°C, while at lower temperature an amorphous

film was observed. Annealing of V_2O_5 films in vacuum at 400°C or higher causes a reduction to VO_2, as reported by Ningyi et al. [29]. The oxide reduction follows a sequence with several vanadium oxides formed in the intermediate steps: $V_2O_5 \rightarrow V_3O_7 \rightarrow V_4O_9 \rightarrow V_6O_{13} \rightarrow VO_2$ [29]. Publication III and IV report mainly on synthesis-structure relations of V_2O_5 thin films deposited on MgO (100) and silicon substrates under varying deposition condition and deposition techniques.

There are only few investigations on mechanical and tribological properties of V_2O_5 thin films, since they are more of interest for electronic and optical applications. Lugscheider et al. reported the hardness of vanadium oxide coatings with polycrystalline VO_2 and V_2O_5 phases being in the range of 13-18 GPa [44]. Gulbiński et al. reported the correlation between friction coefficient and testing temperature, recorded during a temperature cycle of 100-700°C against an alumina ball as counterpart [45]. According to their observation, the friction coefficient decreases from a high value of 0.8 at 100°C to 0.4 at 500°C and then to about 0.3 where melting induced effects occur. The almost identical friction coefficient during the cooling sequence confirms the stability of V_2O_5 coatings. In publication V the tribological behaviour of V_2O_5 single-layer as well as VN-V_2O_5 bi-layer coatings was investigated in the temperature range between 25 and 600°C. The friction coefficient of V_2O_5 single-layer coatings decreases from 0.55 at room temperature to ~ 0.39 at 300°C and reaches its lowest value of 0.15 at 600°C.

3. Thin film synthesis

To obtain required coating properties for several applications, numerous deposition techniques have been developed. The most important aspects of the deposition techniques used for this thesis are included in the following chapter.

3.1. Physical Vapour Deposition

In the Physical Vapour Deposition (PVD) process, the transport of material to the substrate results from different physical phenomena. Generally, PVD techniques are based on the common steps of transition from a liquid or solid phase to the vapour phase, transport of the vapour from the source to the substrate, and finally its condensation followed by nucleation and growth. These processes mostly take place in vacuum in order to minimize collisions during the transport of vaporized coating material and avoid involuntary reactions. Nowadays, numerous deposition process variations and modifications have been developed for different applications and are in industrial use. PVD methods include sputtering, evaporation, ion plating and ion-assisted sputtering [46-51]. Details on differences between these processes can be found in [48,52]. The main advantages of these methods rely on the variation of coating materials which can be deposited, and the deposition temperatures, from less than 100°C up to 500°C and more, that allows the deposition of coatings on a diversity of substrate materials [46,47]. Coatings synthesized by PVD, however, are usually far from their state of thermodynamical equilibrium [46-50]. The coatings investigated in this thesis were deposited by the PVD technique using an unbalanced magnetron sputtering (UBMS) system in dc and/or pulsed dc mode operated in reactive or nonreactive atmosphere.

3.2. Magnetron sputtering

Sputtering is a momentum transfer process where energetic particles (inert gas atoms, e.g. Ar) are accelerated towards a target, resulting in direct ejection of surface atoms, i.e. transferring them from the solid to the vapour phase [48,53]. The energetic Ar ions, which show higher velocities and energies than evaporated atoms, originate from the glow discharge which is ignited between target and substrate [53].

Figure 3.1 shows schematically the basic elements of a typical direct current (dc) diode system which mainly consists of two electrodes facing each other. The target is referred to as the cathode since it is connected to the negative side of the direct current power supply in

order to sustain the glow discharge [49]. The substrates, which are placed at the opposite anode, can be either grounded or negatively or positively charged (bias voltage). Before the ignition of the glow discharge, an inert gas, e.g. Ar, is inserted into a chamber which is evacuated prior to deposition to a pressure typically in the range of 10^{-3} Pa. The Ar^{+} ions bombard the target and the momentum transfer causes the neutral atoms of the target source to be dislodged. These atoms transit through the discharge and condense onto the substrate. The power dissipated at the target by the high ion currents accelerated to the cathode causes an increased heating. Therefore, such systems are usually water cooled from the backside to protect the cathode and prevent the target from melting.

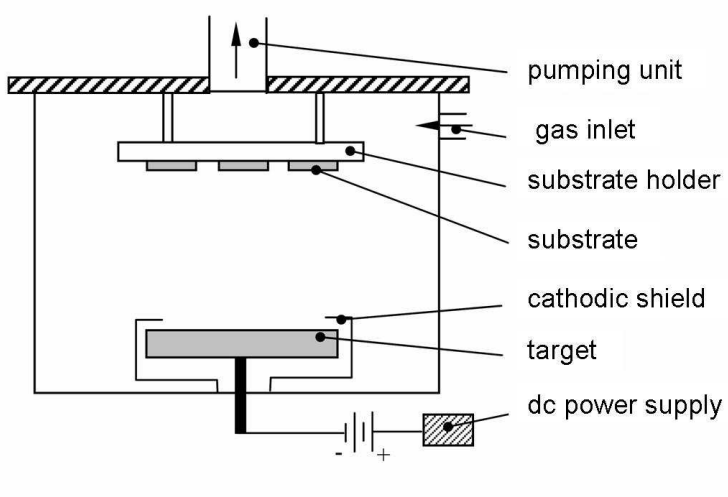

Figure 3.1: Principle of a dc planar diode sputtering system.

Several different sputtering methods are widely used for the deposition of thin films in different practical applications. Sputter systems are usually powered by direct current (dc). Other deposition techniques are working with radio frequency (rf), pulsed dc or alternate current (ac) power supplies [48,54]. In a dc planar diode arrangement, the ions are generated relatively far away from the target, thus, having a higher probability to loose energy on their way which results in rather low deposition rates. These limitations have been overcome by applying magnetic fields generated by magnets behind the target which is known as the magnetron sputtering technique. The applied magnetic fields parallel to the target and perpendicular to the electric field concentrate the electrons near the target and lead to an increased ionization of the sputtering gas due to the higher concentration of charged particles.

The increase of the positive ion production rate leads to a higher deposition rate at much lower working gas pressures [55-58].

Generally, two different types of magnetrons can be used: the conventional balanced magnetron (CBM) and the unbalanced magnetron (UBM) configurations, as shown in Figure 3.2a and b, respectively. In case that all the field lines loop between the two magnets, the magnetic system is called a conventional balanced magnetron. Otherwise, if the field lines are partially open towards the substrate, it is termed unbalanced magnetron (UBM) [59]. In an unbalanced magnetron configuration, where some magnetic field lines do not loop between the outer and the inner magnet, the plasma expands away from the target area (Figure 3.2b) [60,61]. As a result, some secondary electrons escaping from the target follow the magnetic field lines towards the substrate and undergo ionizing collisions with gas atoms. As there is a net movement of negative charge from the magnetron region, positive ions can also be attracted to the substrate influencing the ad-atom mobility as well as film nucleation and growth kinetics. Consequently, there is a higher ion and electron bombardment of the substrate. The energy of ion flux can be adjusted by varying the magnetic field achieved by using stronger central or stronger outer magnets or by applying a bias potential to the substrate [52,60-64].

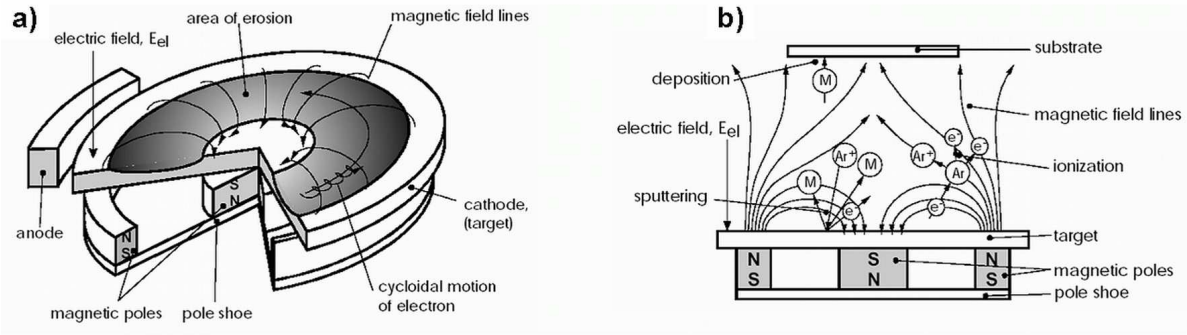

Figure 3.2: Planar magnetron configuration a) balanced magnetron, b) unbalanced magnetron [50,56].

If the working gas atmosphere used to obtain the sputtering process is inert (e.g. Ar) and the plasma consists only of the working gas and the sputtered particles, the process is termed non-reactive. However, if at least one of the film components is added to the deposition chamber in the form of a gas, such as N_2, O_2 as within this thesis, it becomes part of the plasma and contributes actively to the process of film growth. Such deposition technique is termed reactive magnetron sputtering [66,67].

3.3. Pulsed dc magnetron sputtering

Pulsed magnetron sputtering is a well-developed technology, particularly for the deposition of dielectric coatings used in microelectronics [68-75]. Pulsing of the magnetron discharge can eliminate or significantly reduce the arcing problem and stabilizes the deposition process. Pulsed dc magnetron sputtering is mainly based on the regular interruption of the sputtering cycle (negative target voltage) by pulses during which the target voltage acquires a small positive value with frequencies up to several 100 kHz. The operating conditions are typically optimized empirically, and are dependent on the properties of the pulsed plasma in the immediate vicinity of the magnetron. The correct selection of pulse parameters such as frequency, pulse length, pulse pause and pulse voltage can result in extended arc-free operating conditions [72]. Two principal methods of pulsing have been proposed: asymmetric bipolar pulsing and unipolar pulsing. Asymmetric bipolar pulsing in the medium frequency range (10-350 kHz) has become established as one of the main techniques for deposition of oxide and nitride films [72-76].

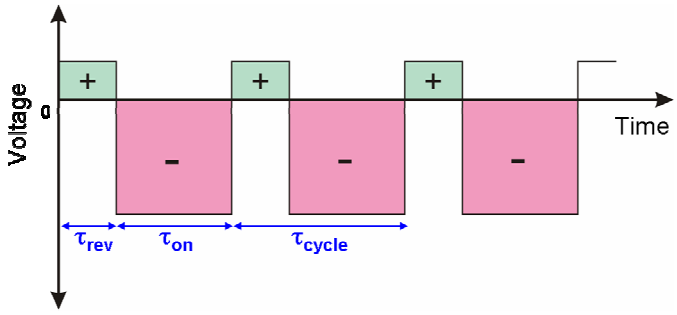

Figure 3.3: The voltage sequence applied to asymmetric bi-polar pulsed dc sputtering [76].

Figure 3.3 illustrates a typical voltage sequence used in pulsed dc sputtering. The power is applied to the target for a time τ_{on} (on-time) during which a negative voltage pulse of a few hundred volts is applied to the target. At the end of τ_{on}, the power is usually switched to a small positive voltage (typically 10% of the nominal voltage), which is termed as 'reverse time' τ_{rev}. The duty cycle, η, is defined as the ratio of negative pulse period (τ_{on}) to overall period ($\tau_{on}+\tau_{rev}$).

One of the main advantages of pulsing is to prevent the problem associated with the continuous dc reactive sputtering, namely the arc events at the target when depositing dielectric materials. Arc-free operation requires the 'on-time' to be sufficiently short to avoid

charge build-up that can cause arcing and the 'reverse time' to be sufficiently long to fully discharge the surfaces in order to avoid charge accumulation in sequential 'on' and 'reverse' cycles. Furthermore, recent investigations have shown that pulsing the magnetron discharge significantly modifies the characteristics of the deposition plasma and lead to an increased ion energy and ion flux which may contribute to the improvement of film structure, film density and stoichiometry, as well as the mechanical and tribological properties of the coatings [72,73]. Within this thesis, the pulsed dc approach for depositing V_2O_5 thin films was particularly used to gain additional control over ion energy and ion flux to the substrate and to promote polycrystalline growth with certain preferential orientation.

3.4. Coatings deposition

Within this work, the TiN, VN and V coatings investigated in Publications I and II were deposited from a Ti or V target (ø 75×6 mm), respectively with an unbalanced dc magnetron sputtering system (Leybold Z-400), as shown in Figure 3.4. The deposition process was carried out at a constant working gas pressure of 0.25 Pa. To support film growth, a negative substrate bias of -50 V was applied to attract ions close to the substrates and enhance the ad-atom mobility of the films. Depending on the coatings investigated, the deposition process was operated in reactive or nonreactive atmosphere (see Publications I and II for details).

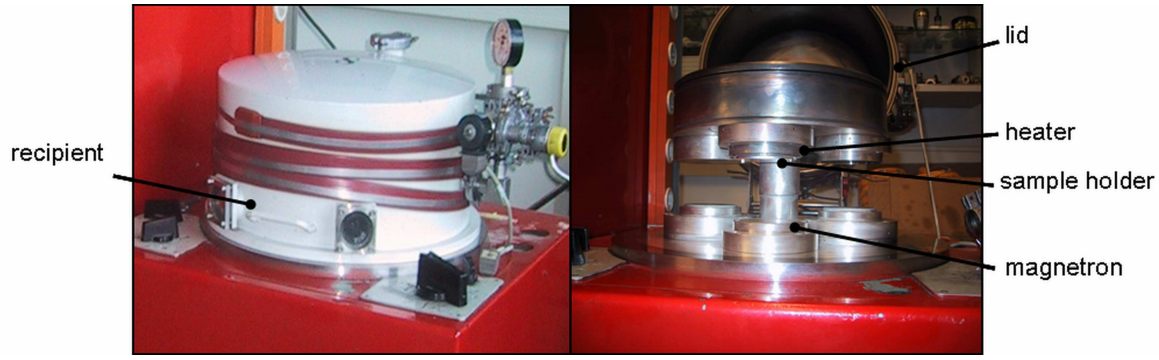

Figure 3.4: Leybold Z-400 unbalanced magnetron puttering system.

Figure 3.5 shows the deposition system used for coatings investigated in Publications III, IV and V. This device is equipped with three V targets (ø 50.8×6.35 mm) mounted to a cluster of three unbalanced magnetrons (AJA cluster with A320-XP magnetrons). Sputtering was conducted in a reactive atmosphere applying dc and pulsed dc discharges. The substrates were positioned parallel to the magnetron cluster and were rotated at approximately 10 revolutions

per minute during deposition to obtain uniform thin films. The total gas pressure for both sputtering modes was kept constant at 0.28 Pa while the target current was set to 0.35 A at each magnetron for all experiments. Furthermore, the samples were heated from the reverse side and after reaching deposition temperature, a period of 30 minutes was used to establish a homogeneous temperature distribution. The sample temperature was determined using a k-type thermocouple attached to the substrate holder. For the pulsed dc magnetron sputtered films, three bipolar pulsed dc power supplies (MKS RPG-50) were used to generate the plasma. The target pulsing frequency was kept constant at 100 kHz with 16% duty cycle. In this case, each magnetron acts alternatively as an anode and a cathode during the pulse cycle.

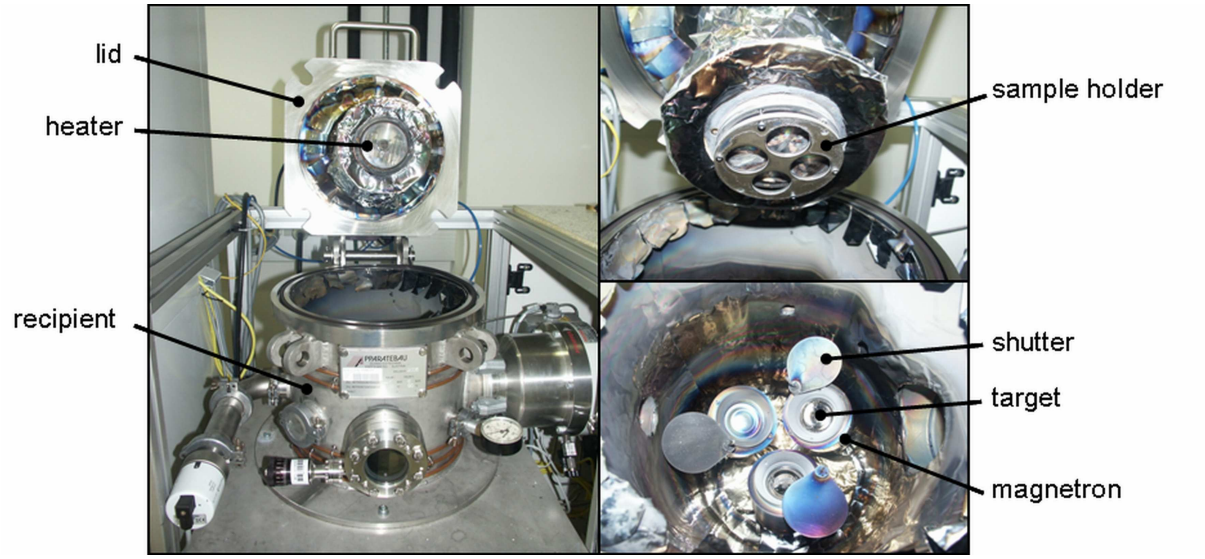

Figure 3.5: Deposition system equipped with the coupled configuration of three unbalanced magnetrons, the corresponding shutter protection and the rotatable sample stage with heater and sample holder.

4. Nucleation and thin film growth

In thin film technology, the microstructure of the coatings has a significant influence on their mechanical, tribological and oxidation properties. Thin films exhibit a wide variety of microstructures which can be characterized in terms of grain size, phase composition, surface morphology and crystallographic orientation. During the evolution of the structure, different mechanisms occur which are all influenced by the deposition method and process parameters. Detailed discussions on the fundamental structure forming phenomena of thin films can be found in several textbooks and publications [77-83]. In the following chapter, a short summary of the mechanisms involved in the growth process will be presented.

4.1. Structure evolution mechanisms

The growth processes controlling microstructure evolution include nucleation, island growth, coalescence of islands, formation of polycrystalline islands and channels, development of a continuous structure and film growth [84,85]. After arriving at the surface, particles, atoms or ions are either adsorbed or directly reflected, depending on the appearance of the substrate surface. Usually, most particles remain on the substrate surface for a certain time, and if they encounter a stable lattice site during their diffusion time, nucleation starts (see Figure 4.1).

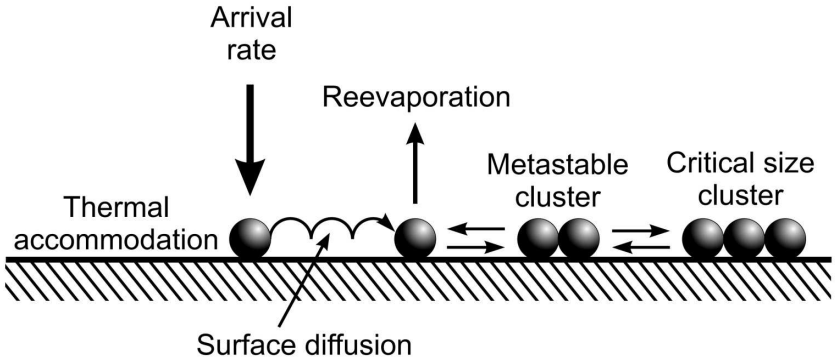

Figure 4.1: Processes in the nucleation and growth of crystals on a substrate [77].

Sufficiently high impingement rates can lead to the formation of metastable and stable clusters which can continuously grow by binding of diffusing ad-atoms or by direct capture of

atoms from the vapour phase. Once a metastable cluster exceeds a critical size, adjacent crystals come into contact and the coalescence stage starts. To form a single crystal film, atoms of the film material in the vapour must arrive at the substrate surface, adhere to it and settle into possible equilibrium positions before structural defects are left behind the growth front. To form an amorphous film, on the other hand, atoms must be prevented from seeking stable equilibrium positions once they arrive at the growth surface. The nucleation phenomena are influenced by several parameters during deposition such as energy distribution of impinging ions, substrate temperature, the ad-atom-substrate affinity or stress/strain state with film thickness [79-85].

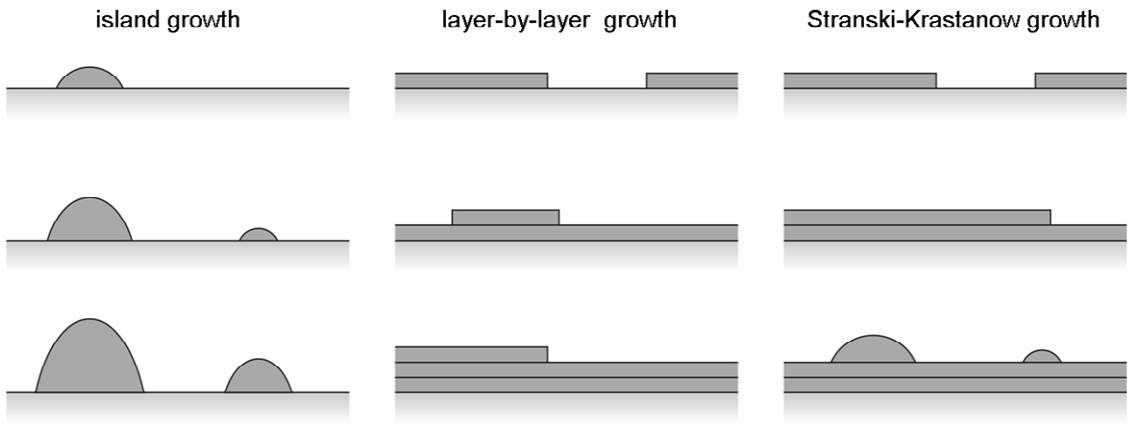

Figure 4.2: Schematic representation of possible film growth mechanisms [79].

Figure 4.2 shows three different growth modes, each of them depending on the predominant energy distribution. If the binding energy between the ad-atoms is equal to or smaller than that between film atoms and substrate, then layer-by-layer growth (Frank van der Merwe growth) appears. Here, a second monolayer will only occur after the first monolayer has fully covered the surface. When the ad-atoms are stronger bonded to each other than to the substrate, small clusters and islands are nucleated directly on the substrate surface. Due to the coalescence of growing islands, a continuous film lately covers the whole substrate. This mechanism is termed as island growth (Volmer Weber growth), as illustrated in Figure 4.2 [79,81]. These two growth modes can also be combined, which is often referred to Stranski-Krastanow growth. Typically, after forming of 5-6 monolayers, further layer-by-layer growth becomes unfavourable and island growth appears. However, the mechanisms driving the transition from layer-by-layer growth to islands growth are not yet fully understood [77]. One

explanation might be the release of elastic energy between film and substrate due to the lattice mismatch [79].

4.2. Structure zone models

In general, the evolution of film structure and its morphology is determined by the elementary processes of diffusion and the fundamental phenomena of structure formation during grain growth. Since these processes and phenomena, i.e. nucleation, crystal growth and recrystallization, have an Arrhenius type behaviour with temperature, their rates are controlled by their corresponding activation energies. In addition to ad-atom mobility, other parameters such as the deposition rate, impurities, energetic bombardment etc. determine the film growth. To represent the influence of several deposition parameters on the final film structure and morphology, various structure zone models (SZMs) has been published by many authors [85-91]. Since the microstructure of thin films is strongly influenced by the surface mobility or the temperature on the growing surface, the SZMs are often represented as function of the homologous temperature, i.e. the ratio between the substrate temperature and the melting temperature of the deposited material. Movchan and Demchishin [93] were the first to define three structure zone models classified by the homologous temperature. To extend this concept, a similar model was derived by Thornton [86,87], where additionally to temperature, the inert gas pressure, i.e. argon, was introduced as a variable. This model was further modified by Messier et al. [88], whereas the gas pressure was replaced by the substrate bias voltage which affects the energy of impinging ions during film growth. Nearly all published SZMs use the terminology introduced by Movchan and Demchishin (zone I, II and III) [93] and by Thornton (zone T) [86,87]. A comparison of different SZMs and detailed explanations can be found in literature [49,54,89-92].

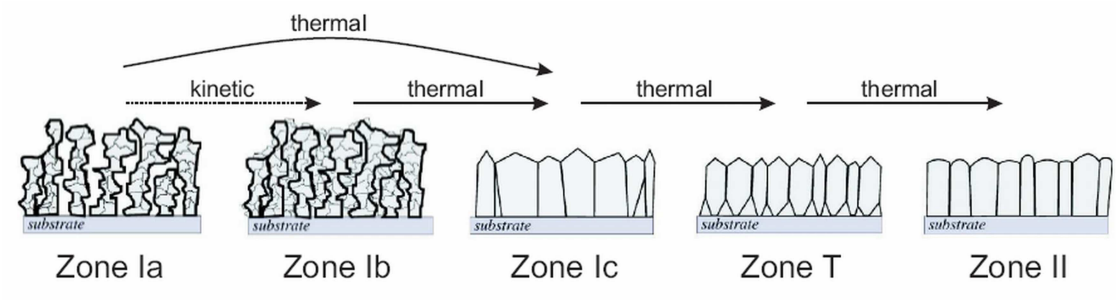

Figure 4.3: Schematic structure zone model as published by Mahieu et al. [91].

In the following, the structure zone model as published by Mahieu et al. [91] will be presented briefly (see Figure 4.3). Since the diffusion processes and structure formation phenomena are not only controlled by the substrate temperature, but by the total energy flux to the growing surface, the use of quantitative temperature values is avoided in this model.

Zone Ia At very low temperature, the ad-atoms have little or no mobility and they cannot overcome the diffusion barrier. Consequently, the ad-atoms stick to the growing film at the place they hit it (known as hit-and-stick growth or "ballistic" deposition). The resulting structure is only influenced by the incoming direction of the material flux. In this case, a columnar structure separated by voids is developed which is mainly caused by roughening and self-shadowing (see Figure 4.3). The Zone Ia structure can also be obtained at higher temperature by using a high deposition rate, where ad-atoms are buried by the high flux of incoming particles and diffusion processes are suppressed. In general, the films deposited under zone Ia conditions exhibit an amorphous-like structure or consist of small grains due to the very limited ad-atom mobility. They usually have low density and do not show a specific crystallographic direction perpendicular to the substrate.

Zone Ib Deposition of thin films under zone Ia conditions, but with continuous bombardment by energetic particles, leads to a different structure. Due to the energetic bombardment, the voids between the columns will be filled by atoms and a more dense columnar structure is observed. The transition from zone Ia to zone Ib is only possible by energetic bombardment and not by increasing the temperature. Since the mobility of ad-atoms is mainly controlled by kinetic energy and is not thermally induced, an amorphous-like film with no preferential orientation is developed.

Zone Ic At higher temperature, the thermally induced mobility and nucleation increases and crystalline islands are formed. Since the ad-atoms in zone Ic are able to overcome the diffusion barrier, a polycrystalline random growth with faceted structure is observed, while grains are terminated by the planes of lowest crystallographic growth rate. However, the ad-atoms are unable to diffuse from one grain to another; thus, there is no real interaction or competition between neighbouring grains. Therefore, the columns are separated by grain boundaries while voids between the columns are filled due to the increased ad-atom mobility.

Zone T Further increase in temperature leads to the diffusion of ad-atoms from one grain to another. Due to the high mobility, grain growth and faceting occur, whereas the planes with lowest perpendicular growth rate form the resulting facets. Since no recrystallization or restructuring can happen, the grains with the geometrically fastest growing

direction perpendicular to the substrate will overgrow the other grains. Consequently, V-shaped, faceted grains develop. The out-of-plane alignment is completed at a certain film thickness while at higher film thickness, a columnar structure with faceted tops can be observed.

Zone II At higher temperatures, recrystallization and restructuring take place. Former stable nuclei or islands become unstable and incorporation of islands into other islands by ripening, cluster diffusion or grain boundary migration occurs. Since the unstable islands are dissolved in more stable islands, no V-shape overgrowth is observed. In this growth region, a columnar structure with approximately straight columns throughout the whole film thickness is formed. Due to the thermodynamically most stable situation, the columns are oriented with the plane of lowest surface energy parallel to the substrate. Further increase in temperature gives rise to the effect of recrystallization and restructuring, thus increasing the lateral size of the resulting columns.

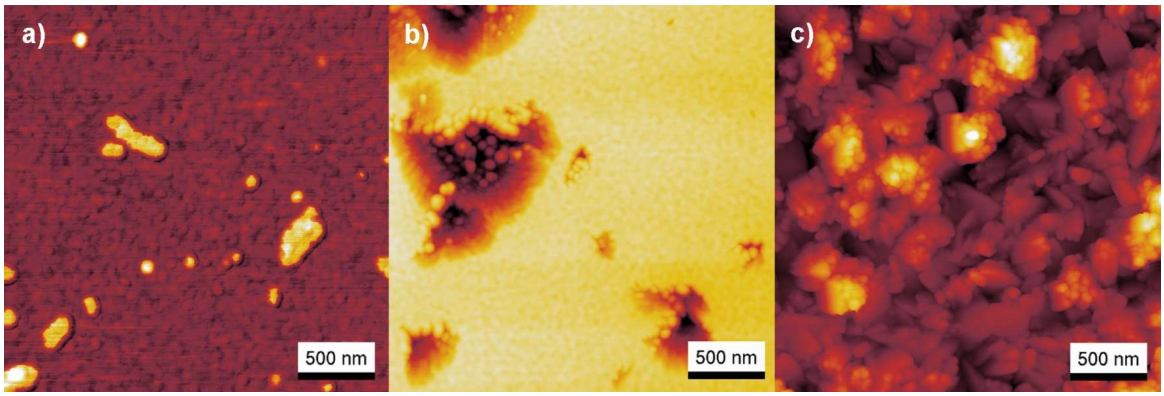

Figure 4.4: AFM images of a) an amorphous V_2O_5 film grown at room temperature (z-scale: 10 nm), b) the transition from amorphous to crystalline film growth at 80°C (z-scale: 70 nm) and c) a polycrystalline V_2O_5 film grown at 300°C (z-scale: 140 nm).

Publication III and IV provide an insight into structure evolution of V_2O_5 thin films for different deposition techniques at various deposition temperatures. The observed results showed that the variation of deposition temperature and change in the energy flux regarding to different deposition modes influence the thin film microstructure. Figure 4.4 presents the AFM images of dc magnetron sputtered V_2O_5 films deposited onto MgO (100) substrate at different deposition temperatures (see Publication III). In this case, a transition from amorphous to polycrystalline growth with increasing deposition temperature due to the

increased mobility of ad-atoms on the surface and enhanced diffusion could be observed. The AFM image of a V_2O_5 film deposited at 300°C shows the granular structure, where a morphology characterized by small plates could be found.

5. Tribology

Tribology can be defined as the science and technology of interacting surfaces in relative motion, and covers the field of friction, wear and lubrication [94,95]. During the industrial revolution, friction and wear became increasingly important, since reducing or controlling friction and wear play a significant role to extend the machinery lifetime and efficiency and to save energy. An etablished tribology related engineering concept is to apply a thin layer on one or both contacting surfaces in relative motion to improve the tribological performance. Development of a new class of low-friction coatings based on lubricious oxides is the central point within this thesis. Therefore, a brief overview of tribological aspects is presented in the following chapter.

5.1. Theories of friction and wear

Friction is the resistance encountered by one body when moving over another. The resistive force, which acts tangentially to the interface, perpendicular to the normal force and opposite to the direction of motion, is known as friction force. The ratio between the frictional force and the normal load is defined as coefficient of friction μ, and is often abbreviated as COF. Friction is characterised by three basic laws stated as follows [94-96]:

1. The friction force is proportional to the normal force.
2. The friction force is independent of the apparent area of contact. Thus large and small objects may have the same COF.
3. The friction force is independent of the sliding velocity.

The first two laws are generally well obeyed while the third law of friction is rather less well founded. It is well known that the friction force required to start sliding is usually greater than the force required to maintain sliding. But once the sliding is established, the coefficient of dynamic friction (for surfaces in motion) is found for many systems to be nearly independent of sliding velocity. The friction coefficient is not an inherent material property, but is dependent on various parameters, e.g. the sliding distance, sliding velocity, normal load or the environment. Suh and Sin presented in 1981 a new concept of friction, called the “genesis of friction” [97]. They point out that, during sliding, the frictional behaviour undergoes six different stages before reaching the steady state. There are three basic mechanisms behind friction: adhesion of the flat portions of the sliding surfaces, ploughing by wear particles and hard asperities and deformation of surface asperities, as shown in Figure

5.1. According to this theory, the mechanical properties affect the frictional behaviour to a greater extent than chemical properties when sliding occurs without a significant interfacial temperature rise. Depending on the tribosystem, one of these mechanisms turns into the dominant effect while the contribution of each basic mechanism is determined by the interface, the material pairing, the operation conditions and the environment [97].

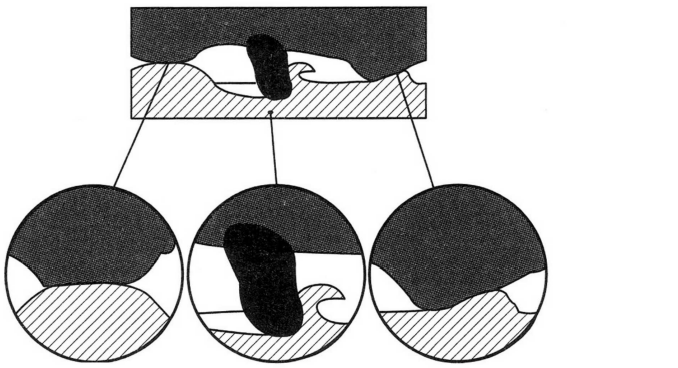

Figure 5.1: The three components of sliding friction a) adhesion, b) ploughing, c) asperity deformation [98].

Figure 5.2 shows the previously mentioned six stages of friction in sliding contact during the initial period of sliding [97]. In stage 1, the friction coefficient is mainly controlled by ploughing of the surface by asperities. Adhesive wear plays a minor role due to the surface contamination such as oxidation, while occurring asperity deformation affects the static coefficient of friction and the surface is easily polished. Ploughing of the surface leads to the removal of the oxides. Once the surface contaminations are removed, the bare surface will appear which results in a slight increase in the coefficient of friction due to the increased adhesion (stage 2). During stage 3, the friction coefficient increases further due to a rapid increase in the number of wear particles in the sliding contact as a consequence of higher wear rates. Some of the wear particles are trapped between the surfaces, causing ploughing. Once the overall number of wear particles reaches an equilibrium between the particles entering and leaving the interface, a constant friction coefficient can be observed in stage 4. In the case that two identical materials slide against each other, stage 4 represents the steady state friction. For two different materials, i.e. a hard counterpart sliding against a soft specimen, the asperities of the hard surface are gradually removed and the surface of the hard material gets polished. As a consequence, wear particles cannot anchor easily to such a

polished surface and the friction coefficient decreases due the reduction of ploughing and asperity deformation (stage 5). As the hard surface becomes mirror smooth to a maximum extent, the softer surface also acquires a mirror finish, leading to a steady state value of friction coefficient, as shown in stage 6. The shown development of the friction coefficient is valid for a steel contact and may change in several ways for other materials [97]. Although many friction theories have been developed to explain these mechanisms, it is not possible to predict the resulting friction coefficient for a given situation.

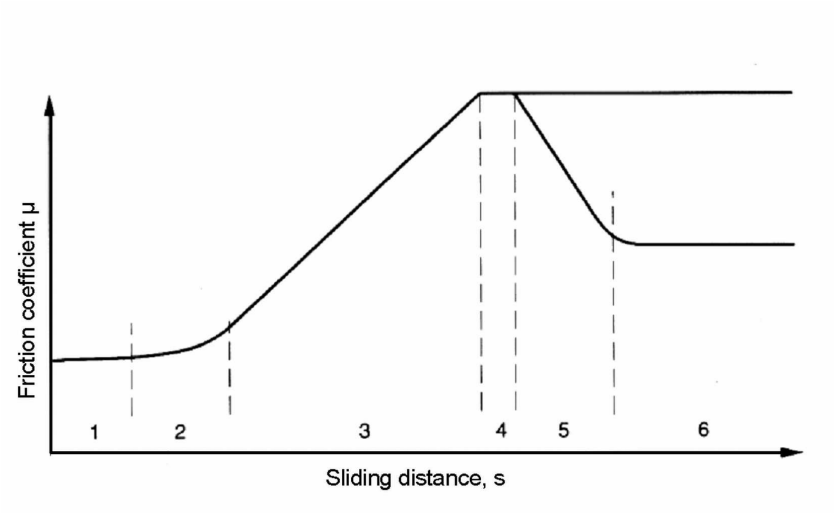

Figure 5.2: Stages in friction coefficient vs. sliding distance for steel counterparts [97].

Another important topic is wear which is defined as the material removal from solid surfaces as a result of one contacting surface moving over another. Wear appears simultaneously to friction as a result of the same tribological contact processes and their interrelationship is still not well understood in detail. To quantify and compare wear effects for design and material development purposes, the wear coefficient or wear rate is widely used. The term wear rate describes (see Equ. 5.1) the rate of material removal or dimensional change due to wear per unit of exposure parameter, for example, volume V of removed material per applied load F_N and sliding distance s [13,95-98] and is often given with the dimensions [10^{-6}mm^3/Nm]:

$$K = \frac{V}{F_N \cdot s} \qquad \text{Equ. (5.1)}$$

According to the observation of Holm and Archard in 1953, the wear rate is inversely proportional to the hardness of the material [96,98]. Generally, wear occurs by mechanical

and/or chemical means, and usually increases at elevated temperatures. There are different ways of classifying wear mechanisms. However, no general agreement has been reached up to now. The most common classification was done by Blau (1989) who defined four basic wear mechanisms: adhesion, abrasion, surface fatigue and tribochemical reaction, as illustrated in Figure 5.3 [13], When two surfaces slide against each other, asperity junctions are formed. These junctions are sheared during the relative tangential motion until they break. Some of them break through some surfaces usually inside the weaker body, resulting in the transfer of small particles to the other contact surface. This phenomenon is called adhesive wear, see Figure 5.3a. The physical and chemical properties of the interacting materials, the mode and value of loading and properties of the contacting surfaces such as contamination or roughness determine the adhesion tendency of the materials in contact [95,98-100].

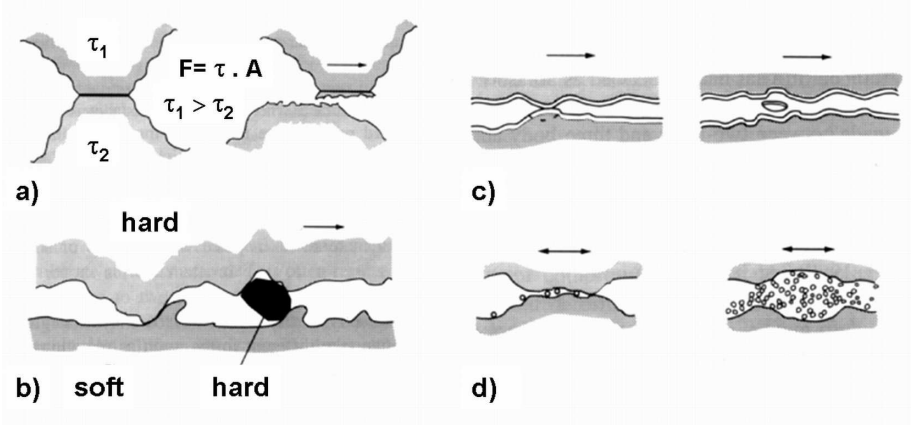

Figure 5.3: The four main wear mechanisms a) adhesion, b) abrasion, c) surface fatigue, d) tribochemical reaction [13].

Abrasive wear occurs, when asperities of a rough, hard surface or hard particles slide on a softer surface and damage the interface by plastic deformation or fracture, see Figure 5.3b. It covers two types of situations, known as two-body abrasion and three-body abrasion. In case of two-body abrasion, the abrasive material is fixed to one of the rubbing surfaces (e.g. grinding, cutting, machining), whereas for three-body abrasion, loose abrasive particles can move between both surfaces (e.g. polishing). Surface fatigue wear (Figure 5.3c) originates from surface and subsurface cracks induced by repeated loading and unloading cycles which eventually, after a critical number of cycles, will result in delamination of long and thin wear debris. In tribochemical wear, the wear process is dominated by chemical reactions of the sliding surfaces with each other, and with the corrosive environment resulting in removal of

material and wear debris, see Figure 5.3d. Elevated temperatures, typically in the range of 700°C to 1300°C in cutting applications, promote these reactions. Oxidative wear is the most common tribochemical wear process, where in the absence of sliding a thin oxide layer may form which can be continuously removed by a rubbing action [99,100].

5.2. Tribological coatings: contact mechanisms

In the middle of the 20th century, attention focused on discrete components, their interactions and also on the modelling and study of contacts at the asperity level. To optimize the properties of two surfaces in contact and to achieve the required friction and wear performance, a fundamental understanding of the mechanisms involved in tribological contacts at different scale levels is necessary. Gradually, attention has been focused on the tribological mechanisms in a coated contact at the molecular and atomic level.

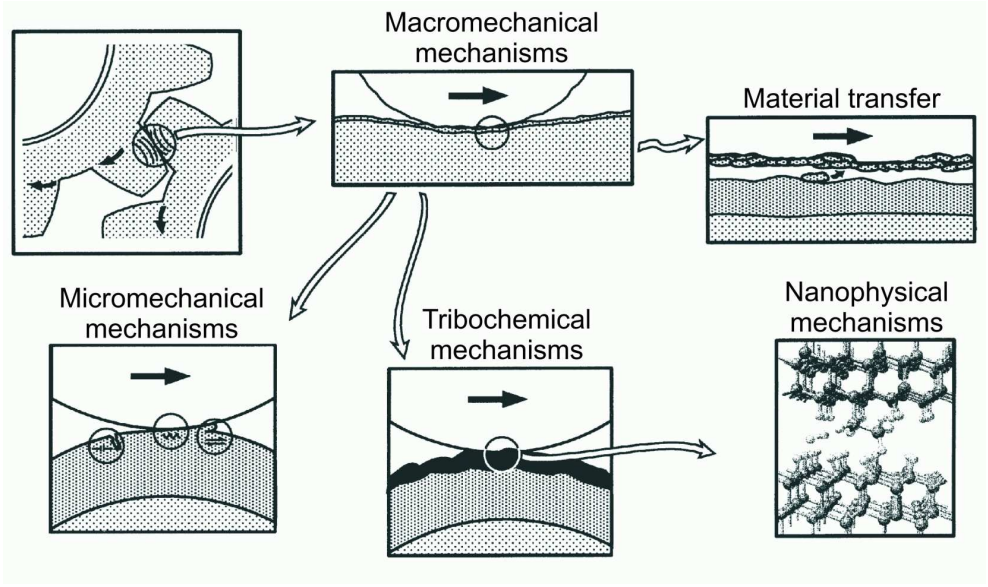

Figure 5.4: Schematic representation of the tribological contact mechanism relations according to Holmberg and Matthews [13,100].

As illustrated in Figure 5.4, Holmberg and Matthews classified the tribological mechanisms of coated surfaces as being macromechanical, micromechanical, tribochemical as well as mechanisms of material transfer and the nanophysical contact [13,99,101].

Macromechanical tribological mechanisms describe the friction and wear phenomena by considering the stress and strain distributions in the entire contact, the resulted elastic and plastic deformations, the wear particle formation and its dynamics. In contacts with one or

two coated surfaces, the tribological process is controlled by four main parameters: the coating to substrate hardness and elasticity relationship, coating thickness, the surface roughness and the size and hardness of the debris and tribolayers in contact. The mechanisms involved are very different depending on whether the coating and the substrate are soft or hard (their deformability and not only their hardness) [13,101].

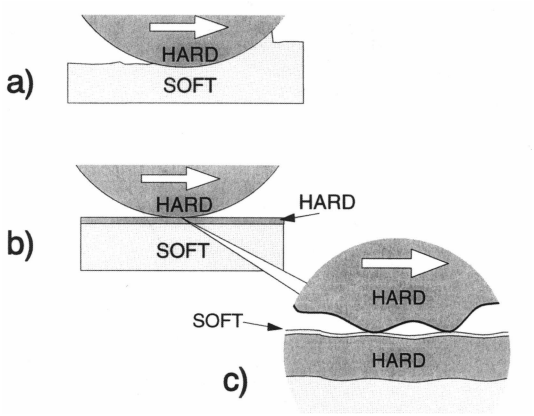

Figure 5.5: Schematic illustration of a hard slider moving over a) soft counterface, b) hard coating on a soft substrate and c) a hard coating with a soft microfilm at the top [13].

The friction force is ideally calculated as the product of contact area and the shear strength. Thus, low friction coefficients are favoured by low shear strength and small contact areas. Soft films provide a low shear strength but the contact area can be large because of the low load carrying capacity resulting in lower adhesion and ploughing effects (see Figure 5.5a). Hard coatings can reduce the contact area by decreasing the ploughing component which also increases the wear resistance (Figure 5.5b). However, hard coatings mostly show a high friction coefficient caused by their higher shear strength. The combination of both a hard coating and a thin soft film at the top is often beneficial to optimize the response to deformation forces, and is very popular in many tribological applications. The soft layer can accommodate the shear stresses while the hard coating provides the load support and good wear protection. A further benefit of having a soft phase present is that it may trap wear debris, and therefore take it out of the system, and reduce it possibility to act as an abrasive (Figure 5.5c).

Micromechanical tribological mechanisms embrace the formation of the stress and strain at an asperity level, the crack generation and propagation, material liberation and single particle formation. Shear and fracture are basic mechanisms for the nucleation and

propagation of a crack which might result in material liberation and wear scare formation. One approach to consider micromechanical tribological mechanisms is by using the velocity accommodation concept developed by Berthier et al [102]. According to Berthier et al., there are four mechanisms by which velocity differences between contacting surfaces can be accommodated: elastic deformation, fracture, shear and rolling. These basic mechanisms may occur in either of the two surfaces (first bodies) or in the layer between them (third body).In the contact with a coated surface, the situation is even more complex since the number of sites for velocity accommodation increases. In this case, velocity accommodation can take place also at the interface between the substrate and the coating, within the coating and within a microfilm on top of the coating. Holmberg and Matthews [103] extended this velocity accommodation concept in the form of an energy accommodation approach, which identifies the elastic modulus, shear strength and fracture toughness as key material parameters for the study of micromechanical tribological mechanisms.

Tribochemical mechanisms take place at the surfaces during sliding contact, and are strongly influenced by high local pressure and the flash temperatures which can exceed 1000°C in the tribological contact zone. The formation of low shear strength microfilms on hard coatings and the oxidation of soft coatings are two main surface phenomena for which the chemical effects are essential. In environments containing oxygen, a thin oxide layer can be formed very quickly on most surfaces. The oxidation on the coating surface may influence in different ways the tribological properties, which are strongly dependent on the nature, the thickness, the adherence and the hardness of the formed oxide.

Mechanisms of material transfer occur from liberated wear particles that are reattached to the surface. Material transfer takes place on both micro- and macro-level but it is mainly the macro material transfer that influences the friction and wear behaviour.

Nanophysical contact mechanisms include all friction and wear phenomena related to the interaction between molecules and atoms, such as the effects of van der Waal’s forces and related interatomic phenomena, and are determined by the crystal structure and bonding structure of materials.

6. Coating characterisation

The coatings investigated in this work were characterized with respect to their chemical composition and microstructure as well as mechanical and tribological properties. Different common experimental techniques were used to assess these properties which are briefly explained in this section. Furthermore, some selected methods are described in more detail in the following chapter.

X-ray Diffraction (XRD) reveals the evaluation of the crystalline structure and phase composition in Bragg-Brentano geometry [104].

Scanning electron microscopy (SEM) provides information of the surface- and coating morphology, microstructural changes after dry sliding tests and supplies high magnification images and compositional maps by scanning a focused electron beam over the sample [104,105].

Differential scanning calorimetric (DSC) and simultaneous thermo-gravimetric (TGA) analysis are applied to characterise the thermal stability of the coatings in a wide temperature range with respect to their oxidation behaviour.

Atomic force microscopy (AFM) is used for studying short-range order on a surface and obtaining topographical information of the films on a nanometer scale.

Nanoindentation is used to obtain values of the hardness and Young´s modulus of the films according to the proposed evaluation method by Oliver and Pharr [106]. More information regarding to this method can be found in references [107,108].

6.1. High temperature tribotesting

To apply friction and wear, different experimental apparatus have been used. One of the most common methods applied to obtaining friction and wear data is the ball-on-disc test. The principle of the test is that the ball (counterpart), which is weighted with a defined load, is pressed on the rotating sample during the total sliding distance causing wear on the coating and on the counterpart itself. The disc speed, controlled by the radius and circular speed, can reach up to 2 ms^{-1} while a Linear Voltage Displacement Transducer measures the friction force at the selected recording rate. Dividing the friction force through the normal force caused by the load delivers the friction coefficient. The tribological behaviour of the coatings in this thesis was studied up to 700°C using a high temperature ball-on-disc tribometer. The parameters used for the ball-on-disc tests conducted in this work are given in Publications I, II

and V. The resulting wear track of the coatings after ball-on-disc tests is investigated with an optical profiling system revealing information about the depth and the volume of the displaced material without any physical contact to the surface.

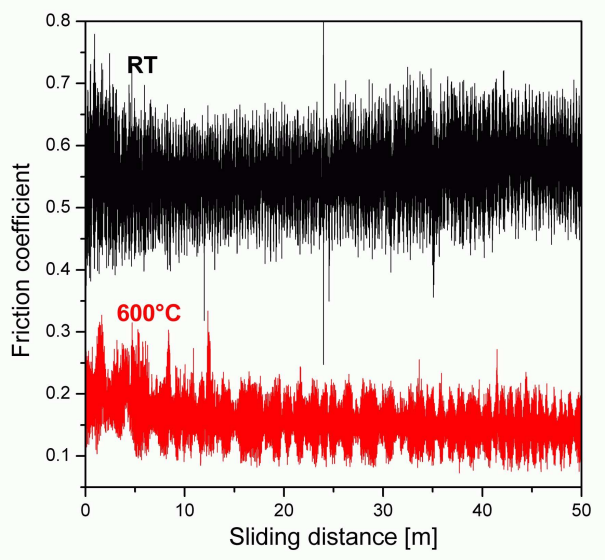

Figure 6.1: Recorded friction coefficients of V_2O_5 single-layer coatings vs. sliding distance.

An example of recorded friction coefficient over the sliding distance is shown in Figure 6.1 where a significant reduction of COF of V_2O_5 single-layer coatings with increasing the temperature can be seen. The lowest COF ($\mu \sim 0.15$) of V_2O_5 single-layer coating is reached at 600°C where thermally activated processes seem to be necessary to promote low friction due to the easy shearing of V_2O_5 lattice planes.

6.2. Raman spectroscopy

Raman scattering was first discovered by Krishna and Raman in 1928 and arises from an interaction of light with the optical and vibrational oscillations of molecules [109,110]. Besides the absorption of light, a small fraction of the incident photons will be scattered either with the same frequency (Rayleih scattering) or a different, material specific frequency (Raman scattering). Scattering of an incident photon results in a loss or gain of energy, depending onto whether the molecule is in an excited vibrational state or not, leading to Stokes or anti-Stokes Raman scattering. Both Stokes and anti-Stokes peaks are symmetrically positioned about the Rayleigh scattering, but of different intensities. Further, anti-Stokes

scattering depends on the existence of thermally activated lattice vibrations and, thus, yields a very weak intensity, whereas Stokes scattering is only weakly influenced by the temperature.

Raman spectroscopy is an excellent way to identify materials via fingerprints by comparing the recorded spectrum with a database containing reference spectra and also to determine the structure of materials, since it is sensitive to the length, strength and arrangement of atomic bonds. It is common to illustrate the Raman spectra in terms of the difference between the frequency of the Rayleigh- and the Stokes-scattering, the so-called Raman shift as a function of wave number in reciprocal centimetres. The Raman shift depends on the crystallinity, the defects, structural disorder and stresses in materials. Furthermore, quantitative information can be obtained from the Peak intensities, whereas the Peak position provides information about the stoichiometry [110-113]. Especially the good lateral resolution of Raman spectroscopy combined with a very surface-sensitive information depth give rise to the utilization of this method in the field of thin film technology. A combination of an optical microscope with a laser providing monochromatic light of high intensity and a sensitive detector offers a possible measurement setup for Raman investigations. Different exciter wavelengths are in use depending on the Raman active mode of the investigated material [114].

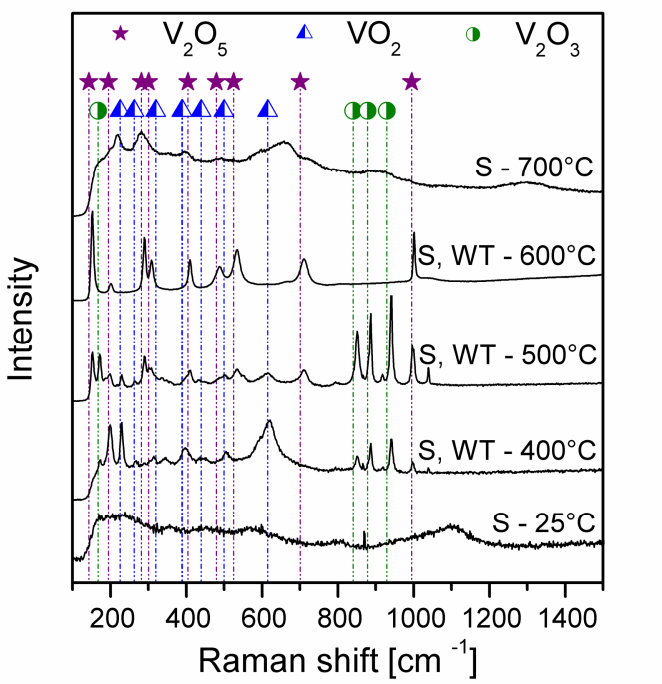

Figure 6.2: Raman spectra of VN coatings after high temperature tribometer testing against alumina at different temperatures, S…surface and WT…wear track.

Within this work (Publications I-IV), Raman measurements were performed by a confocal Raman spectroscope which provides a high spatial resolution while a He-Ne laser with an excitation wave length of 632.8 nm was used. In Publication I and II, Raman spectroscopy was applied for studying the wear tracks of TiN, VN and V coatings, to identify the possible oxides generated during dry sliding experiments at elevated temperatures. Figure 6.2 shows the Raman spectra of VN coatings after dry sliding tests against alumina balls at different temperatures up to 700°C where different vanadium oxides could be easily distinguished. The observed vanadium oxides corresponding to VO_2, V_2O_3 and V_2O_5 indicate the ongoing oxidation reactions above 400°C (see Publication II). A detailed study on structural changes of deposited V_2O_5 coatings at different deposition temperatures and after annealing using also Raman spectroscopy is presented in Publications III and IV.

6.3. Transmission electron microscopy (TEM)

Transmission electron microscopy (TEM) is a special technique among electron microscopy whereby an electron beam is transmitted through an ultra-thin specimen, interacting with the specimen as it passes through it. The most common TEM (conventional TEM) is operated with high-energy electrons (10-120 keV). The specimens for TEM investigation must be prepared as a thin foil, or etched to obtain some portion of the specimen thin enough for the beam to penetrate. Preparation techniques to achieve an electron transparent region include ion beam milling and wedge polishing. The focused ion beam (FIB) is a common new technique to prepare thin samples for TEM examination from larger specimens which is explained in detail in references [115,116]. Most materials require extensive sample preparation to produce a sample thin enough to be electron transparent, which makes TEM analysis a relatively time consuming process.

The basic principle of TEM is very similar to a conventional microscope operating with visible light which contains elements like condenser lenses, sample manipulator, and an objective to form the primary image. However, in practice the light is coming from an electron source and the optical lenses are substituted by electromagnetic complements with a variable focal length to magnify or condense the image. Moreover, a complex sample handling system for tilting and translating with a very high mechanical stability, and a fluorescent screen to convert electrons into light are required [117]. The two possible TEM operation modes are diffraction mode and imaging mode. Basically, the only difference between these two modes is the strength of the intermediate lens. In diffraction mode, the

specimen is illuminated with a parallel electron beam. To determine the crystallographic relation between two neighbouring crystallites or the orientation of specific ones, the diffraction pattern volume must be limited to this area. This is achieved by inserting a selected area aperture in the image plane of the objective lens resulting in selected area electron diffraction (SAED) which provides information that is equivalent to XRD [117]. In the imaging mode, the objective lens system is focused on the objective image plane. An objective aperture in the back focal plane is intended to set the objective lens at the optimum value. According to its position around the direct beam or any diffracted beam in the diffraction pattern, either bright-field (BF) or dark-field (DF) images can be observed [104].

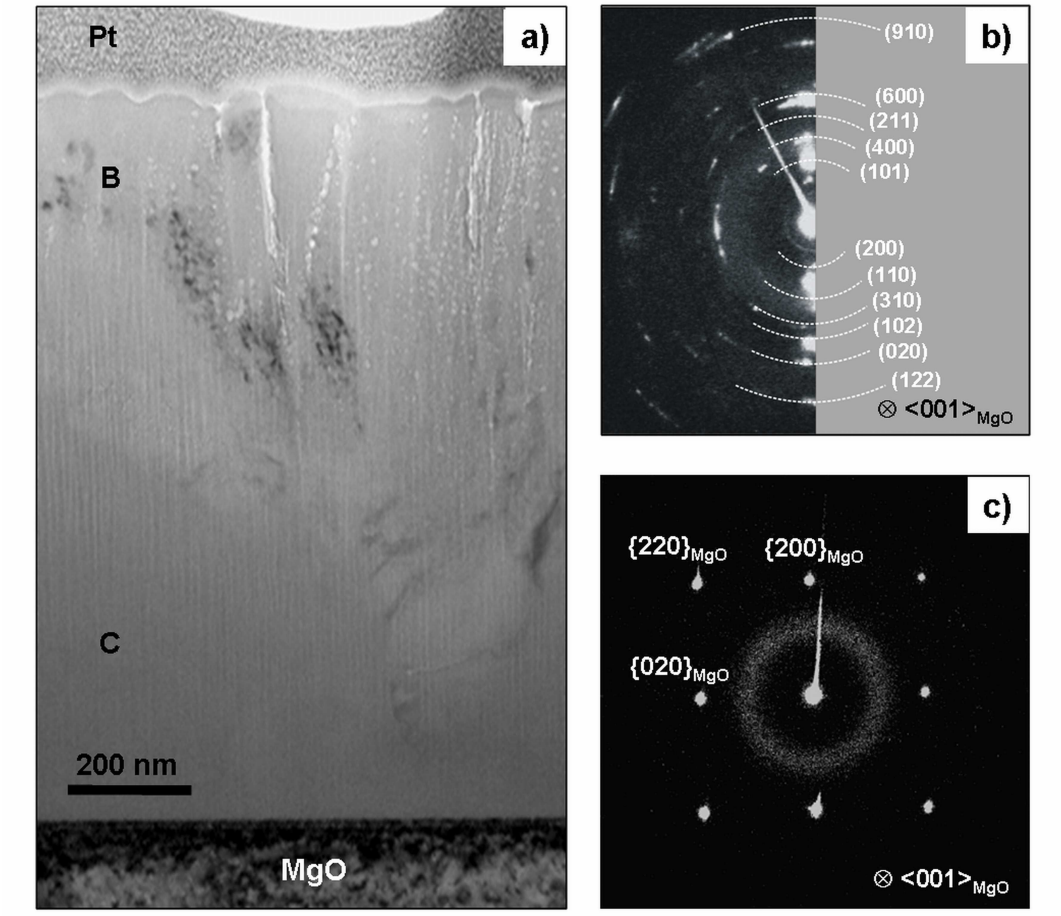

Figure 6.3: a) TEM cross-sectional bright-field image of a V_2O_5 film deposited on MgO (100) at 80°C, b) corresponding SAD patterns taken from the upper region (B) of the film and c) the lower part of the film (C) and adjacent substrate.

In Publication III, the microstructure investigation of synthesised V_2O_5 thin films grown at different substrate temperatures was accomplished by TEM using bright- and dark-field

imaging. For TEM investigations in this thesis, the cross-sectional TEM samples were prepared by focused ion beam (FIB). To obtain detailed information of the crystal structure, selected area electron diffraction (SAED) was used. Figure 6.3 presents a TEM cross-sectional bright-field image of the V_2O_5 film deposited on MgO (100) at 80°C with corresponding SAED patterns taken from two different regions of the film. Figure 6.3(a) displays the presence of discrete crystalline grains within a flat and uniform matrix. According to the SAED pattern of the polycrystalline region taken from the upper part of the film in Figure 6.3(b), the d-spacings match very well to orthorhombic α-V_2O_5 crystal lattice. A comparison between BF and DF images of the V_2O_5 film deposited on MgO (100) at 300°C at the same position can be seen in Publication III.

7. Summary and conclusions

The need to design a new class of low-friction coatings for tribological applications in the medium- and high-temperature range, and to fill the gap between room temperature low-friction coatings (e.g. DLC or MoS_2) and high temperature low-friction coatings such as previously developed TiAlVN or AlCrVN, represent the driving force which leads to the investigation of coatings based on lubricious oxides as conducted within this work.

In the first step, TiN, VN and V coatings were used as model systems to be characterized in the temperature range from room temperature up to 700°C with respect to their oxidation behaviour at elevated temperatures, and to study the influence of the formed oxides on the tribological properties of the coatings. TiN coatings showed only minor changes in friction coefficient over the whole temperature range, while wear increased with raising temperature. The onset of oxidation and the appearance of rutile TiO_2 in the wear track occurred at temperatures above 300°C, while no efficient lubrication or wear protection could be observed. A detailed study on the oxidation behaviour of these coatings under ultra-high vacuum conditions by X-ray photoelectron spectroscopy (XPS), reported by Glaser et al. [118], showed that the TiN surface oxidises partially to a mixture of TiO_2 and Ti oxynitride (TiO_xN_y) at elevated temperatures ($\geq$ 600°C), while on the surface of VN only vanadium oxides are formed. The observed Ti oxynitride phase may be responsible for the poor self-lubrication properties of TiN coatings at elevated temperatures. On the contrary, VN and V coatings show promising tribological properties reaching low friction coefficients at temperatures above 400°C. Both coatings investigated showed the expected vanadium oxides (VO_2, V_2O_3, V_6O_{13} and V_2O_5) at elevated temperatures which improve the tribological performance during high-temperature dry sliding tests. To combine the solid oxide lubrication effect in the temperature range between 400°C and 600°C with sufficient wear resistance, an oxide layer of overcritical thickness has to be formed on the coating surface. Such an oxide layer seems to be stable and efficient after reaching a certain oxidation temperature. It is particularly interesting that even a soft substrate like V can be protected by a sufficiently thick oxide. The lowest friction value of 0.25-0.27 was observed at 700°C, due to the formation of easy-shearable V_2O_5 and the subsequent melting of this phase which has a low melting point of ~ 680°C, resulting in liquid lubrication.

Since these vanadium oxides formed in situ during high-temperature dry sliding, in particular V_2O_5, have the potential to work as a lubricious tribofilm and to provide low

friction and wear protection it is obvious that the next step is the deposition of V_2O_5 thin films, which defines the main focus of the present work.

V_2O_5 thin films were grown on (100) oriented MgO and Si substrates using dc and bipolar pulsed dc reactive magnetron sputtering, in order to study in detail the interrelationships between deposition conditions, growth and the structural evolution, and the influence of these parameters on the resulting mechanical properties of the coatings.

The effect of deposition temperature (varying between 26°C and 300°C) on structure and surface morphology was first investigated by depositing V_2O_5 thin films on MgO (100) by dc reactive magnetron sputtering. The V_2O_5 thin films grown at room temperature exhibited an amorphous structure with a smooth morphology. The onset of crystallisation during thin film growth occurs at ~ 80°C, where the film region close to the substrate is mostly amorphous and the region near to the surface polycrystalline, as derived from TEM analysis. Increasing the deposition temperature to 80°C and above, favours the onset of crystallisation and subsequent grain growth due to the increase in ad-atom mobility on the surface and enhanced diffusion. The V_2O_5 films deposited at temperatures above 100°C were polycrystalline, exhibiting the orthorhombic α-V_2O_5 phase with (200) preferred orientation and with a plate-like morphology. The results obtained for dc magnetron sputtered V_2O_5 thin films on Si (100) at 26, 100 and 300°C revealed that the transition from amorphous to polycrystalline growth with (200) preferred orientation with increasing deposition temperature is independent of the substrate used, and the increasing crystallinity leads to an increase in hardness and Young's modulus. The films deposited by pulsed dc magnetron sputtering exhibit a polycrystalline α-V_2O_5 structure over the whole deposition temperature range due to the increased energy and flux of ions bombarding the substrate by applying the pulsed dc mode. It seems that there is a change in the preferred orientation from (001) to (110) with increasing deposition temperature. The hardness of these films decreases with increasing deposition temperature while the Young's modulus is almost unaffected.

Finally, to verify the suitability of V_2O_5 as low-friction coating and to gain a detailed understanding of the influence of sputtering mode, structure and growth orientation of the V_2O_5 films on their tribological performance, dry sliding experiments of V_2O_5 single-layer and VN-V_2O_5 bi-layer coatings were performed in the temperature range between 25 and 600°C. Structural investigations revealed that the V_2O_5 single-layer and the V_2O_5 top-layer of dc sputtered VN-V_2O_5 coatings have preferred (200) orientation while the V_2O_5 top-layer of pulsed dc VN-V_2O_5 coatings shows preferred (110) growth. The investigated coatings show

high friction and wear at room temperature and do not provide the expected lubrication. However, the friction coefficient of all investigated coatings decreases with increasing temperature, where thermally activated processes seem to be necessary to promote the low friction effect. Growth orientation and film structure seem to determine this onset temperature, and both together with the surface morphology determine the frictional behaviour. Furthermore, also the wear resistance is improved with increasing testing temperature. The use of V_2O_5 acting as a solid lubricant in the case of biased V_2O_5 single-layer and pulsed dc VN-V_2O_5 bi-layer coatings has advanced the operating range for tribological performance to lower temperatures. A reduced friction ($\mu \sim 0.39$) could be observed at 300°C, reaching low friction coefficients (0.29-0.15) at 600°C which are lower in comparison to the friction values of the V and VN coatings investigated within this work.

The investigations conducted in the present thesis have confirmed that V_2O_5 provides low friction and wear protection in the temperature range between 300 and 600°C due to its substantial beneficial lubricious effect. However, there is still a gap between room temperature and 300°C which should promote the development of novel tribological coatings with lubricious capability. Besides V_2O_5, oxides with high ionic potentials such as WO_3, MoO_3, Re_2O_7 and Nb_2O_5 are expected to provide low friction and wear and could be used in new concepts for tribological applications [6]. According to the obtained findings within this work, the lubrication effect of V_2O_5 is a thermally induced process, and the onset of this thermal activation might depend on its melting point. Thus, the application temperature of lubricious oxides might be defined by their melting temperature. By taking this finding into consideration, Re_2O_7 with a melting point of 296°C may be a good candidate to provide low friction at temperatures below 300°C, while Nb_2O_5 (melting point ~ 1460°C) might be capable to offer sufficient lubricity at temperatures above 600°C. Nevertheless, a systematic investigation on the deposition and tribological behaviour of the mentioned oxides and a distinct understanding of the underlying tribological mechanisms is a prerequisite to succeed in applying such oxides as solid lubricants in a wide variety of tribological systems.

8. References

[1] L. Hultman, J.E. Sundgren, in: Handbook of Hard Coatings, Deposition Technologies, Properties and Applications, (R.F. Bunshah, S.M. Rossnagel, G.E. McGuire, eds.), Noyes Publications, New Jersey, 2001.

[2] A. Erdemir, in: Modern Tribology Handbook, (B. Bhushan, ed.), vol. 2, CRC Press, Boca Raton, 2001, pp. 787.

[3] W.-D. Münz, J. Vac. Sci. Technol. A4/6 (1986) 2717.

[4] S. PalDey, S. C. Deevi, Mat. Sci. Eng. A342 (2003) 58.

[5] C.P. Constable, J. Yarwood, P.Eh. Hovsepian, L.A. Donohue, D.B. Lewis, W.-D. Münz, J. Vac. Sci. Technol. A 18 (4) (2000) 1681.

[6] A. Erdemir, Tribol. Lett. 8 (2000) 97.

[7] A.A. Voevodin, J. Bultman, J.S. Zabinski, Surf. Coat. Technol. 107 (1998) 12.

[8] R. Gilmore, M.A. Baker, P.N. Gibson, W. Gissler, Surf. Coat. Technol. 105 (1998) 12.

[9] M. Woydt, A. Skopp, I. Dörfel, K. Witke, Wear 218 (1998) 84.

[10] M. N. Gardos, H.-S. Hong, W.O. Winer, Tribol. Trans. 22 (1990) 209.

[11] M. Gardos, Tribol. Trans. 31 (1988) 427.

[12] M. Gardos, Tribol. Lett. 8 (2000) 65.

[13] K. Holmberg, A. Matthews, Coatings Tribology: Properties, Techniques and Applications in Surface Engineering, vol. 28 of Tribology Series, Elsevier, Amsterdam, 1994.

[14] P.H. Mayrhofer, P.E. Hovsepian, C. Mitterer, W.-D. Münz, Surf. Coat. Technol. 177-178 (2004) 341.

[15] R. Franz, J. Neidhardt, B. Sartory, R. Kaindl, R Tessadri, P. Polcik, V.-H. Derflinger, C. Mitterer, Tribol. Lett. 23 (2) (2006) 101.

[16] A. Magnéli, Acta Crystallogr. 6 (1953) 495.

[17] G. Andersson, Acta Chem. Scand. 8 (1954) 1599.

[18] A. Erdemir, Surf. Coat. Technol. 200 (2005) 1792.

[19] A. Dietzel, Z. Elektrochem. 48 (1942) 9.

[20] H. Meidia, A.G. Cullis, C. Schönjahn, W.-D. Münz, J.M. Rodenburg, Surf. Coat. Technol. 151-152 (2002) 209.

[21] W.-D. Münz, D.B. Lewis, P.Eh. Hovsepian, C. Schönjahn, A. Ehiasarian, I.J. Smith, Surf. Eng. 17 (1) (2001) 15.

[22] L.A. Donohue, W.-D. Münz, D.B. Lewis, J. Cawley, T. Hurkmans, T. Trinh, I. Petrov, J.E. Greene, Surf. Coat. Technol. 93 (1997) 69.

[23] W.-D. Münz, L.A. Donohue, P.Eh. Hovsepian, Surf. Coat. Technol. 125 (2000) 269.

[24] W.M. Rainforth, Z. Zhou, J Physics.: Conf. Ser. 26 (2006) 89.

[25] P.Eh. Hovsepian, D.B. Lewis, W.-D. Münz, Surf. Coat. Technol. 133-134 (2000) 166.

[26] P.Eh. Hovsepian, D.B. Lewis, Q. Luo, W.-D. Münz, P.H. Mayrhofer, C. Mitterer, Z. Zhou, W.M. Rainforth, Thin Solid Films 485 (2005) 160.

[27] D.B. Lewis, S. Creasy, Z. Zhou, J.J. Forsyth, A.P. Ehiasarian, P.Eh. Hovsepian, Q. Luo, W.M. Rainforth, W.-D. Münz, Surf. Coat. Technol. 177-178 (2004) 252.

[28] Z. Zhou, W.M. Rainforth, D.B. Lewis, S. Creasy, J.J. Forsyth, F. Clegg, A.P. Ehiasarian, P.Eh. Hovsepian, W.-D. Münz, Surf. Coat. Technol. 177-178 (2004) 198.

[29] Y. Ningyi, L. Jinhua, and L. Chenglu, Appl. Surf. Sci. 191 (2002) 176.

[30] K. Kutschej, P.H. Mayrhofer, M. Kathrein, P. Polcik, C. Mitterer, Surf. Coat. Technol. 188-189 (2004) 358.

[31] G. Gassner, P.H. Mayrhofer, K. Kutschej, C. Mitterer, M. Kathrein, Tribol. Lett. 17/4 (2004) 751.

[32] P. Balog, D. Orosel, Z. Cancarevic, S. Schön, M. Jansen, J. Alloys Comp. 429 (2007) 87.

[33] R. Enjalbert and J. Galy, Acta Crystallogr. C: Cryst. Struct. Commun. 42 (1986) 1467.

[34] A. Byström, K.A. Wilhelmi, O. Brotzen, Acta Chem. Scand. 4 (1950) 1119.

[35] H.G. Bachmann, F.R. Ahmed, W.H. Barnes, Z. Kristallogr. 115 (1961) 110.

[36] J. Galy, A. Ratuszna, J. Iglesias, A. Castro, Solid State Sci. 8 1438 (2006).

[37] C.V. Ramana, O.M. Hussain, B.S. Naidu, P.J. Reddy, Thin Solid Films 305 (1997) 219.

[38] A. Gies, B. Pecquenard, A. Benayad, H. Martinez, D. Gobeau, H. Fuess, A. Levasseur, Solid State Ionics 176 (2005) 1627.

[39] S.H. Lee, H.M. Cheong, M.J. Seong, P. Liu, C.E. Tracy, A. Mascarenhas, J.R. Pitts, S.K. Deb, Solid State Ionics 165 (2003) 111.

[40] L. J. Meng, R. A. Silva, H. N. Cui, V. Teixeira, M. P. dos Santos, Z. Xu, Thin Solid Films 515 (2006) 195.

[41] S. P. Lim, J. D. Long, S. Xu, K. Ostrikov, J. Phys. D: Appl. Phys. 40 (2007) 1085.

[42] M. Benmoussa, E. Ibnouelghazi, A. Bennouna, E. Ameziane, Thin Solid Films 265 (1995) 22.

[43] C. Ramana, R. Smith, O. Hussain, and C. Julien, J. Vac. Sci. Technol. A 22 (2004) 2453.

[44] E. Lugscheider, O. Knotek, K. Bobzin, S. Bärwulf, Surf. Coat. Technol. 133-134, (2000) 362.

[45] W. Gulbinski, T. Suszko, W. Sienicki, B. Warcholinski, Wear 254, 129 (2003).

[46] E. Moll in: Advanced Techniques for Surface Engineering, (W. Gissler, H.A. Jehn, eds.), Kluwer Academic Publisher, Dordrecht (1992), pp. 181.

[47] B. Rother, J. Vetter, Plasmabeschichtungsverfahren und Hartstoffschichten, Deutscher Verlag für Grundstoffindustrie, Leipzig, 1992.

[48] R.F. Bunshah, D.M. Mattox, Deposition Technologies for Films and Coatings, Developments and Applications, Noyes Publications, New Jersey, 1982.

[49] G. Kienel, K. Röll, Vakuumbeschichtung 2, Verfahren und Anlagen, VDI Verlag, Düsseldorf, 1995.

[50] R.A. Häfer, Oberflächen- und Dünnschicht- Technologie, Teil I: Beschichtungen von Oberflächen, Springer Verlag, Berlin, 1987.

[51] S.S. Eskildsen, C. Mathiasen, M. Foss, Surf. Coat. Technol., 116-119 (1999) 18.

[52] H. Frey, VakuumBeschichtung 1, Plasmaphysik-Plasmadiagostik-Analytik, VDI Verlag, Berlin, 1995.

[53] K-P. Müller, Praktische Oberflächentechnik, vorbehandeln, beschichten, prüfen, Vieweg, (3. ed.), Braunschweig, 1999.

[54] M. Konuma, Film Deposition by Plasma Techniques, Springer Verlag, Berlin, 1992.

[55] A. Grill, Cold Plasma in Materials Fabrication, IEEE Press, New York, 1994.

[56] B.N. Chapman, Glow Discharge Processes, John Wiley Inc., New York, 1984.

[57] F.F. Chen, Plasma Physics and Controlled Fusion, Plenum Press, New York, 1984.

[58] G. Franz, Oberflächentechnologie mit Niederdruckplasmen, Beschichten und Strukturieren in der Mikrotechnik, Springer Verlag, (2nd ed.), Berlin, Heidelberg, 1994.

[59] M. Zongxin, L. Guoqing, C. Deliang, H. Kaiyu, L. Cui, Surf. Coat. Technol. 193 (2005) 46.

[60] B. Window, N. Savvides, J. Vac. Sci. Technol. A 4(3) (1986) 453.

[61] B. Window, Surf. Coat. Technol. 81 (1996) 92.

[62] I. Petrov, V. Orlinov, I. Ivanov, J. Kourtev, Contrib. Plasma Phys. 28 (3) (1988) 265.

[63] I. Petrov, F. Adibi, J.E. Greene, W.D. Sproul, W.-D. Münz, J. Vac. Sci. Technol. A 10 (1992) 3283.

[64] I. Ivanov, P. Kazansky, L. Hultman, I. Petrov, J.-E. Sundgren, J. Vac. Sci. Technol. A 12 (2) (1994) 314.

[65] P. H. Mayrhofer, Materials Science Aspects of Nanocrystalline PVD Hard Coatings, PhD Thesis, University of Leoben, 2000.

[66] R. F. Bunshah, C.V. Deshpandey, J. Vac. Sci. Technol. A 3/3 (1985) 553.

[67] L. I. Maissel, Handbook of Thin Film, McGraw-Hill, New York, 1983.

[68] O. Zywitzki, G. Hoetzsch, Surf. Coat. Technol. 86-87 (1996) 640.

[69] W.D. Sproul, M.E. Graham, M.S. Wong, S. Lopez, D. Li, R.A. Scholl, J. Vac. Sci. Technol. A13 (1995) 1188.

[70] A. Belkind, A. Freilich, R. Scholl, Surf. Coat. Technol. 108-109 (1998) 558.

[71] P. Kelly, R. Arnell, J. Vac. Sci. Technol. A 17 (1999) 945.

[72] P.J. Kelly, C.F. Beevers, P.S. Henderson, R.D. Arnell, J.W. Bradley, H. Bäcker, Surf. Coat. Technol. 174-175 (2003) 795.

[73] H. Bäcker, P.S. Henderson, J.W. Bradley, P.J. Kelly, Surf. Coat. Technol. 174-175 (2003) 909.

[74] S. Schiller, K. Goedicke, J. Reschke, V. Kirchhoff, S. Schneider, F. Milde, Surf. Coat. Technol. 61 (1993) 331.

[75] P. Kelly, R. Arnell, Vacuum 56, 159 (2000).

[76] A. Belkind, A. Freilich, J. Lopez, Z. Zhao, W. Zhu, K. Becker, New J. Phys. 7 (2005) 90.

[77] J.E. Greene, in: Handbook of Crystal Growth, (D.T.J. Hurle, ed.), Vol. 1, Elsevier, 1993, pp. 640.

[78] P.B. Barna, in: Proc. Diagnostics and Applications of Thin Films (L. Eckertová, T. Ruzicka eds.), Institute of Physics Publishing, 1992, pp. 295.

[79] J.E. Greene, in: Handbook of Deposition Technologies for films and coatings, (R.F. Bunshah, ed.), Noyes Publications, Park Ridge,1994, pp. 681.

[80] H.A. Jehn, in Advanced Techniques for Surface Engineering, (W. Gissler, H.A. Jehn, eds.), Kluwer Academic Publishers, Amsterdam, 1993, pp. 5.

[81] M. Ohring, Materials Science of Thin Films, Deposition and Structure, Academic Press, San Diego, (2nd ed.), 2002.

[82] Y. Pauleau, P. B. Barna, Protective Coatings and Thin Films, Kluwer Academic Publishers, Dordrecht, 1997.

[83] I. Petrov, L. Hultman, J.-E. Sundgren, J.E. Greene, J. Vac. Sci. Technol. A 10 (1992) 265.

[84] I. Petrov, P.B. Barna, L. Hultman, J.E. Greene, J. Vac. Sci. Technol. A 21 (2003) 117.

[85] P.B. Barna, M. Adamik, Thin Solid Film 317 (1998) 27.

[86] J. A. Thornton, J. Vac. Sci. Technol. 11 (1974) 666.

[87] J. A. Thornton, Annu. Rev. Mater. Sci. 7 (1977) 239.

[88] R. Messier, A.P. Giri, R.A. Roy, J. Vac. Sci. Technol. A 2 (1984) 500.

[89] D.L. Smith, Thin-Film Deposition: Principles & Practice, McGraw-Hill Inc., New York, 1995.

[90] J.B. Wachtman, R.A. Haber, Ceramic films and coatings, Noyes Publications, Westwood, New Jersey, USA, 1993.

[91] S. Mahieu, P. Ghekiere, D. Depla, R. De Gryse, Thin Solid Films 515/4 (2006) 1229.

[92] E. Mirica, G. Kowach, H. Du, Cryst. Growth Des. 4/1 (2004) 157.

[93] B. Movchan, A. Demchishin, Physics of Metals and Metallography 28 (1969) 83.

[94] E. Rabinowicz, Friction and Wear of Materials, John Wiley Inc. (2nd ed), New York, 1995.

[95] I. Hutchings, Tribology - Friction and Wear of Engineering Materials, Edward Arnold, London, 1992.

[96] F. Bowden, D. Tabor, The Friction and Lubrication of Solids, Clarendon Press, Oxford, 1954.

[97] N. Suh, H. Sin, Wear 69 (1981) 91.

[98] B. Bhushan, Principles and Application of Tribolog, John Wildey Inc., New York, 1999.

[99] K. Holmberg, A. Matthews, H. Ronkainen, Tribology Int. 31 (1998) 107.

[100] K. Holmberg, H. Ronkainen, A. Matthews, Ceramics Int. 26 (2000) 787.

[101] A. Matthews, S. Franklin, K. Holmberg, J. Phys. D: Appl. Phys. 40 (2007) 5463.

[102] Y. Berthier, M. Godet, M. Brendle, Tribol. Trans. 32 (1989) 490.

[103] K. Holmberg, A. Mattews, in: Modern Tribology Handbook, (B. Bhushan), vol. 2, CRC Press, Boca Raton, 2001, pp. 828.

[104] W. Gissler, J. Huapt, in: Advanced Techniques for Surface Engineering, (W. Gissler, H.A. Jehn, eds.), Kluwer Academic Publisher, Dordrecht (1992) pp. 313.

[105] J.B. Bindell, in: Encyclopedia of Materials Characterization: Surfaces, Interfaces, Thin Film, (C.R. Brundle, C.A. Evans, Jr., S. Wilson, eds.), Butterworth-Heinemann, Boston, 1992, pp. 70.

[106] W. Oliver and G. Pharr, J. Mater. Res. 7 (1992) 1564.

[107] A. Fischer-Cripps, Nanoindentation, Springer, (2nd ed), New York, 2004.

[108] A. Fischer-Cripps, Surf. Coat. Technol. 200 (2006) 4153.

[109] W. Demtröder, Experimentalphysik 3: Atome, Moleküle und Festkörper, Springer, Berlin, 1996.

[110] R. McCreery, Raman Spectroscopy for Chemical Analysis, vol. 157 of Chemical Analysis, Jonh Wiley Inc., New York, 2000.

[111] W. B. White, in: Encyclopedia of Materials Characterization: Surfaces, Interfaces, Thin Film, (C.R. Brundle, C.A. Evans, Jr., S. Wilson, eds.), Butterworth-Heinemann, Boston, 1992, pp. 428.

[112] R.J. Capwell, F. Spagnolo, M.A. DeSesa, Appl. Spectrosc. 26 (1972) 537.

[113] J.C. Parker, R.W. Siegel, Appl. Phys. Lett. 57 (1990) 943.

[114] D.J. O'Connor, B.A. Sexton; R.St.C. Smart, Surface Analysis Methods in Materials Science, Springer, Berlin, 2003.

[115] L. Giannuzzi, F. Stevie, Micron 30 (1999) 197.

[116] J. Mayer, L. Giannuzzi, T. Kamino, J. Michael, MRS Bulletin 32 (2007) 400.

[117] B. Fultz a, J. Howe, Transmission Electron Microscopy and Difractometry of Materials, Springer, (2nd ed), Berlin, 2002.

[118] A. Glaser , S. Surnev, F.P. Netzer, N. Fateh, G.A. Fontalvo, C. Mitterer, Surf. Sci. 601 (2007) 1153.

9. Publications

9.1. List of included publications

I. Influence of high-temperature oxide formation on the tribological behaviour of TiN and VN coatings,
N. Fateh, G. A. Fontalvo, G. Gassner, C. Mitterer
Wear 262 (2007) 1152-1158.

II. The beneficial effect of high-temperature oxidation on the tribological behaviour of V and VN coatings,
N. Fateh, G. A. Fontalvo, G. Gassner, C. Mitterer
Tribology Letter 28 (2007) 1-7.

III. Synthesis-structure relations for reactive magnetron sputtered V_2O_5 films,
N. Fateh, G.A. Fontalvo, L. Cha, T. Klünsner, G. Hlawacek, C. Teichert, C. Mitterer
Surface & Coatingd Technology 202 (2008) 1551-1555.

IV. Structural and mechanical properties of dc and pulsed dc reactive magnetron sputtered V_2O_5 films,
N. Fateh, G. A. Fontalvo, C. Mitterer
Journal of Physics D: Applied Physics 40 (2007) 7716-7719.

V. Tribological properties of reactive magnetron sputtered V_2O_5 and VN-V_2O_5 coatings,
N. Fateh, G. A. Fontalvo, C. Mitterer
Submitted for Publication

9.2. Publications related to this work

VI. Oxidation of vanadium nitride and titanium nitride coatings,
A. Glaser, S. Surnev, F.P. Netzer, N. Fateh, G.A. Fontalvo and C. Mitterer
Surface Science 601(2007) 1153-1159.

9.3. My contribution to the included publications

	Conception and planning*	Experiments	Analysis and interpretation	Manuscript preparation*
Publication I	100	90	90	90
Publication II	100	90	90	90
Publication III	100	60	90	100
Publication IV	100	100	100	100
Publication V	100	100	100	100

* Supervision is not included

Publication I

Influence of high-temperature oxide formation on the tribological behaviour of TiN and VN coatings

N. Fateh, G. A. Fontalvo, G. Gassner, C. Mitterer

Wear 262 (2007) 1152-1158

Influence of high-temperature oxide formation on the tribological behaviour of TiN and VN coatings

N. Fateh, G. A. Fontalvo, G. Gassner, C. Mitterer

Department of Physical Metallurgy and Materials Testing, University of Leoben, Franz-Josef-Strasse 18, A-8700 Leoben, Austria

Abstract

The formation of thin reaction films in sliding contacts has provided the basis for the recent development of adaptive, self-lubricating coatings with optimum tribological properties. The aim of this study was to characterize TiN and VN coatings deposited by reactive unbalanced magnetron sputtering with respect to their oxidation behaviour at elevated temperatures and to correlate the formed oxides to the tribological properties. Dry sliding experiments were performed in the temperature range between 25°C and 700°C. Oxide phases were identified by X-ray diffraction and Raman spectroscopy after tribometer testing. In the case of TiN coatings, only minor changes in the friction coefficient were detectable in the investigated temperature range. The onset of oxidation of TiN coatings, as evidenced by DSC and TGA, occurred at 600°C-700°C and yields the formation of rutile. In the case of VN coatings, oxidation starts at about 500°C with the formation of Magnéli phases of vanadium oxides, which were identified by XRD as V_2O_5, VO_2 and V_6O_{13}. In addition, it was found that the friction coefficient decreases continuously at temperatures above 400°C, reaching a value of 0.25 at 700°C due to the formation and melting of V_2O_5 which leads to liquid lubrication.

Keywords: TiN; VN; friction; Magnéli oxides

1. Introduction

Over the last few years, several new solid lubricants and modern lubrication concepts have been developed to achieve low friction and wear and to increase tool performance and lifetime in various tribological applications like high-speed cutting and dry machining processes [1-3]. Nowadays, many new solid lubricating coatings such as diamond-like carbon

(DLC), MoS_2, WC/C, as well as nanocomposite and multilayered coatings are already used for practical applications in drilling, tapping and milling [4,5]. Recently, a low-friction effect for PACVD TiN coatings due to incorporation of chlorine in the TiN matrix has been reported [6]. However, the tribological effectiveness of these solid lubricants often begins to fail at elevated temperatures, in humid atmospheres or due to oxidation [6-8].

To meet the increasing requirements of modern machining applications, a new concept for lubrication was found by using oxide materials. As a matter of fact, oxide materials are interesting for high temperature lubrication because of their expected oxidation stability and low adhesion tendency. A variety of oxide phases called “Magnéli-phase oxides”, which represent oxygen deficient homologous series with planar faults, show easy crystallographic shear planes with reduced binding strength. These oxides are supposed to be ideal high-temperature solid lubricants if they are stable, or act as liquid self-lubricants due to the low melting points of the formed oxide phases [9,10].

Several investigations have been published in which the existence of lubricious oxides on the basis of Ti, Mo, V, Si and W as a result of tribo-oxidation was found [10-13]. The beneficial influence related to Magnéli phases formed by oxidation of VN on the tribological behaviour of TiAlN/VN superlattic coatings and VN coatings has already been reported [9,12,14-16]. The aim of this work was to characterize the respective oxides formed on the surface and in the wear track of TiN and VN coatings at elevated temperatures and to study their influence on the tribological behaviour.

2. Experimental

The coatings investigated in this work were deposited from Ti and V targets (ø 75×6 mm), respectively, with an unbalanced DC magnetron sputtering system and a reactive $Ar+N_2$ discharge. For all the coatings, the deposition process was carried out at a constant temperature of 400°C and a working gas pressure of 0.25 Pa. For the TiN coatings, the N_2 partial pressure was 30 % of the total pressure; for the VN coatings it was decreased to 24 %. The magnetron discharge current was adjusted to 1 A, the applied bias voltage was -50 V. The deposition rates were ~ 1.8 µm/h for TiN and ~ 4 µm/h for VN coatings. After target pre-cleaning and ion etching of the substrates, coatings with an average thickness of 3 µm were deposited. Prior to deposition, all substrates were grounded, polished and ultrasonically cleaned with acetone and ethanol. Low-alloyed steel foils (thickness 0.05 mm) and high-speed

steel discs (DIN 1.3343, AISI M2) with 30 mm diameter and 10 mm height, which were quenched and tempered to a hardness of 65 HRC, were used as substrates.

The tribological behaviour of the coatings on high-speed steel was studied at temperatures from room temperature (RT, ~ 25°C) up to 700°C using a CSM high-temperature ball-on-disc tribometer. Dry sliding tests were conducted in ambient air (relative humidity of 30 to 40 %) under a load of 5 N and a sliding speed of 0.1 m/s using alumina balls of 6 mm in diameter as counterparts. The radius of the wear track was set to 7 mm and the sliding distance to 100 m. The wear tracks on the coatings were investigated using a 3D profiling system (Wyko NT1000).

X-ray diffraction (XRD) analyses were conducted to determine the film structure and to identify possible oxide phases formed after tribometer testing by comparing to the JCPDS powder diffraction files [17]. The XRD patterns were recorded using a Siemens D 500 Bragg–Brentano diffractometer and Cu–Kα radiation. A scanning electron microscope (SEM, Cambridge Instruments Stereoscan 360) was used to investigate the wear tracks on the coatings and to characterize the oxides on the surface after tribometer testing at elevated temperatures. Identification of tribochemical reactions and the chemical structure of wear products generated during the dry sliding experiments was conducted by Raman spectroscopy using a Horiba Dilor Raman spectrometer with a laser wavelength of 532.2 nm (He-Ne-Laser, 100 mW).

Differential scanning calorimetric (DSC) and simultaneous thermo-gravimetric analysis (TGA) investigations were conducted in a Netzsch-STA 409 C thermal analyzer to characterize the thermal stability of the coatings with respect to their oxidation behaviour. To avoid the influence of the substrate material on the DSC investigation, the coatings were chemically removed from their low-alloyed steel substrates using a hydrochloric acid. The dynamical DSC/TGA experiments were carried out in artificial air (20% O_2, 80% N_2) between room temperature and 1000°C at a heating and cooling rate of 20 K/min. Prior to DSC measurements, temperature and energy were calibrated by use of five standards (tin, zinc, aluminium, silver and gold, each of 99.999 % purity) with an accuracy of ± 0.2 K and ± 0.007 mW, respectively.

3. Results and discussion

3.1. Tribological behaviour

Fig. 1 shows the average steady-state friction coefficient of TiN and VN coatings sliding against alumina balls in ambient air. For the dry sliding experiments, six different temperatures in the range between RT and 700°C were chosen. It can clearly be seen that TiN shows higher friction coefficients over the whole temperature range compared to VN. The friction coefficient of the TiN coatings increases from about 0.5 at RT to values between 0.6 and 0.7 at higher temperatures. Also in the case of VN, the values increase for temperatures up to 400°C. Above 400°C, the friction coefficient decreases continuously with increasing temperature reaching a value of 0.25 at 700°C. This low-friction effect agrees with earlier studies on TiAlN/VN superlattices, Ti-Al-V-N and Cr-Al-V-N coatings [18-20].

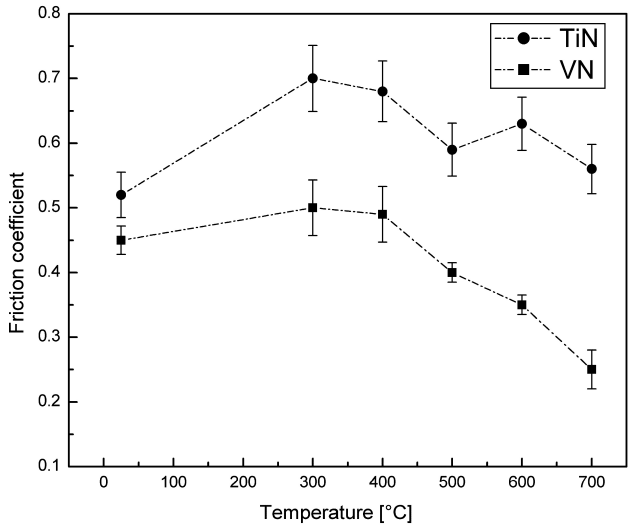

Fig. 1. Temperature dependence of the friction coefficient for TiN and VN coatings.

Investigation of the wear tracks after tribometer testing by 2D/3D profilometry showed differences in the wear behaviour of TiN and VN coatings with increasing temperature. 2D surface profiles of the wear tracks after testing at RT, 400 and 600°C are shown in Fig. 2 and 3D profiles after testing at 600°C in Fig. 3. In the case of TiN coatings, wear and consequently the amount of produced wear debris increases continuously with raising temperature until at 700°C the coating is completely worn through. In Fig. 3(a) some

transferred material is visible at both sides of the wear track and wear plough tracks in the direction of sliding. On the contrary, VN coatings show no visible wear after testing at RT. However, at 300°C the wear behaviour is similar to TiN. With increasing temperature, higher amounts of transferred material appear in the wear tracks indicating the formation of a third body during the tests, as Fig. 3(b) clearly shows.

The increase in the friction coefficient at elevated temperatures might be related to the production of coating wear debris with diameters larger than the peak to peak roughness values of both surfaces, slider and coating, which interact with both surfaces by scratching or getting crushed in the contact [21]. In the case of TiN, the slight decrease in the friction coefficient at temperatures above 400°C (which is above the deposition temperature used in this work) might be connected to the softening of the coating due to annihilation of growth-related defects [31] and thus, to a reduction of the adhesive and ploughing components of the friction force.

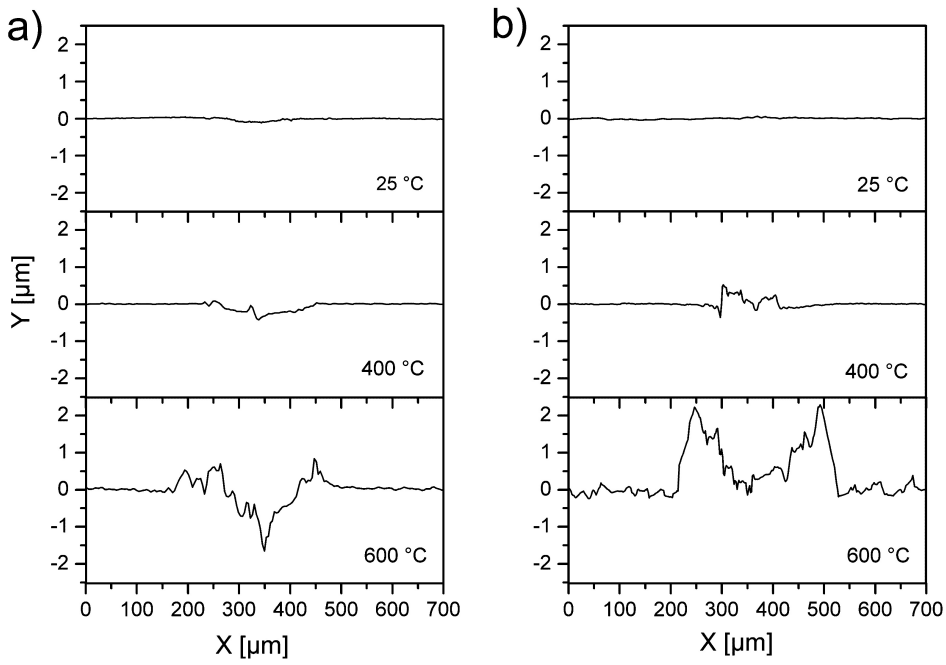

Fig. 2. Two-dimensional profiles of the wear tracks of: (a) TiN and (b) VN coatings after ball-on-disc tests against alumina at 25°C, 400°C and 600°C.

The formed wear debris acts as an abrasive leading to further material removal from the coating. This is the case for VN and TiN, whereas particularly softening leads to higher wear with increasing temperature. For carbon steels, it has been shown that mechanically stable

oxide scales may act as protective layers, and even if they are partially removed they can still protect the surface if wear particles are transferred back to the wear track forming load-bearing compact layers [22,23]. TiN oxidizes mainly at temperatures above 600°C (see below), and although Fig. 2 indicates that wear particles are partially back-transferred to the wear track at 600°C, whether the surface oxide layer nor back-transferred material can protect the surface effectively against wear. The tribological behaviour of VN differs from that of TiN at temperatures above 400°C. As surface investigations showed (see below), an oxide layer which consists mainly of the Magnéli phase V_2O_5 forms on the VN surface during the heating step. This oxide shows low shear strength due to its crystallographic structure leading to lower friction coefficients [10]. During the test, the oxide layer is partially removed and wear debris is formed which acts as a third body. Wear debris particles are partially back-transferred to the wear track and additional tribo-chemical reactions take place, leading to the formation of other oxides than those formed during the heating step (see below). The oxides formed during heating and the oxide glazes formed in the wear track during testing protect the coating from wear, in the same way as previously described for steels.

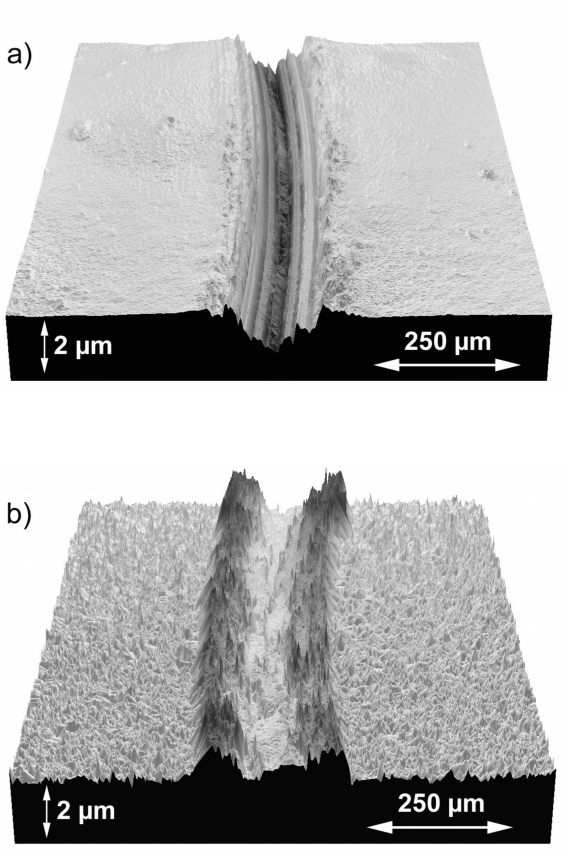

Fig. 3. Three-dimensional profiles of the wear tracks of: (a) TiN and (b) VN coatings after ball-on-disc tests against alumina at 600°C.

3.2. Surface investigations

Fig. 4 shows XRD patterns of TiN and VN coatings after the ball-on-disc tests. The total temperature exposure time during tribological tests in air at different test temperatures was about 2 h. The XRD patterns of the TiN coatings (see Fig. 4(a)) reveal an fcc TiN structure, where all peaks are shifted to lower diffraction angles than the standard value of TiN. A possible reason can be the influence of deposition parameters and the resulting residual compressive stresses, as proposed by Constable et al. [24]. The patterns of TiN coatings show no evidence of significant changes in structure with increasing test temperatures up to 600°C. After a tribotest at 700°C, a few new peaks were detected which could be identified as TiO_2 (rutile). It should be noted that in this case obviously the formed rutile on the TiN coating does not have any significant beneficial tribological influence (see Fig. 4(a)).

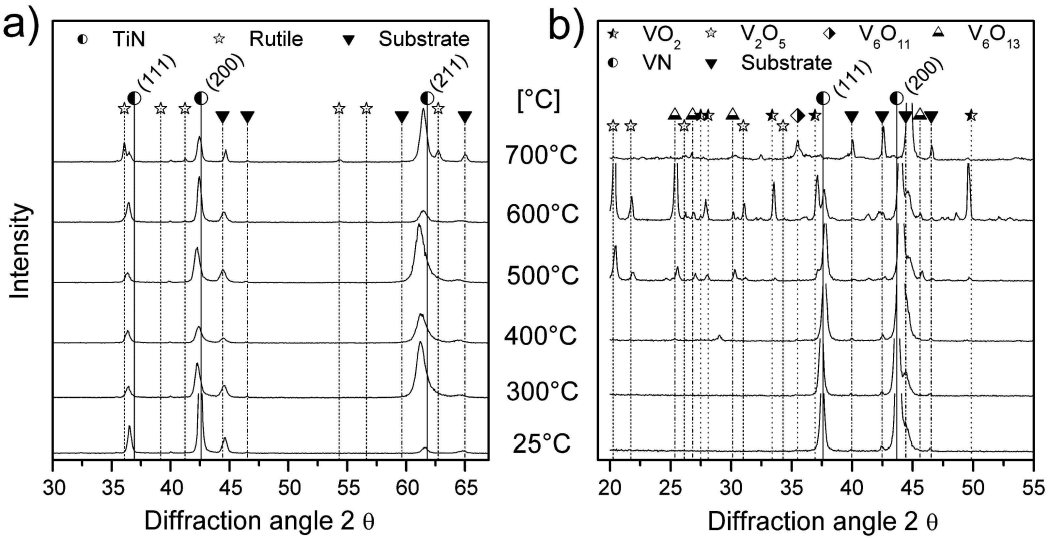

Fig. 4. XRD patterns of: (a) TiN and (b) VN coatings after high-temperature tribometer testing up to 700°C.

The XRD investigations show that the VN coatings (see Fig. 4(b)) exhibit an fcc VN structure, which is stable up to 400°C. After ball-on-disc testing at 500°C, the XRD patterns indicate generation of various vanadium oxides on the coating surface which can be assigned to the lubricious Magnéli oxide series V_nO_{2n-1} and V_nO_{3n-1} with n = 1,2,3, etc. Most oxide peaks were identified as V_2O_5 and VO_2. There are also some minor peaks corresponding to V_6O_{13}. These results agree widely with the published data in refs. [19,25]. When the temperature increases up to 600°C, the VO_2 and V_6O_{13} peaks become more pronounced. This is related to oxide reduction following the sequence $V_2O_5 \rightarrow V_3O_7 \rightarrow V_4O_9 \rightarrow V_6O_{13} \rightarrow VO_2$, as reported in [26,27]. As the test temperature rises to 700°C, the VN coating peaks disappear

and the intensity of the substrate peaks increases indicating that the coating is almost completely oxidized and partially removed in the wear track. Increasing the temperature leads to the reduction of V_2O_5 as stated before. Thus, no V_2O_5 peaks, but lower oxidized vanadium like V_6O_{11} and V_6O_{13} was found. Further, it is known that bulk V_2O_5 melts at approximately 685°C and reaches its boiling point at 1750°C [26]. As no evidence of crystalline V_2O_5 was found after testing at 700°C, the drop of the friction coefficient could be attributed to the melting of V_2O_5 which yields liquid lubrication. For further investigation of the oxidation behaviour, the surface morphology of the coatings was analysed by SEM after the tribological tests. Fig. 4 shows a SEM image of the surface of a VN coating after testing at 700°C. The whole coating exhibits a uniformly oxidized surface with a needle-like morphology which indicates the solidification of a liquid phase. This might be the reason for the vanishing fcc coating peaks observed in the XRD investigations (see Fig. 4). It is also assumed that most of the liquid oxide phase is moved away from the disc surface due to centrifugal forces during ball-on-disc testing, where consequently the needle-like structures seen in Fig. 5 result from crystallization of a very thin vanadium oxide layer wetting the steel surface, thus explaining the low intensity of the oxide peaks seen in Fig. 4(b).

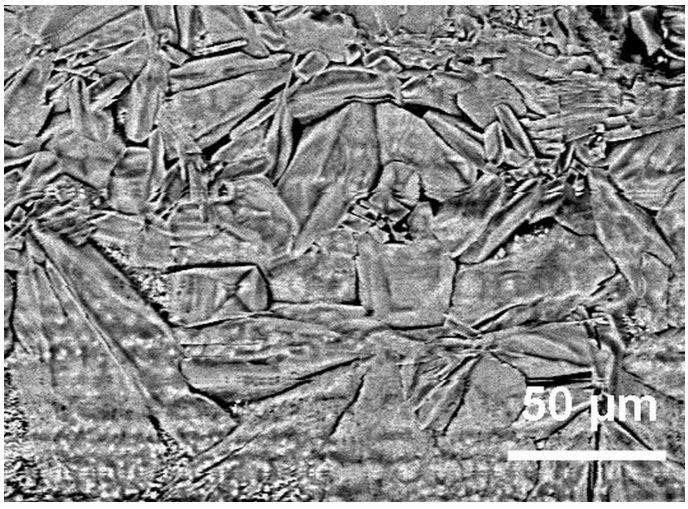

Fig. 5. SEM micrograph of the oxidized VN coating after ball-on-disc testing at 700°C.

Different areas of the wear tracks were investigated using Raman spectroscopy. Fig. 6 shows Raman scattering spectra of TiN and VN coatings after tribometer testing at different temperatures. To illustrate the possible changes, the Raman spectra of the unaffected TiN and VN coating surface were taken as a reference after testing at RT (see Fig. 6 for TiN and VN).

At temperatures below 400°C, there were no significant changes visible, neither on the coating surfaces nor in the wear tracks of the TiN coatings. However, the spectrum of the wear track after ball-on-disc testing at 400°C shows two broad peaks at approximately 443 and 610 cm^{-1}. This spectrum is in good agreement with the published Raman data of rutile TiO_2 in Fig. 6(a) [28,29]. Increasing the temperature to 700°C leads also to the formation of rutile, however, not only in the wear track but also on the TiN surface. This result agrees well with the XRD results obtained for the coating surface at the same temperature (see Fig. 4(a)). In different areas of the wear track generated on the TiN coating at 700°C, peaks of oxidized substrate material (Fe_2O_3 and Fe_3O_4) were found which indicates the already mentioned coating failure during the tribometer test.

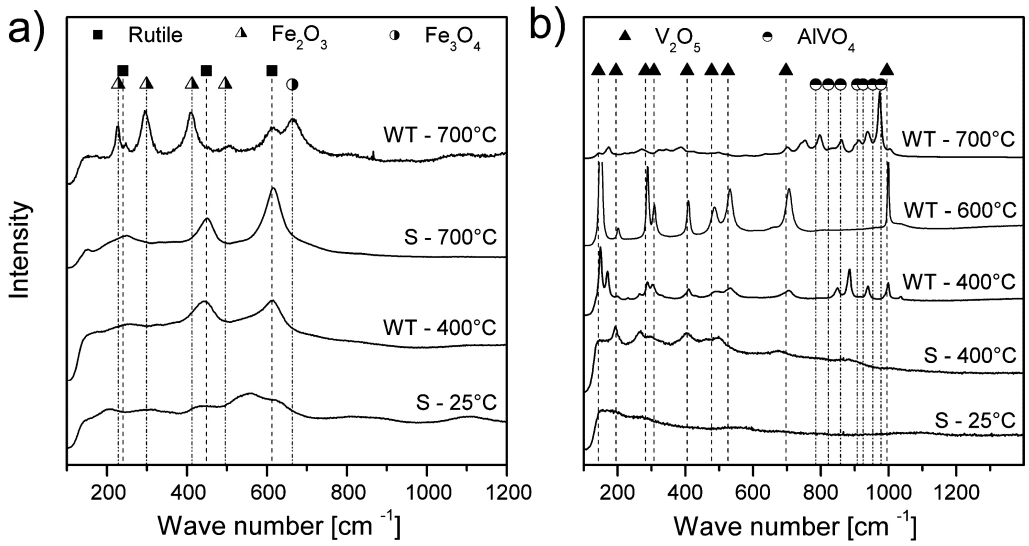

Fig. 6. Raman spectra of: (a) TiN and (b) VN coatings after high temperature tribometer testing. S: surface and WT: wear track.

Raman investigations of VN coatings show no evident changes after tribo-testing up to 400°C (see Fig. 6(b)). The spectrum obtained for 400°C shows some minor peaks for the coating surface indicating the presence of V_2O_5. In the wear track produced at 400°C, a high amount of V_2O_5 and a new phase corresponding to $AlVO_4$ could be detected (see the range between 800 and 1000 cm^{-1} in Fig. 6(b)). The $AlVO_4$ phase forms from a reaction between V_2O_5 and Al_2O_3 [30]. The generation of $AlVO_4$ is assumed to be an interaction between the formed V_2O_5 and the alumina counterpart during the tribological test. At 600°C, the spectrum shows sharp peaks which fit well to the V_2O_5 standard peaks (see Fig. 6(b)). A further increase in test temperature to 700°C leads to a reduction of the amount of V_2O_5. The

spectrum of the wear track indicates a predominant $AlVO_4$ phase indicating that any V_2O_5 formed in the wear track has reacted with the alumina ball during the test.

3.3. DSC investigations

Fig. 7 shows the results of dynamic DSC/TGA measurements of TiN coating material in artificial air. Compared to measurements in inert argon atmosphere where no distinct observations in the DSC/TGA signals were made [31], several ongoing reactions can be detected during measurements in air (see Fig. 7(a)). Both the DSC and TGA signals indicate ongoing oxidation starting at ~ 300°C, leading to a pronounced increase in sample mass for temperatures higher than 600°C. Our previous investigations on TiN coatings in the same DSC/TGA system [32] confirmed the commonly observed onset of oxidation of ~ 600°C [1]. The minor reactions taking place at lower temperatures are thus related to the large surface of the powder used for DSC/TGA analysis and are, consequently, not relevant for the oxidation of TiN coatings. After the complete thermal cycle, the sample mass has increased from 25.60 mg to 32.41 mg (~ 130%). Nevertheless, no material evaporation was indicated by DSC/TGA. The oxidation reaction is completed during sample heating, since no further reactions and no additional mass gain can be observed by TGA during cooling. Additionally, even a second heating/cooling cycle of the pre-oxidized material shows no further reactions of the coating material (see Fig. 7(b)).

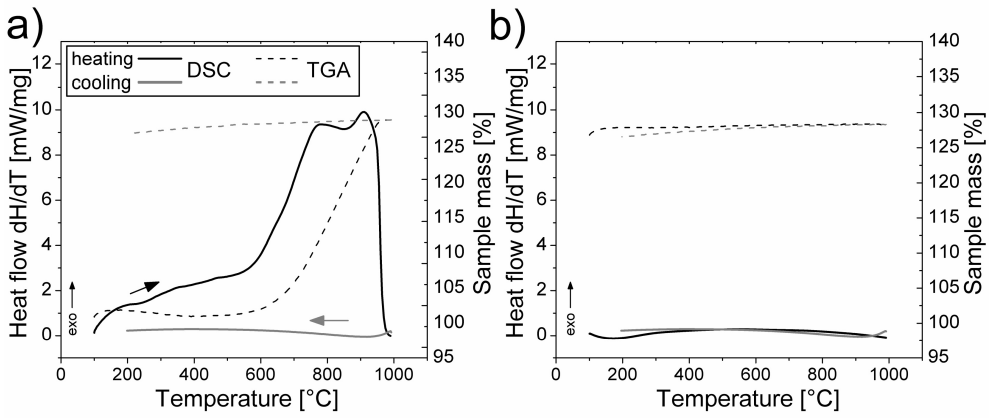

Fig. 7. (a) DSC/TGA heating/cooling cycle of TiN to 1000°C in artificial air atmosphere at 20K/min and (b) rerun measurement of pre-oxidized coating material.

Similar to the observations for TiN, DSC/TGA measurements of VN coating material in argon atmosphere show no distinct ongoing reactions [25]. DSC/TGA measurements in air,

however, indicate massive oxidation of VN starting at ~ 500°C and leading to a gain in sample mass at a temperature above 400°C (see Fig. 8(a)). Herein, several peaks at ~ 500, 650 and 800°C signify the oxidation processes. At ~ 910°C, the superposed endothermal melting of the partially oxidized VN material takes place. The molten phase solidifies again at ~620°C during cooling, indicated by a pronounced exothermal peak. Nevertheless, also in the molten state, the oxidation processes continue since the sample mass steadily increases up to ~ 130% where the temperature becomes too low during cooling, (see the TGA signal in Fig. 8(a)), indicating their uncompleted state. A rerun measurement of the already pre-oxidized coating material clearly displays melting of the material during heating at ~ 670°C (see the endothermal peak in Fig. 8(b)). Oxidation of the material continues at higher temperatures, where the gain in sample mass can be observed in the TGA signal increasing from 48.67 mg (100%) to 66.86 mg (~ 135%). During this second heating/cooling cycle, the oxidation processes seem to be completed, as no additional mass gain during subsequent cooling is indicated. The advanced coating material oxidation leads to a pronounced shift of the exothermal peak signifying solidification to a temperature, which is ~ 90°C lower compared to the first heating/cooling cycle.

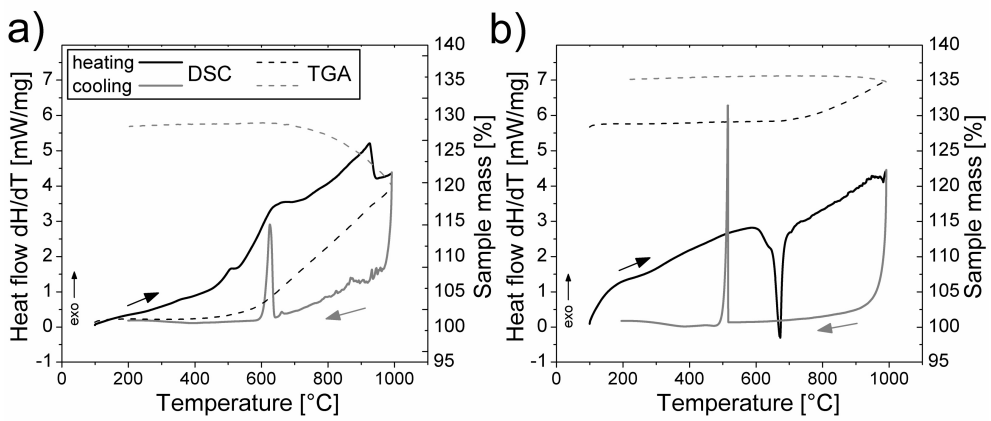

Fig. 8. (a) DSC/TGA heating/cooling cycle of VN to 1000°C in artificial air atmosphere at 20K/min and (b) rerun measurement of pre-oxidized coating material.

4. Conclusions

The aim of this work was to study the oxidation behaviour of sputtered TiN and VN coatings at elevated temperatures and its influence on the tribological properties. TiN coatings showed only minor changes in friction coefficient over the whole temperature range, while wear increased with raising temperature. At 700°C an evident formation of rutile TiO_2 on the

coating surface could be observed. According to Raman measurements, the onset of oxidation and the appearance of rutile in the wear track occur at temperatures above 300°C. However, this oxide offers no efficient lubrication or wear protection. On the contrary, for VN coatings, a continuous decrease in friction coefficient at temperatures above 400°C was found. Pronounced coating oxidation at temperatures above 400°C in air atmosphere was proven by DSC/TGA measurements. After testing at 500°C, Magnéli oxide phases on the sample surface were identified by XRD, with V_2O_5 and VO_2 representing the dominating phases. The lowest friction coefficient of 0.27 was found after tribometer testing at 700°C. According to the XRD and SEM results, the entire coating was fully oxidized forming a liquid lubricant. Further, a high amount of $AlVO_4$ formed due to an interaction of vanadium oxides with alumina could be detected in the wear track by Raman spectroscopy. Finally, it can be concluded, that VN coatings, compared to TiN coatings, offer self-lubricious abilities at elevated temperatures achieving low friction coefficients during high-temperature dry-sliding against alumina.

Acknowledgements

This work was supported by the Austrian NANO Initiative via a grant from the Austrian Science Fund FWF within the project “LowFrictionCoatings”.

References

[1] W.-D. Münz, J. Vac. Sci. Technol. A 4 (6) (1986) 2717-2725.

[2] S. PalDey, S.C. Deevi, Mat. Sci. Engin. A 342 (2003) 58-79.

[3] R. Gilmore, M.A. Baker, P.N. Gibson, W. Gissler, M. Stoiber, P. Losbichler, C. Mitterer, Surf. Coat. Technol. 108-109 (1998) 345-351.

[4] J.M. Carrapichano, J.R. Gomes, R.F. Silva, Wear 253 (2002) 1070-1076.

[5] B. Navinsek, P. Panjan, M. Cekada, D.T. Quinto, Surf. Coat. Technol. 154 (2002) 194-203.

[6] M. Stoiber, E. Badisch, C. Lugmair, C. Mitterer, Surf. Coat. Technol. 163-164 (2003) 451-456.

[7] A. Erdemir, M. Halter, G.R. Fenske, Wear 205 (1997) 236-239.

[8] E. Badisch, G.A. Fontalvo, M. Stoiber, C. Mitterer, Surf. Coat. Technol. 163-164 (2003) 585-590.

[9] A. Magnéli, Acta Crystallogr. 6 (1953) 495-500.

[10] E. Lugscheider, O. Knotek, K. Bobzin, S. Bärwulf, Surf. Coat. Technol. 133-134 (2000) 362-368.

[11] M.N. Gardos, Tribol. Trans. 22 (2) (1990) 209-220.

[12] M. Woydt, A. Skopp, I. Dörfel, K. Witke, Wear 218 (1998) 84-95.

[13] A. Skopp, M. Woydt, Tribol. Trans. 38 (2) (1995) 233-242.

[14] C.P. Constable, J. Yarwood, P.Eh. Hovsepian, L.A. Donohue, D.B. Lewis, W.-D. Münz, J. Vac. Sci. Technol. A 18 (4) (2000) 1681-1689.

[15] H. Meidia, A.G. Cullis, C. Schönjahn, W.-D. Münz, J.M. Rodenburg, Surf. Coat. Technol. 151–152 (2002) 209-213.

[16] W.-D. Münz, D.B. Lewis, P.Eh. Hovsepian, C. Schönjahn, A. Ehiasarian, I.J. Smith, Surf. Eng. 17 (1) (2001) 15-27.

[17] PCPDFWIN v. 2.2, JCPDS-International Centre for Diffraction Data, Swarthmore, PA, 2001.

[18] P.H. Mayrhofer, P.E. Hovsepian, C. Mitterer, W.-D. Münz, Surf. Coat. Technol. 177-178 (2004) 341-347.

[19] K. Kutschej, P.H. Mayrhofer, M. Kathrein, P. Polcik, C. Mitterer, Surf. Coat. Technol. 188-189 (2004) 358-363.

[20] R. Franz, J. Neidhardt, B. Sartory, R. Kaindl, R Tessadri, P. Polcik, V.-H. Derflinger, C. Mitterer, Tribol. Lett. 23 (2) (2006) 101-107.

[21] K. Holmberg, A. Matthews, Coatings Tribology, Elsevier, Amsterdam, 1994, p. 105.

[22] G. A. Fontalvo, C. Mitterer, Wear 258 (2005) 1491-1499.

[23] F.H.Stott, Tribology International 31 (1998) 61-71.

[24] C.P. Constable, D.B. Lewis, J. Yarwood, W.-D. Münz, Surf. Coat. Technol. 184 (2004) 291-297.

[25] G. Gassner, P.H. Mayrhofer, K. Kutschej, C. Mitterer, M. Kathrein, Tribol. Lett. 17/4 (2004) 751-756.

[26] N.N. Greenwood, A. Earnshaw, Chemistry of the Elements, 2nd ed., Butterworth-Heinemann, Oxford, 1997.

[27] Y. Ningyi, L. Jinhua, L. Chenglu, Appl. Surf. Sci. 191 (2002) 176-180.

[28] W.H. Weber, R. Merlin, Raman Scattering in Materials Science, Springer, Berlin, 2000.

[29] M. Franck, J.-P. Celis, J.R. Roos, J. Mater. Res. 10 (1) (1995) 119-125.

[30] D.B. Lewis, S. Creasey, Z. Zhou, J.J. Forsyth, A.P. Ehiasarian, P.Eh. Hovsepian, Q. Luo, W.M. Rainforth, W.-D. Münz, Surf. Coat. Technol. 177–178 (2004) 252-259.

[31] P.H. Mayrhofer, A. Hörling, L. Karlsson, J. Sjölén, T. Larsson, C. Mitterer, L. Hultman, Appl. Phys. Lett. 83 (2003) 2094-2051.

[32] C. Mitterer, F. Holler, F. Üstel, D. Heim, Surf. Coat. Technol. 125 (2000) 233-239.

Publication II

The beneficial effect of high-temperature oxidation on the tribological behaviour of V and VN coatings

N. Fateh, G. A. Fontalvo, G. Gassner, C. Mitterer

Tribology Letters 28 (2007) 1-7

The beneficial effect of high-temperature oxidation on the tribological behaviour of V and VN coatings

N. Fateh, G. A. Fontalvo, G. Gassner, C. Mitterer

Department of Physical Metallurgy and Materials Testing, University of Leoben, Franz-Josef-Strasse 18, A-8700 Leoben, Austria

Abstract

The mechanisms for frictional self-adaptation of advanced hard coatings with optimum tribological properties are based on the formation of thin reaction films in sliding contacts. The aim of this work was to characterize VN and V coatings deposited by unbalanced magnetron sputtering and to determine the influence of oxide phase formation on their friction and wear properties during high-temperature exposure in ambient air. Dry sliding experiments were performed in the temperature range between 25°C and 700°C. Structural changes and oxide phases were identified by X-ray diffraction and Raman spectroscopy after tribometer testing. The friction coefficient of the V coatings decreases from about 1.05 at RT to 0.27 at 700°C, while the VN coating has a lower coefficient of friction (~ 0.45) at RT which further decreases at temperatures above 400°C. The onset of rapid oxidation of V and VN coatings, as evidenced by differential scanning calorimetry (DSC) and thermo-gravimetric analysis (TGA), occurred at 400-450°C with the formation of vanadium oxides, which were identified by XRD as V_2O_5, VO_2 and V_6O_{13}. For both coatings evaluated, a significant decrease of the friction coefficient at temperatures above 400°C was observed reaching a value of 0.25-0.27 at 700°C, due to the formation of V_2O_5, giving rise to solid lubrication, and subsequent melting of this phase at temperatures above 600°C, leading to liquid lubrication.

Keywords: V; VN; friction; lubricious oxides

1. Introduction

Over the last few years, several research activities have focused on development of new solid lubricants and modern lubrication concepts to achieve low friction and wear and to

extend the lifetime of tools and engineering components [1-3]. Especially the oxide materials have become interesting for tribological applications due to their expected oxidation stability, low adhesion tendency and their low tribo-oxidation sensitivity [4,5]. A recently introduced new concept for low friction coatings in intermediate to high-temperature applications is the formation of lubricious surface oxides, the so-called Magnéli phases. These are supposed to be ideal high-temperature solid lubricants due to their easy crystallographic shear planes and they also act as liquid self-lubricious films due to their often low melting points. Possible metals forming Magnéli phase oxides are W, Mo, Ti, and V [6-12].

The beneficial influence of molten oxide phases on friction has already been reported in the case of V alloyed solid solution as well as superlattice coatings [13-15]. The lubricating effect of vanadium oxides has recently been demonstrated in high-temperature tribological testing of VN coatings [16,17]. The purpose of the present study was to characterize VN and V coatings prepared by unbalanced magnetron sputtering and to verify the expected lubricious oxide concept. Main emphasis was laid on a potential formation of lubricious oxides, in particular on the comparison of oxide formation on soft metallic V and on hard VN coating.

2. Experimental

The coatings investigated in this work were deposited from a V target (⌀ 75×6 mm), with an unbalanced DC magnetron sputtering system. For both coatings, the deposition process was carried out at a constant temperature of 450°C and a working gas pressure of 0.25 Pa. The applied substrate bias voltage was -50 V. The average thickness of VN and V coatings was 3.2 and 5.6 µm, respectively. The coatings were grown on ground and polished high-speed steel discs (DIN 1.3343, AISI M2), which were quenched and tempered to a hardness of 65 HRC, and on iron foils (thickness 0.05 mm).

Dry sliding ball-on-disc experiments were conducted using coated high-speed steel discs at temperatures from room temperature (RT, ~ 25°C) up to 700°C in ambient air using alumina balls of 6 mm diameter as counterpart. For both coating systems, the sliding speed was kept constant at 0.1 m/s and the wear track radius at 7 mm. For the VN coatings, the sliding distance was 100 m and the load 5 N. In the case of pure V coatings, the sliding distance was reduced to 10 m and the load to 1 N in order to avoid failure of the coating. After the tribometer tests, the wear tracks on the coatings were characterized using an optical 3D white light profiling system (Wyko NT 1000).

X-ray diffraction (XRD) analysis was conducted to investigate the phase composition and identify possible oxide phases formed after tribometer testing using a Siemens D 500 Bragg-Brentano diffractometer and Cu–Kα radiation. Raman spectroscopy was conducted to observe structural changes and identify tribochemical reactions generated during the sliding experiments using a Horiba Dilor Raman spectrometer with a laser wave length of 532.2 nm (He-Ne-Laser, 100 mW). Scanning electron microscopy (SEM, Zeiss EVO 50) and energy-dispersive electron probe microanalysis (EDX, Oxford instrument Inca) were also used to characterize film microstructure and to investigate the wear tracks on the coatings.

Differential scanning calorimetry (DSC) and simultaneous thermo-gravimetric analysis (TGA) investigations were conducted in a Netzsch-STA 409 C thermal analyzer to characterize the thermal stability of the coatings with respect to their oxidation behaviour. The dynamical DSC/TGA experiments were carried out in artificial air (20 % O_2, 80 % N_2) between room temperature and 1000°C at a heating and cooling rate of 20 K/min. Prior to DSC measurements, temperature and energy were calibrated by use of five standards (Sn, Zn, Al, Ag, and Au, each of 99.999 % purity) with an accuracy of ± 0.2 K and ± 0.007 mW, respectively. To avoid the influence of the substrate material on the DSC investigation, the coatings were chemically removed from their iron foil substrates using a 10 % hydrochloric acid.

3. Results and discussion

3.1. Tribological behaviour

The average steady-state friction coefficient of V and VN coatings sliding against alumina balls in ambient air at different temperatures is shown in Fig. 1. Sliding tests show pure V coatings to have a much higher friction coefficient up to 500°C compared to VN coatings. At room temperature, a friction coefficient of ~ 1.05 was obtained for the V coating, while VN shows a significantly lower value (~ 0.45). At 500°C, both coatings show almost the same friction coefficient of ~ 0.4-0.5, which decreases continuously for a further increase of the testing temperature, reaching the lowest value of 0.24-0.27 at 700°C. This low friction effect agrees with earlier studies where V incorporation provided a lubrication mechanism due to oxide formation at moderate or/and high temperatures [13-16].

Two-dimensional surface profiles of the wear tracks after tribometer testing at RT, 300°C, 500°C, and 600°C are shown in Fig. 2 for VN and V coatings. It should be mentioned first

that the mean surface roughness of the samples (R_a), as measured by white light profilometry, increases with increasing test temperature. This indicates surface oxidation during the heating step. In the case of VN coatings, there is no visible wear after testing at RT, as Fig. 2a clearly shows. The increase in the friction coefficient from RT to 300°C might be related to the generation of loose wear debris of both slider and coating, which interact with both surfaces by scratching or getting crushed in the contact [18]. This is supported by the increasing wear track depth and material accumulation at the borders of the wear track (see Fig. 2a). At temperatures above 400°C, an oxide layer which consists mainly of V_2O_5 forms on the VN surface during the heating step, as already described in [17]. With increasing temperature, material accumulation increases as shown in Fig. 2a, indicating an increasing amount of oxidized and transferred material in the wear track acting as third body.

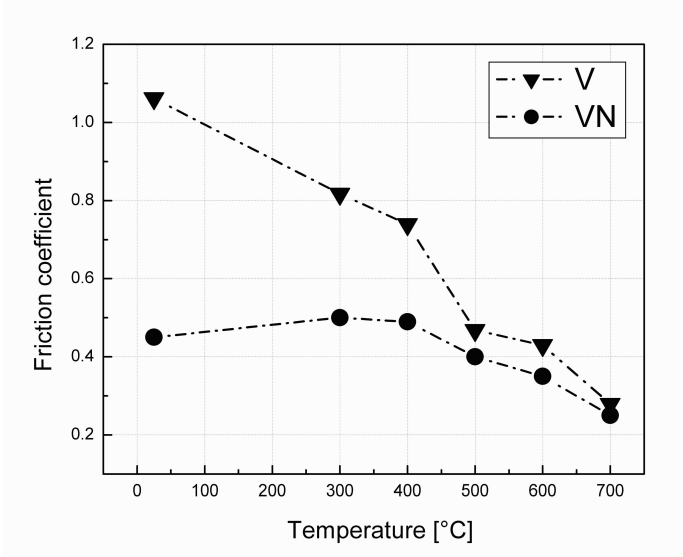

Fig. 1. Friction coefficient of the V and VN coatings from RT-700°C against alumina.

In the case of V coatings, the predominant wear mechanism for temperatures below 500°C is abrasion as evidenced by the deep grooves in Fig. 2b. Depth of the wear track and produced wear debris tend to decrease from RT to 400°C. At temperatures above 500°C, the wear mechanism changes and no significant material removal is visible in the wear track indicating massive oxidation and material transfer. Further increase in temperature results in a higher amount of oxidized and transferred material indicating the formation of a third body during the test, as Fig. 2b clearly shows. The SEM micrograph in Fig. 3 shows the wear scar of the V coating after tribometer testing at 600°C, where faceted features on the surface can be observed. EDX analyses showed that both surface and wear track of the coating were entirely

composed of V and O. The smeared appearance indicates the formation of a soft V-O phase during the test, while the dendritic nature [13,14] of a molten and subsequently solidified V_2O_5 phase is absent.

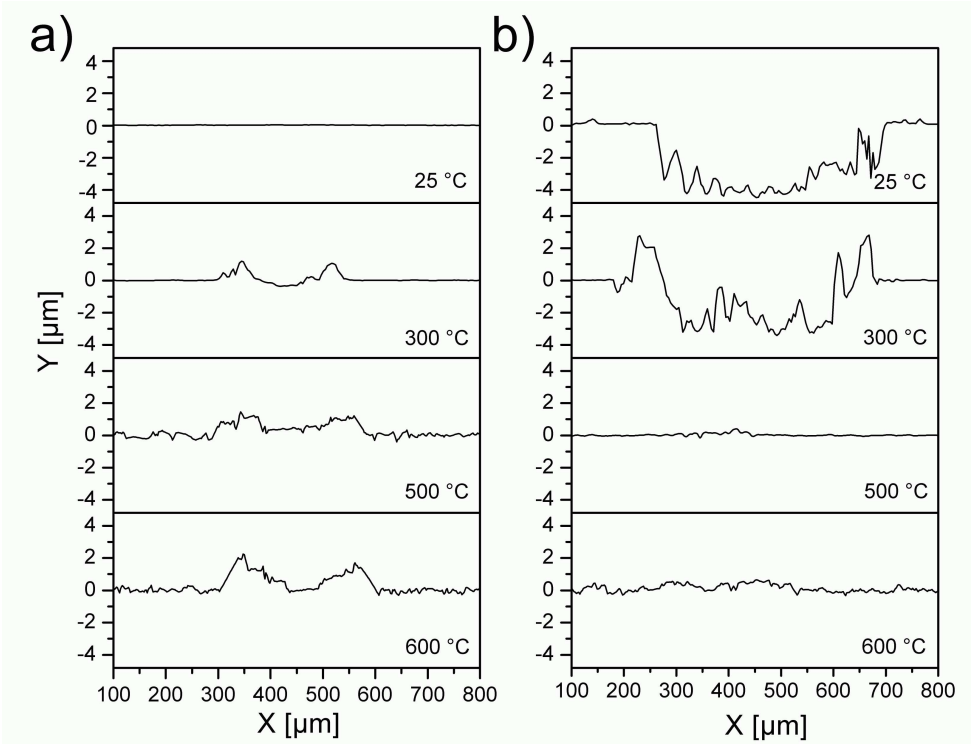

Fig. 2. 2D profiles of the wear tracks of a) VN and b) V coatings after ball-on-disc tests against alumina at 25, 300, 500 and 600°C.

From literature [19,20] it is known that both friction coefficient and wear are considered to be dependent on the nature, the thickness and the adherence of the oxide layer generated on the surface of a solid. For many metals, there is a transition temperature above which a continuous oxide layer is established which gives reduced resistance to sliding and good protection against wear. It is supposed that the oxide layers formed on the V coatings at temperatures below 500°C do not reach the sufficient thickness to act as a protective layer and prevent mechanical wear. However, if the oxide scale formed during heating and oxide glazes in the wear track allow easy shear due to their crystallographic structure, they should be the reason for the drop in the friction coefficient of V coatings with increasing temperature [21, 22]. The oxides formed at temperatures above 500°C are assumed to be mechanically stable and thus protect the coating against wear. In order to verify this suggestion, another test at 600°C with the same test condition was carried out. Only the sliding distance was increased

from 10 to 100 m. The friction coefficient observed in this case remains identical with an average value of 0.43 and the wear track looks similar to that in Fig. 3 with no evidence of material removal but a smeared oxide layer. This supports the assumption of a protective oxide layer.

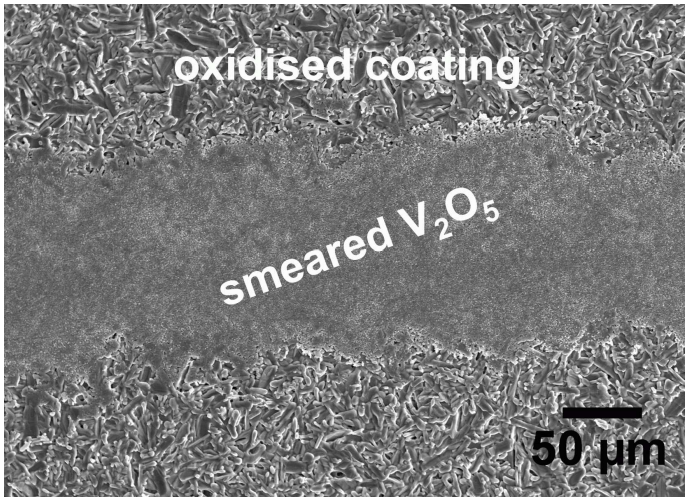

Fig. 3. SEM micrograph of the wear track of the V coating after dry sliding against alumina at 600°C and 100 m sliding distance.

3.2. Surface investigations

The XRD patterns of V and VN coatings in the as-deposited state and after ball-on-disc tests at different temperatures are shown in Fig. 4. Both coatings are stable up to a test temperature of 400°C; no significant oxidation could be observed. As the test temperature increases to 500°C, the XRD peaks indicate the generation of various oxides on the coatings surface which can be identified as V_2O_5, VO_2 and V_6O_{13}. In the case of V coatings annealed at temperatures above 500°C, the XRD peaks show a huge deviation from the standard value of V indicating the incorporation of oxygen in the V matrix. It seems that VO_2 and V_6O_{13} are the dominating phases formed on the oxidized V coating at 500°C, whereas V_2O_5 peaks predominate in the XRD patterns of the oxidized VN surface. Increasing the temperature to 600°C leads to massive oxidation of the coating surface. The fractions of V_2O_5 and V_6O_{13} increase in both cases. At 600°C, considerable oxidation of the V coating has taken place since only a very weak signal of the V peaks can be observed. As the test temperature rises to 700°C, the V and VN coating peaks disappear and the intensity of the substrate peaks increases in both cases. This suggests that at such a high temperature the V and VN coatings are completely oxidized and removed from the surface due to melting of the V_2O_5 phase. In

particular, V_2O_5 shows a melting point of 685°C and a boiling point of 1750°C [21,23]. Thus, the low friction coefficient of 0.24-0.27 measured at 700°C should be related to sliding over the molten V_2O_5 phase.

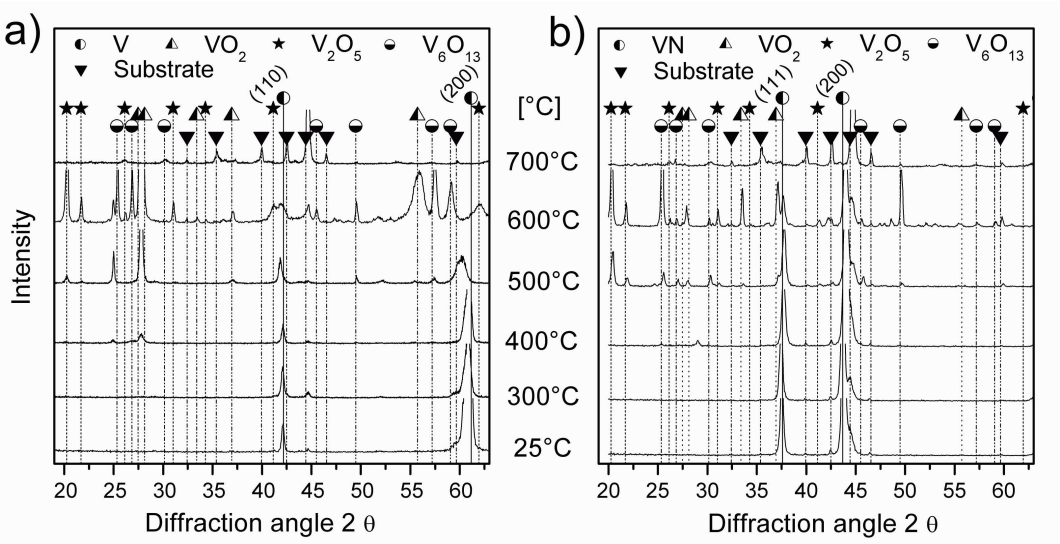

Fig. 4. XRD patterns of a) V and b) VN coatings after high-temperature tribometer testing against alumina up to 700°C.

For a further investigation of oxidation products, the surface of V and VN coatings, different areas of the wear track and wear debris have been analysed by Raman spectroscopy after testing at different temperatures (see Fig. 5). At room temperature, there are no significant peaks because of the weak intensity of the Raman active scattering mode of V and VN coatings. In the case of V coatings, different sharp peaks could be observed after ball-on-disc tests at 400°C. These peaks fit well to the VO_2, V_2O_3 and V_2O_5 standard peaks indicating the ongoing oxidation reactions during the tribological test at 400°C on the coating surface as well as in the wear track (see Fig. 5a). At 500°C, the observed V_2O_3 peaks on the coating surface and in different areas within the wear track become more pronounced while the intensity of VO_2 peaks decreases. In the case of VN coatings, the spectrum of the coating surface shows some small peaks indicating the generation of VO_2 and V_2O_5 at 400°C. Peaks corresponding to V_2O_3 could be detected only in the wear track of the VN coating after tribometer testing at 400°C. The spectrum of the surface and the wear track after testing at 500°C shows some distinct peaks indicating VO_2 and V_2O_3 phases besides V_2O_5. The results obtained by Raman spectroscopy suggest that the oxidation of VN coatings might take place at higher temperatures compared to pure V coatings. The change in the onset of oxidation can

be attributed to the more stable bonding configuration of V in the nitride compared to the metallic coating. The appearance of VO_2 and V_2O_3 peaks only in the wear track of VN coatings at 400°C can be the result of higher local flash temperatures in the contact area for the nitride coating [24]. With further increase in test temperature to 600°C, the spectra of both coatings show only sharp peaks corresponding to V_2O_5 which seems to be the most stable oxide in this temperature range (Fig. 5b). A further increase in test temperature to 700°C leads to a reduction of the amount of V_2O_5 for both coatings. In the case of VN coatings, there are several small peaks which could not be identified. As already mentioned, at 700°C the V and VN coatings are completely oxidised and due to the low melting point of V_2O_5 it is assumed that most of the liquid oxide phase is moved away from the surface during the test.

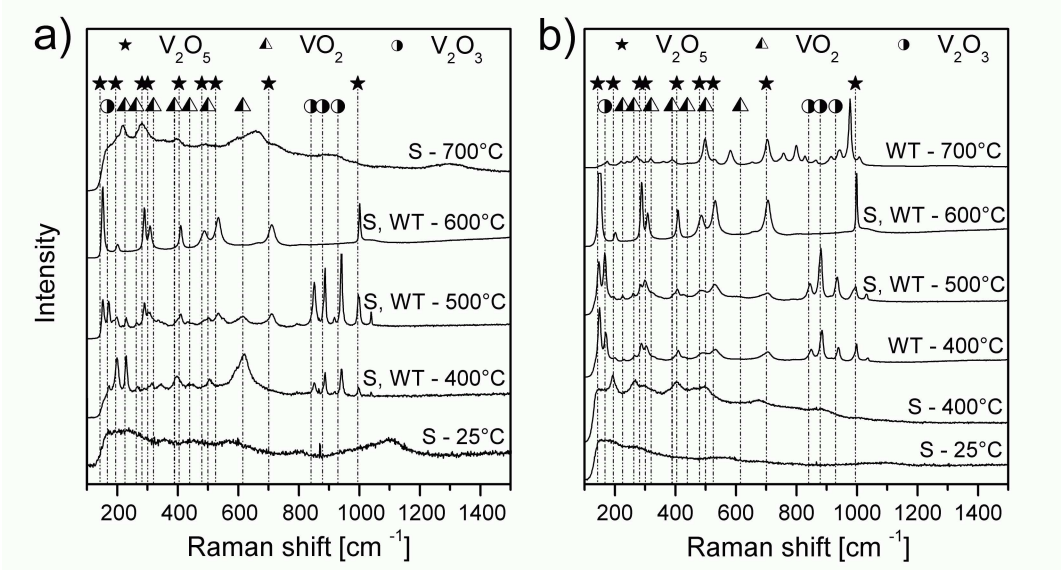

Fig. 5. Raman spectra of a) V and b) VN coatings after high temperature tribometer testing against alumina, S…surface and WT…wear track.

3.3. DSC/TGA investigations

It was shown that in the case of VN protective oxide glazes are already formed at temperatures above 400°C [17], whereas for V coatings higher oxidation temperatures are needed. For further investigation of the oxidation behaviour DSC and TGA analysis were conducted in artificial air for both V and VN coatings.

For V coating material, several ongoing reactions can be observed (cf. Fig. 6a). Both the DSC and TGA signals indicate oxidation reactions starting at ~ 400°C, leading to a pronounced increase in sample mass at higher temperatures. The DSC signal indicates several reaction steps by multiple overlapping exothermic peaks centred around 500 and 620°C. After

the first cycle up to 1000°C, the sample mass has increased to 135% of the initial sample mass. No material evaporation was indicated by DSC/TGA. However, the oxidation reaction is not completed during heating up to 1000°C and continues during cooling until the threshold temperature is too low, indicated by a constant TGA signal after cooling below 700°C in Fig. 6a. During the cooling cycle, a pronounced exothermal reaction is observed at 630°C indicating oxide phase solidification [15,16]. The corresponding melting reaction of the oxidized V coating material was not observed during the DSC heating cycle but may be superposed by the pronounced exothermal oxidation reactions [15].

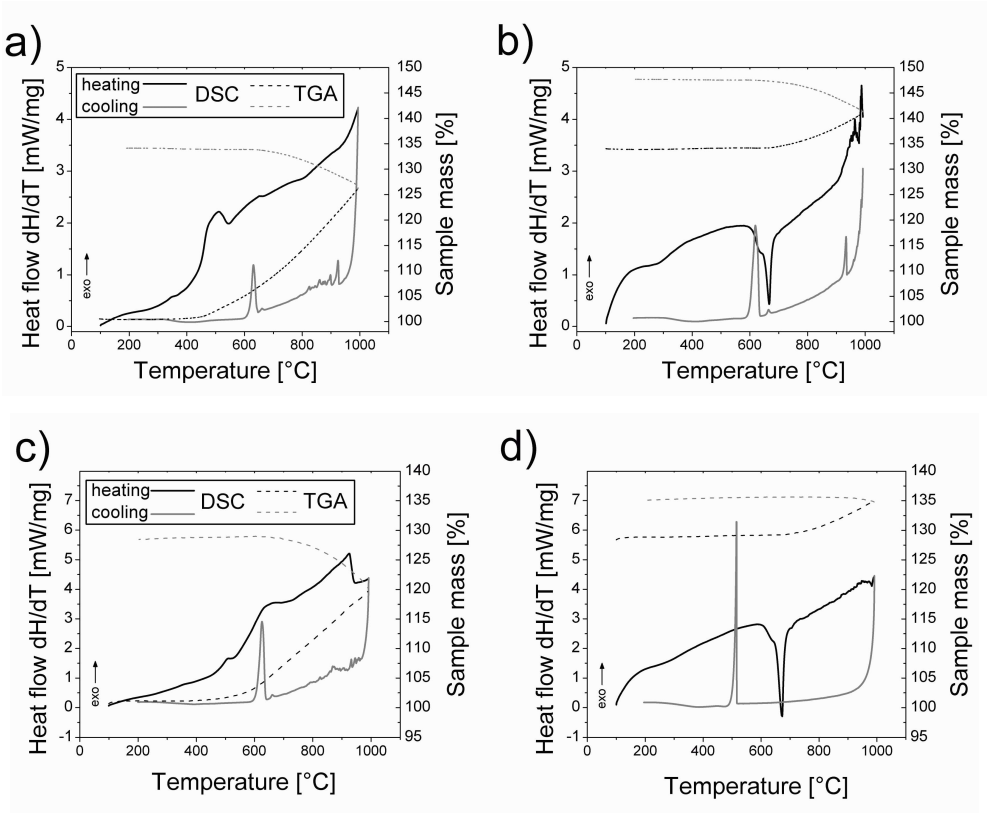

Fig. 6. DSC/TGA heating/cooling cycles of a) V and c) VN coating material up to 1000°C in artificial air at 20 K/min, rerun measurements of pre-oxidized b) V and d) VN coatings.

Comparing the results obtained for VN shown in Fig. 6c, an almost similar oxidation onset temperature between 400 to 450°C was found for both coatings. Additionally, a corresponding mass gain was observed under identical experimental conditions. Further proof for the incomplete oxidation reactions of V and VN coating material after the initial DSC/TGA heating/cooling cycle is observed in rerun measurements of the already pre-oxidized coating materials. The rerun clearly shows further mass gain at temperatures above

600°C (see TGA curves in Fig. 6b and d). The DSC signal clearly displays melting of the formed V-O phases during heating above 590°C for V (Fig. 6b) and above 500°C for VN (Fig. 6d) and subsequent solidification during cooling below 620°C for both coatings. Additionally, the heating above 900°C yields some exothermic reactions for V coatings indicating possible reduction processes of V_2O_5 to other oxides [25,26]. While the oxidation processes seem to be completed for VN, as no further mass gain during subsequent cooling is indicated (see the TGA signal in Fig. 6d), an additional rerun shows even further coating material oxidation for V in the TGA curve at a reduced level and a slight change of the two pronounced melting/solidification reactions in the DSC signal to higher (melting)/lower (solidification) temperatures indicating different formed V-O phases.

Summing up, the tribological behaviour of V containing coatings should be influenced by three factors; (i) the mechanical stability of the oxidized/unaffected coatings system, (ii) the thickness of the oxide scale as determined by oxidation thermodynamics and kinetics and (iii) the chemical nature of the oxide scale formed. It can be assumed that the system VN/V-O with a hard nitride base layer is mechanically more stable than the system V/V-O with the softer V layer. The results of DSC/TGA measurements reveal that the onset of oxidation of both V and VN coatings occurs in a range between 400 and 450°C. Despite these similar onset temperatures, the exothermic and endothermic reactions observed at different temperatures during the DSC measurements indicate different oxidation processes for V and VN coatings, as also supported by Raman Spectroscopy.

4. Conclusions

Within this work, the oxidation behaviour of V and VN coatings and its influence on high-temperature tribological properties has been studied. Differential scanning calorimetry and thermo-gravimetric analysis investigations reveal that the onset of oxidation in the case of V and VN coatings occurs in a range between 400 and 450°C, whereas the oxidation processes of these coatings seems to be different. Both coatings investigated clearly showed the expected vanadium oxides at elevated temperatures which act as an effective lubricant during high-temperature dry sliding tests. The present oxides could be identified as VO_2, V_2O_3, V_2O_5 and V_6O_{13} by X-ray diffraction and Raman investigations. They further revealed that the oxide composition depends on the oxidation temperature, i.e. the higher the temperature, the higher is the amount of V_2O_5 present in oxide layers and oxide glazes. Dry sliding experiments show that the friction coefficient of V coatings at temperatures below 500°C is

much higher than that measured for VN. However, the coatings show promising tribological properties reaching low friction coefficients by solid oxide lubrication in a temperature range between 400 and 600°C. For combining this solid oxide lubrication effect with sufficient wear resistance, an oxide layer of overcritical thickness has to be formed on the surface of the coating, where the critical thickness seems to be dependent on the mechanical properties of the coating material below. The best friction performance was found for both coatings at 700°C, enabling liquid oxide lubrication with a friction coefficient of ~ 0.25.

Finally, it can be concluded that the mechanism of V oxide formation with self-lubricious contributions can be employed to design low-friction coatings over a broad temperature range.

Acknowledgements

This work was supported by the Austrian NANO Initiative via a grant from the Austrian Science Fund FWF within the project “LowFrictionCoatings”.

References

[1] Münz, W.-D.: Titanium aluminum nitride films: A new alternative to TiN coatings. J. Vac. Sci. Technol. A 4 (6), 2717-2725 (1986)

[2] PalDey, S., Deevi, S.C.: Single layer and multilayer wear resistant coatings of (Ti,Al)N: a review. Mat. Sci. Engin. A 342, 58-79 (2003)

[3] Gilmore, R., Baker, M.A., Gibson, P.N., Gissler, W., Stoiber, M., Losbichler, P., Mitterer, C.: Low-friction TiN–MoS_2 coatings produced by dc magnetron co-deposition. Surf. Coat. Technol. 108-109, 345-351 (1998)

[4] Lugscheider, E., Knotek, O., Bobzin, K., Bärwulf, S.: Tribological properties, phase generation and high temperature phase stability of tungsten- and vanadium-oxides deposited by reactive MSIP-PVD process for innovative lubrication applications. Surf. Coat. Technol. 133-134, 362-368 (2000)

[5] Gardos, M.N., Hong, H.-S., Winer, W.O.: Effect of anion vacancies on the tribological properties of rutile (TiO_2-x). Part II. Experimental evidence. Tribol. Trans. 33 (2), 209-220 (1990)

[6] Magnéli, A.: Structures of the ReO_3-type with recurrent dislocations of atoms: homologous series of molybdenum and tungsten oxides. Acta Crystallogr. 6, 495-500 (1953)

[7] Teer, D.G.: New solid lubricant coatings. Wear 251, 1068-1074 (2001)

[8] Carrapichano, J.M., Gomes, J.R., Silva, R.F.: Tribological behaviour of SiN-BN ceramic materials for dry sliding applications. Wear 253, 1070-1076 (2002)

[9] Woydt, M., Skopp, A., Dörfel, I., Witke, K.: Wear engineering oxides/anti-wear oxides. Wear 218, 84-95 (1998)

[10] Erdemir, A.: A crystal-chemical approach to lubrication by solid oxides. Trib. Lett. 8, 97-102 (2000)

[11] Gardos, M.N.: Magnéli phases of anion-deficient rutile as lubricious oxides. Part I. Tribological behaviour of single-crystal and polycrystalline rutile (Ti_nO_{2n-1}). Trib. Lett. 8, 65-78 (2000)

[12] Zabinski, J.S., Sanders, J.H., Nainaparampil, J., Prasad, S.V.: Lubrication using a microstructurally engineered oxide: performance and mechanisms. Trib. Lett. 8, 103-116 (2000)

[13] Kutschej, K., Mayrhofer, P.H., Kathrein, M., Polcik, P., Mitterer, C.: A new low-friction concept for TiAlN based coatings in high-temperature applications. Surf. Coat. Technol. 188-189, 358-363 (2004)

[14] Franz, R., Neidhardt, J., Sartory, B., Kaindl, R., Tessadri, R., Polcik, P., Derflinger, V.H., Mitterer, C.: High-temperature low-friction properties of vanadium-alloyed AlCrN coatings. Tribol. Lett. 23/2, 101-107 (2006)

[15] Mayrhofer, P.H., Hovsepian, P.Eh., Mitterer, C., Münz, W.-D.: Calorimetric evidence for frictional self-adaptation of TiAlN/VN superlattice coatings. Surf. Coat. Technol. 177-178, 341-347 (2004)

[16] Gassner, G., Mayrhofer, P.H., Kutschej, K., Mitterer, C., Kathrein, M.: A new low friction concept for high temperatures: Lubricious oxide formation on sputtered VN coatings. Tribol. Lett. 17/4, 751-756 (2004)

[17] Fateh, N., Fontalvo, G.A., Gassner, G., Mitterer, C.: Influence of high-temperature oxide formation on the tribological behaviour of TiN and VN coatings. Wear 262, 1152-1158 (2007)

[18] Holmberg, K., Matthews, A.: Coatings Tribology, Elsevier, Amsterdam, p. 105 (1994)

[19] Vergne, C., Boher, C., Gras, R., Levaillant, C.: Influence of oxides on friction in hot rolling: Experimental investigations and tribological modelling. Wear 260, 957-975 (2006)

[20] Stott, F.H.: The role of oxidation in the wear of alloys. Tribol. Int. 31, 61-71 (1998)

[21] Greenwood, N.N., Earnshaw, A.: Chemistry of the Elements, second ed., Butterworth-Heinemann, Oxford (1997)

[22] Lugscheider, E., Bärwulf, S., Barimani, C.: Properties of tungsten and vanadium oxides deposited by MSIP-PVD process for self-lubricating applications. Surf. Coat. Technol. 120-121, 458-464 (1999)

[23] Ramana, C.V., Hussain, O.M., Srinivasulu Naidu, B., Reddy, P.J.: Spectroscopic characterization of electron-beam evaporated V_2O_5 thin films. Thin Solid Films 305, 219-226 (1997)

[24] Rabinowicz, E.: Friction and wear of materials, second ed., Wiley-Interscience, New York, p. 96 (1995)

[25] Ningyi, Y., Jinhua, L., Chenglu, L.: Valence reduction process from sol-gel V_2O_5 to VO_2 thin films. Appl. Surf. Sci. 191, 176-180 (2002)

[26] Ramana, C.V., Utsunomiya, S., Ewing, R. C., Becker, U.: Formation of V2O3 nanocrystals by thermal reduction of V2O5 thin films. Solid State Commun. 137, 645-649 (2006)

Publication III

Synthesis-structure relations for reactive magnetron sputtered V_2O_5 films

N. Fateh, G. A. Fontalvo, L. Cha, T. Klünsner, G. Hlawacek, C. Teichert, C. Mitterer

Surface & Coating Technology 202 (2008) 1551-1555

Synthesis-structure relations for reactive magnetron sputtered V_2O_5 films

N. Fateh[a], G. A. Fontalvo[a], L. Cha[a], T. Klünsner[b], G. Hlawacek[b], C. Teichert[b], C. Mitterer[a]

[a] Department of Physical Metallurgy and Materials Testing, University of Leoben, Franz-Josef-Strasse 18, A-8700 Leoben, Austria
[b] Institute of Physics, University of Leoben, Franz-Josef-Strasse 18, A-8700 Leoben, Austria

Abstract

V_2O_5 films were grown onto MgO (100) substrates by reactive magnetron sputtering between 26°C to 300°C to establish a detailed synthesis-structure relation. The effect of deposition temperature on structural characteristics and surface morphology was characterized using X-ray diffraction, Raman spectroscopy, atomic force microscopy and scanning and transmission electron microscopy. Films prepared at room temperature are amorphous while those deposited above 80°C exhibit a polycrystalline structure with the orthorhombic symmetry of the V_2O_5 phase.

Keywords: V_2O_5; Thin films; Atomic force microscopy (AFM); Raman spectroscopy; Transmission electron microscopy (TEM)

1. Introduction

Vanadium pentoxide (V_2O_5) thin films have been studied intensively in recent years due to their attractive physical and chemical properties, particularly its optical properties, which makes them interesting for various applications such as electrochromic devices and optical switches [1,2]. There are some polymorphs of V_2O_5 which are identified in the literature as α-V_2O_5 (orthorhombic), β-V_2O_5 (monoclinic or tetragonal) and δ-V_2O_5 (a modification of β-V_2O_5) [3]. The most stable crystal structure is orthorhombic α-V_2O_5 which belongs to the space group Pmmn (59) with lattice parameters a=11.512, b=3.564 and c=4.368 Å [4]. This structure is characterized by periodic arrangements of edge and corner sharing VO_5 square pyramids. The vanadium atoms form five bonds with oxygen with V-O bond lengths varying

between 1.585 and 2.021 Å. The layers so formed are held together by weak vanadium-oxygen interactions with a distance as large as 2.79 Å. The interaction between the V_2O_5 layers is so weak (van der Waals type) that the crystals cleave easily along the (001) plane, as described in detail by Ramana et al. [5] and Julien et al. [6]. Thus, V_2O_5 should be a promising solid lubricant [7-11]. Recently, several investigations on temperature-structure relationship of amorphous and polycrystalline V_2O_5 films have been reported, where the films were fabricated by different deposition techniques and under varying deposition conditions [6,12-17]. However, the fabrication of V_2O_5 thin films still needs a more detailed characterization for understanding the correlation between the deposition conditions, growth and morphological aspects in order to design well-defined coatings for potential applications. The aim of this work was to prepare V_2O_5 thin films using DC reactive magnetron sputtering over a wide range of substrate temperatures onto MgO (100) substrates and to study the influence of the deposition temperature on their structure and morphology.

2. Experimental details

V_2O_5 films were grown onto MgO (100) substrates which were ultrasonically pre-cleaned in acetone and ethanol prior to deposition. After evacuating the vacuum chamber down to a pressure of 8×10^{-4} Pa, the substrates were thermally cleaned at 750°C for 10 minutes within the deposition chamber. The films were deposited from three metallic vanadium targets (ø 50.8×6.35 mm) with a purity of 99.8 % using unbalanced DC magnetron sputtering in an $Ar+O_2$ atmosphere. The total gas pressure was kept constant at 0.28 Pa, the O_2 partial pressure was 21 % of the total pressure for all deposited V_2O_5 films. The substrates were positioned at a distance of 7 cm from the target center and were rotated at a rate of ~ 10 rotations per minute during deposition to obtain uniform thin films. All films were deposited at floating potential for 60 minutes resulting in an average film thickness of 1.2 µm. The deposition process was carried out at various substrate temperatures of T_s= 26, 80, 100, 150, 230 and 300°C. The samples were heated from the reverse side and after reaching deposition temperature, a period of 30 minutes was used to reach a homogeneous temperature distribution. The sample heater was controlled by an Ogden Microprocessor, while the sample temperature was determined using a thermocouple (type K, Ni-Cr/Ni) which was placed at the steel substrate holder.

X-ray diffraction (XRD) analysis was conducted for structural investigations of the films using a Bragg-Brentano diffractometer (Siemens D500) with Cu–K_α radiation. Raman

spectroscopy measurements were performed using a Horiba Dilor Raman spectroscope with a laser wavelength of 532.2 nm (He-Ne laser) at a power level of 100 mW. In addition, to corroborate the findings from XRD and Raman spectroscopy, atomic force microscopy (AFM, Digital Instruments Nanoscope IIIa) using conventional Si-tips in tapping mode, scanning electron microscopy (SEM, Zeiss EVO 50) and transmission electron microscopy (TEM) were employed. The root mean square (rms) surface roughness, as an integral measure for the vertical film roughness, was also obtained by AFM in the tapping mode from at least three different 10×10 μm scans. Cross -sectional TEM samples were prepared by focused ion beam (FIB) and analyzed using a 200 kV Tecnai F20 TEM. Selected area electron diffraction (SAD) patterns were taken to investigate the crystal structure and orientation.

3. Results and discussion

All deposited V_2O_5 films adhered well to the MgO (100) substrate and had a bright orange appearance. The films exhibited a dense structure with an average thickness of about 1.2 μm according to cross-sectional SEM analysis. XRD patterns of V_2O_5 films deposited onto MgO (100) substrates at different substrate temperatures are shown in Fig. 1.

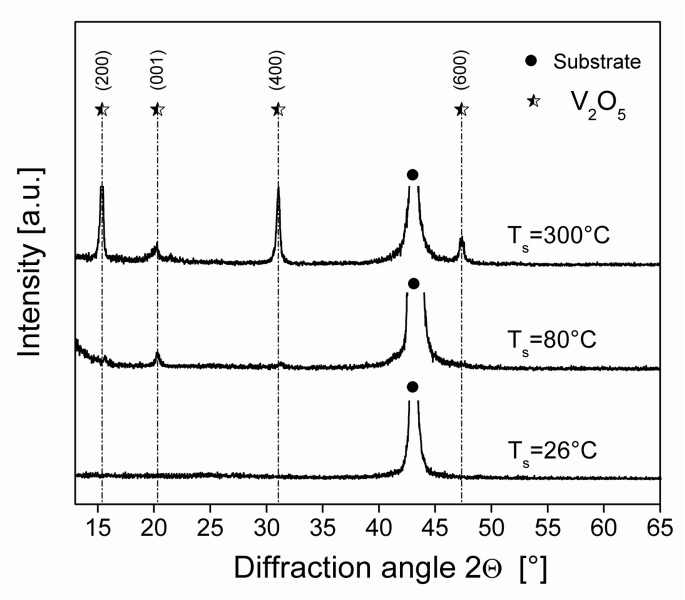

Fig. 1. XRD patterns of V_2O_5 films grown at different temperatures on MgO (100) substrates.

The peak observed at 2θ=43.3° is attributed to the Bragg reflection of the MgO substrate. The XRD pattern of the film grown at room temperature does not evidence any peaks according to the orthorhombic V_2O_5 or any other vanadium oxide which indicates that the

film is amorphous. In the case of the film deposited at 80°C, three small peaks appear at 2θ=15.38°, 20.31° and 31.04° which correspond to the (200), (001) and (400) orientations of the orthorhombic α-V_2O_5 phase according to the JCPDS file (01-077-2418), respectively. This indicates the onset of crystalline V_2O_5 film growth at temperatures around 80°C. The XRD results reveal an increase in the intensity ratios of the V_2O_5 peaks with further increase in deposition temperature up to 150°C (not shown), whereas no structural differences could be observed in the range between 150-300°C (see Fig. 1). The results suggest that the films deposited above 150°C have a preferred (200) growth orientation. The change from an amorphous to a polycrystalline structure of the V_2O_5 films could be attributed to the enhanced ad-atom mobility with increasing deposition temperature [18]. XRD single line profile analysis employing the Pseudo-Voight method [19] yield a mean coherently diffracting domain size of 15 nm for the films deposited at 80 and 100°C which increases to 33 nm for films deposited above 100°C.

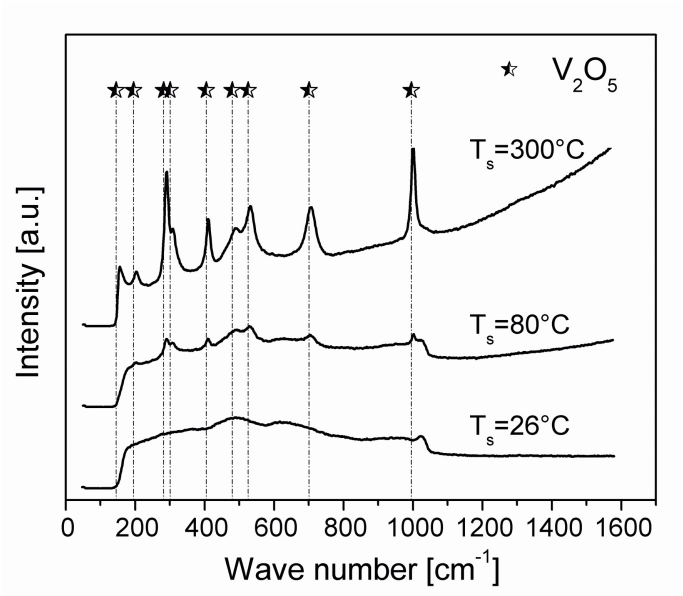

Fig. 2. Raman spectra of V_2O_5 films grown at different temperatures on MgO (100) substrates.

Fig. 2 shows Raman spectra of films deposited at different temperatures which are in good agreement with the XRD results. Raman spectra can be discussed in terms of internal and external vibrations. Internal modes observed in the high-frequency region can be attributed to the stretching and bending of V-O bonds. The external modes, which normally lie in the low-frequency region, can be connected to the relative motion of structural units with respect to each other [15,20,21]. The Raman spectrum of V_2O_5 film grown at room temperature (cf. Fig.

2) clearly demonstrates the amorphous character of the film as no Raman active peaks corresponding to the α-V_2O_5 crystal could be observed. Some low-intensity broad peaks appear in the Raman spectrum of a film deposited at 80°C, indicating the onset of crystalline growth. The spectra of films deposited above 150°C show sharp crystalline features which are in good agreement with the standard Raman peaks for the α-V_2O_5 crystal. Most authors agree that the absorption band located at 995 cm^{-1} is characteristic for V=O double chemical bonds (Vanadyl mode) and corresponds to the stretching of the shortest bond (1.58 Å) between vanadium and oxygen. This mode is an indication of the structural quality and stoichiometry of the film [5,6,15,21]. For the film deposited at 80°C, a small peak at 995 cm^{-1} could be detected which becomes more intense and sharper with increasing deposition temperature of the analysed sample (Fig. 2). This suggests the better crystallinity and stoichiometry of the V_2O_5 films with increasing deposition temperature. A Raman peak at 145 cm^{-1} appears for films deposited at temperatures above 150°C, as clearly seen in the spectrum of the film deposited at 300°C in Fig. 2. Different authors [5,6,21] stated that the presence of this mode indicates the layer-like structure of V_2O_5 films. In the present investigation, this might be interpreted as further indication of the increasing crystallinity of the films with increasing deposition temperature.

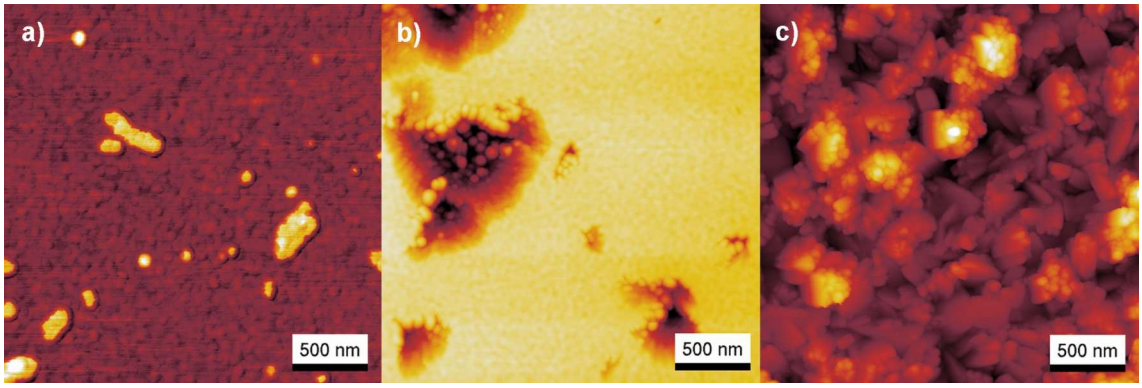

Fig. 3. AFM images of a) an amorphous film grown at room temperature (z-scale: 10 nm), b) the transition from amorphous to crystalline film growth at 80°C (z-scale: 70 nm) and c) a polycrystalline V_2O_5 film grown at 300°C (z-scale: 140 nm).

The morphology of V_2O_5 films as function of the deposition temperature has been studied using AFM in order to understand the microstructure evolution. AFM data of the film deposited at room temperature shown in Fig. 3a verify its amorphous nature as no characteristic features besides 5 nm high contaminations could be revealed. The onset of

crystallisation occurs at 80°C as some fine features with an average size of 50 nm to 100 nm appear on the surface (Fig. 3b). It might be assumed that those features represent clusters of crystalline α-V_2O_5 grains. The AFM image in Fig. 3c clearly shows the granular structure of V_2O_5 film deposited at 300°C, where a morphology characterized by small plates could be found. Fig. 4 shows the variation in rms surface roughness of V_2O_5 films with increasing deposition temperature. The rms values increases from 0.7 nm to 21 nm as the deposition temperature increases from room temperature to 300°C. This is attributed to the transition from amorphous to crystalline growth and promoted grain growth with higher deposition temperatures.

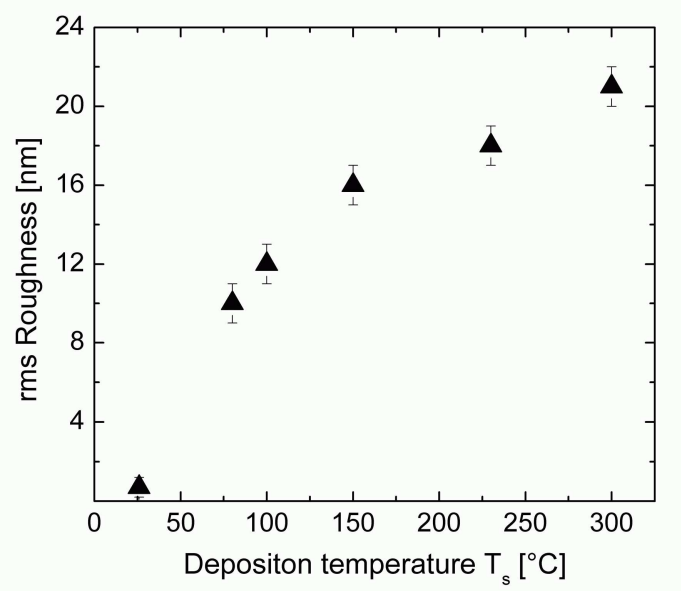

Fig. 4. Variation of rms surface roughness of V_2O_5 films on MgO (100) substrates with increasing deposition temperature.

Fig. 5a shows a bright-field TEM micrograph of a 1.2 µm thick V_2O_5 film deposited on MgO (100) at 80°C. It displays the presence of discrete crystalline grains within a flat and uniform matrix. The fine stripes seen in the bright-field image are induced by FIB preparation damages. Fig. 5b demonstrates SAD pattern of the polycrystalline region taken from the upper part of the film (indicated by "B" in Fig. 5a). The d-spacings of the diffracted spots match very well to orthorhombic α-V_2O_5 crystal lattice. A diffuse ring is slightly visible which indicates that this part of the film is not totally crystallized. The SAD pattern (Fig. 5c) taken from the region near to the substrate (indicated by "C" in Fig. 5a) displays an

amorphous pattern as only a typical diffuse ring besides the diffraction spots of MgO could be observed.

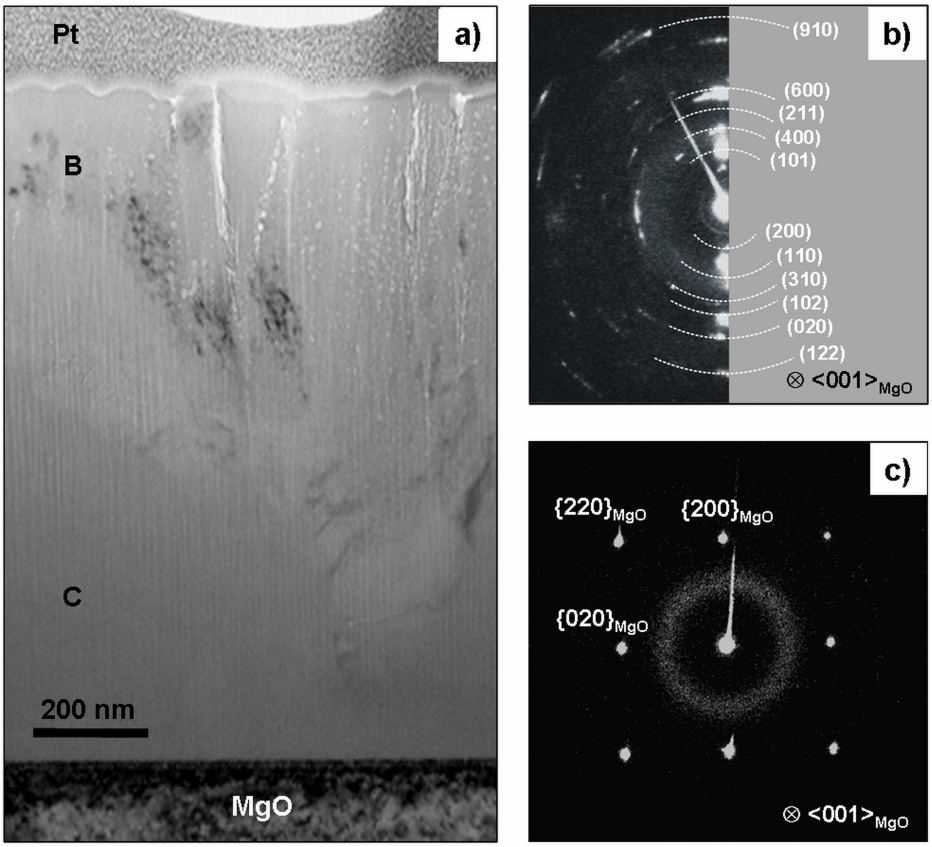

Fig. 5. a) TEM cross-sectional bright-field image of the V_2O_5 film deposited on MgO (100) at 80°C, b) corresponding SAD patterns taken from the upper region (B) of the film and c) the lower part of the film (C) and adjacent substrate.

The bright-field TEM image in Fig. 6a shows that the V_2O_5 film grown at 300°C is clearly polycrystalline. Grains exhibit irregular column shapes and different contrasts. The corresponding dark-field image of the same area is shown in Fig. 6b. The bright areas demonstrate the crystallites having a same orientation where some of them range from the bottom to the top of the film. Fig. 6c and d show SAD patterns of the upper and lower part of the film deposited at 300°C, respectively. Except the diffraction spots from the MgO substrate (see Fig. 6d), all diffracted spots in Figs. 6c and d, in which the intensities varies with orientations, belong to orthorhombic α-V_2O_5. It indicates that the crystallized film has preferred orientations with the MgO substrate for the deposition conditions used.

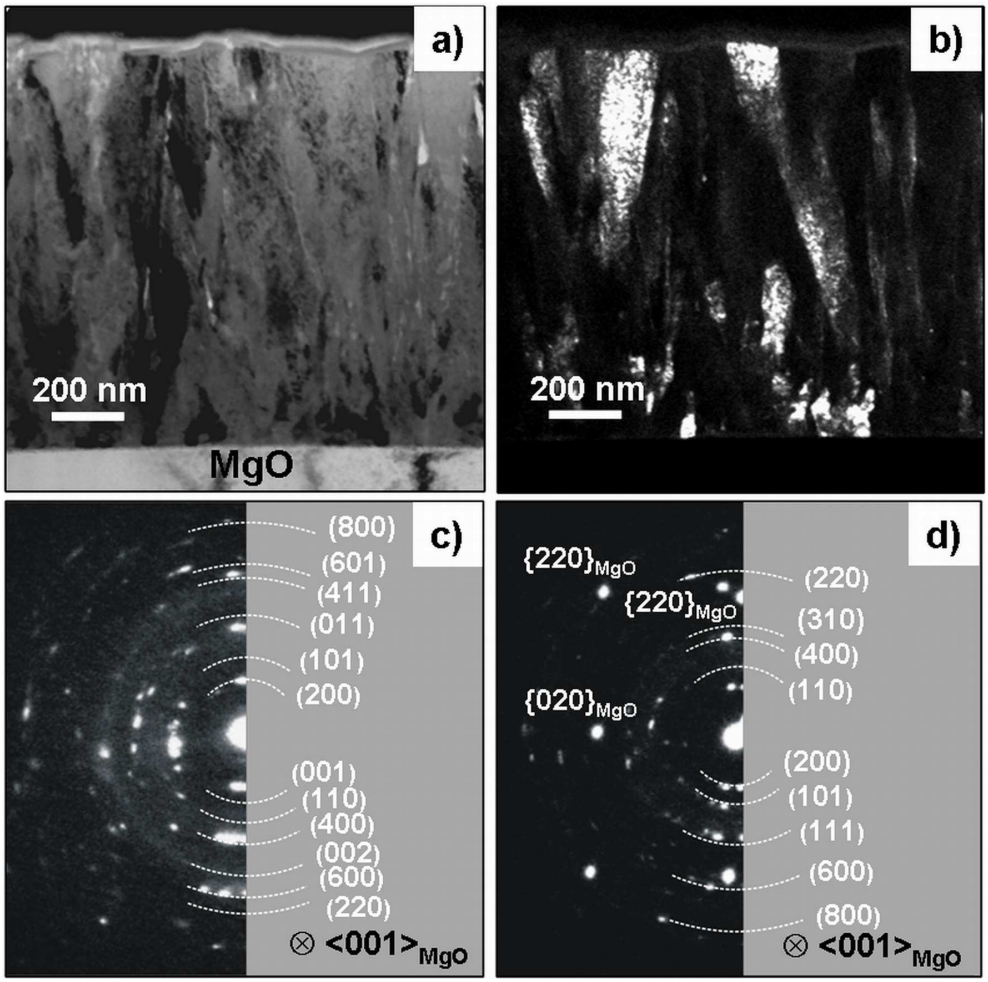

Fig. 6. a) Bright-field TEM image and b) the corresponding dark field image of the V_2O_5 film deposited on MgO (100) at 300°C. SAD patterns taken from c) the upper part of the film and d) the lower part of the film and adjacent substrate.

4. Conclusions

From the results presented here it is obvious that the deposition temperature plays an important role in nucleation and growth of V_2O_5 films deposited onto MgO (100) substrates using reactive DC magnetron sputtering. According to the XRD, Raman, AFM and TEM investigations in this work, the V_2O_5 films grown at room temperature exhibited an amorphous structure with a smooth morphology. The onset of crystallisation during thin film growth occurred at ~ 80°C, where the film region close to the substrate is mostly amorphous and the region farer away from the substrate has been crystallized, as derived from TEM analysis. The V_2O_5 films deposited at temperatures above 100°C were polycrystalline exhibiting the orthorhombic α-V_2O_5 phase and irregular column shapes. AFM results showed an increase in rms surface roughness of V_2O_5 films from 0.7 to 21 nm with increasing

deposition temperature. From the obtained results it can be concluded that deposition at room temperature dose not provide sufficient thermal energy for ad-atom mobility, resulting in an amorphous film structure. Increasing the deposition temperature to 80°C and above favours the onset of crystallization and subsequent grain growth due to the increase in mobility of ad-atoms on the surface and enhanced diffusion.

Acknowledgements

This work was supported by the Austrian NANO Initiative via a grant from the Austrian Science Fund FWF within the project “LowFrictionCoatings”. Valuable discussions with C. Scheu on the TEM investigations are greatly acknowledged.

References

[1] M. K. Yurdakoc, R. Haffiner, D. Honicke, Mater. Chem. Phys. 44 (1996) 276.

[2] G. S. Nadkarni, V. S. Shirodkar, Thin Solid. Films 105 (1983) 115.

[3] P. Balog, D. Orosel, Z. Cancarevic, S. Schön, M. Jansen, J. Alloys Compd. 429 (2007) 87.

[4] R. Enjalbert, J. Galy, Acta Crystallogr. A 42 (1986) 1467.

[5] C. V. Ramana, O. M. Hussain, B. S. Naidu, P. J. Reddy, Thin Solid Films 305 (1997) 219.

[6] C. Julien , J. P. Guesdon, A. Gorenstein, A. Khelfa, I. Ivanov, Appl. Surf. Sci. 90 (1995) 389.

[7] E. Lugscheider, S. Bärwulf, C. Barimani, Surf. Coat. Technol. 120-121 (1999) 458.

[8] N.N. Greenwood, A. Earnshaw, Chemistry of the Elements, 2nd ed., Butterworth-Heinemann, Oxford, 1997.

[9] G. Gassner, P.H. Mayrhofer, K. Kutschej, C. Mitterer, M. Kathrein, Tribol. Lett. 17/4 (2004) 751.

[10] N. Fateh, G. Gassner, G. A. Fontalvo, C. Mitterer, Wear 262 (2007) 1152.

[11] N. Fateh, G. Gassner, G. A. Fontalvo, C. Mitterer, Tribol. Lett. 28 (2007) 1.

[12] C.V. Ramana, R.J. Smith, O.M. Hussain, C.M. Julien, Chem. J. Vac. Sci. Technol. A 22 (2004) 2453.

[13] C.V. Ramana, R.J. Smith, O.M. Hussain, C.M. Julien, Mater. Sci. Eng. B 111 (2004) 218.

[14] A. Gies, B. Pecquenard, A. Benayad, H. Martinez, D. Gobeau, H. Fuess, A. Levasseur, Solid State Ionics 176 (2005) 1627.

[15] S.H. Lee, H.M. Cheong, M.J. Seong, P. Liu, C.E. Tracy, A. Mascarenhas, J.R. Pitts, S.K. Deb, Solid State Ionics 165 (2003) 111.

[16] L. J. Meng, R. A. Silva, H. N. Cui, V. Teixeira, M. P. dos Santos, Z. Xu, Thin Solid Films 515 (2006) 195.

[17] S. P. Lim, J. D. Long, S. Xu, K. Ostrikov, J. Phys. D: Appl. Phys. 40 (2007) 1085.

[18] J.A. Thornton, J. Vac. Sci. Technol. 11 (1974) 666.

[19] T. H. Dekeijser, J. I. Langford, E. J. Mittemeijer, A.B.P. Vogels, J. Appl. Crystallogr. 15 (1982) 308.

[20] C. Julien , I. Ivanov, A. Gorenstein, Mater. Sci. Eng. B 33 (1995) 168.

[21] G. J. Fang, Z.L. Liu, Y. Wang, Y.H. Liu, K.L. Yao, J. Vac. Sci. Technol. A 19 (2001) 887.

Publication IV

Structural and mechanical properties of dc and pulsed dc reactive magnetron sputtered V_2O_5 films

N. Fateh, G. A. Fontalvo, C. Mitterer

Journal of Physics D: Applied Physics 40 (2007) 7716-7719

Structural and mechanical properties of dc and pulsed dc reactive magnetron sputtered V_2O_5 films

N. Fateh, G. A. Fontalvo, C. Mitterer

Department of Physical Metallurgy and Materials Testing, University of Leoben, Franz-Josef-Strasse 18, A-8700 Leoben, Austria

Abstract

Vanadium pentoxide (V_2O_5) thin films were deposited onto Si (100) substrates using dc and pulsed dc reactive magnetron sputtering at 26, 100 and 300°C to investigate the influence of substrate temperature and sputtering mode on their structural and mechanical properties. X-ray diffraction (XRD), Raman spectroscopy and scanning electron microscopy (SEM) revealed that the structural characteristics and the surface morphology of the V_2O_5 films depend on both sputtering mode and deposition temperature. With increasing deposition temperature, the films deposited by dc sputtering show a transition from amorphous at room temperature to polycrystalline growth with a preferred (200) orientation. This leads to an increase of hardness and elastic modulus of the films from 3.2±0.1 and 79.4±3.2 GPa at 26°C to 4.8±0.6 and 129.2±6.4 GPa at 300°C, respectively. In contrast, the films deposited by pulsed dc sputtering exhibit a polycrystalline α-V_2O_5 structure over the whole temperature range. The hardness of these films decreases with increasing deposition temperature while the Young's modulus is almost unaffected.

Keywords: V_2O_5 thin films; magnetron sputtering; Raman; hardness

1. Introduction

The attractive multifunctional properties of V_2O_5, especially in thin film form, have attracted interest for various applications such as catalysis, electrochromic devices and optical switches [1,2]. There are some polymorphic phases of V_2O_5 which are identified in the literature as α-V_2O_5 (orthorhombic), β-V_2O_5 (monoclinic or tetragonal) and δ-V_2O_5 (a modification of β-V_2O_5) [3]. The orthorhombic α-V_2O_5 shows the most stable crystal

structure belonging to the Pmmn (59) space group with lattice parameters a = 11.512, b = 3.564 and c = 4.368 Å [4]. The crystal structure of α-V_2O_5 is built up from VO_5 square pyramids shearing edges and corners. The so formed V_2O_5 layers are held together by week V-O interactions (van der Waals type) which allow the crystals to cleave easily along (001) planes, as described in detail by Ramana et al. [5] and Julien et al. [6]. Thus, V_2O_5 should be a promising solid lubricant [7-11]. Recently, several investigations on structural and optical properties of V_2O_5 films prepared by various deposition techniques and under varying deposition conditions have been reported [6,12-19]. However, understanding the role of the deposition process to control the crystallinity, crystallographic orientation, morphology of the V_2O_5 films and consequently their mechanical properties requires detailed investigations. The purpose of the present work was to grow V_2O_5 thin films onto Si (100) substrates using dc and pulsed dc reactive magnetron sputtering and to study the effect of deposition technique and deposition temperature on their structural and mechanical properties.

2. Experimental details

V_2O_5 thin films were deposited onto Si (100) substrates which were ultrasonically pre-cleaned in acetone and ethanol prior to deposition. After evacuating the vacuum chamber down to a pressure of 8×10^{-4} Pa, the substrates were thermally cleaned at 750°C for 10 minutes within the deposition chamber. The films were deposited from three V targets (⌀ 50.8×6.35 mm) mounted to a cluster of three unbalanced magnetrons (AJA cluster with A320-XP magnetrons), focused to the substrate holder (AJA SHQ400). Sputtering was done in a mixture of Ar and O_2 applying dc and pulsed dc discharges. The total gas pressure for both sputtering modes was kept constant at 0.28 Pa while the O_2 partial pressure was 21 % of the total pressure for all deposited V_2O_5 films. The target current was set to 0.35 A per magnetron for all experiments. The substrates were positioned parallel to the magnetron cluster in a distance of 7 cm and were rotated at approximately 10 revolutions per minute during deposition to obtain uniform thin films. All films were deposited at floating potential. As observed in our experiments, the growth rate obtained by dc sputtering is higher than the one of the pulsed dc process. To keep the film thickness constant at approximately 1.2 µm, the films were deposited for 60 and 90 minutes by dc and pulsed dc sputtering, respectively. For the pulsed dc films, three bipolar pulsed dc power supplies (MKS RPG-50) were used to generate the plasma. The target pulsing frequency was kept constant at 100 kHz with 16% duty cycle. The deposition process for both techniques was carried out at three different

substrate temperatures, T_s= 26, 100 and 300°C. The samples were heated from the reverse side and after reaching deposition temperature, a period of 30 minutes was used to establish a homogeneous temperature distribution. The sample temperature was determined using a k-type thermocouple attached to the substrate holder.

The film structure was determined by X-ray diffraction (XRD) analysis using a Siemens D500 diffractometer in Bragg-Brentano configuration and Cu–K_α radiation. Raman spectroscopy measurements were performed at room temperature in air using a LABRAM confocal-Raman spectroscope with a laser wavelength of 632.8 nm (He-Ne laser) at a power level of 100 mW. To investigate possible structural changes in the films at elevated temperatures, V_2O_5 films deposited at 300°C in dc and pulsed dc mode were annealed in vacuum ($P \leq 1.5 \times 10^{-3}$ Pa, T_a=500°C) for 10 min and then analysed with Raman spectroscopy. The surface morphology of the films was investigated using scanning electron microscopy (SEM, Zeiss EVO 50). Hardness and Young's modulus of the films were evaluated by nanoindentation (UMIS II Nanoindenter) using a Berkovich diamond tip with a constant load of 3 mN. The presented values are averaged from 20 indents.

3. Results and discussion

Fig. 1 presents XRD patterns of dc and pulsed dc sputtered V_2O_5 films deposited onto Si (100) substrates at 26, 100 and 300°C. The results reveal that the film structure depends strongly on both substrate temperature and sputtering mode. The XRD pattern of the film deposited in dc mode at room temperature indicates an amorphous structure. As the substrate temperature increases to 100°C, the typical peaks of polycrystalline α-V_2O_5 appear. The peaks located at 2θ = 15.38°, 31.04° and 47.34° correspond to the (200), (400) and (600) reflections, respectively, of the orthorhombic α-V_2O_5 phase according to the JCPDS file (01-077-2418). The film deposited at 300°C shows no detectable changes in the XRD pattern compared to the film grown at 100°C. The results suggest that the films deposited at 100 and 300°C grow with a preferred (200) orientation. The change from amorphous to polycrystalline structure of the V_2O_5 films could be attributed to the enhanced ad-atom mobility with increasing deposition temperature [20]. More details on the structural characterization of dc sputtered V_2O_5 films can be found in a previous publication [19]. XRD single-line profile analysis employing the Pseudo-Voight method [21] yield a mean coherently diffracting domain size of 35 nm along (200) for the film deposited at 100°C which increases to 54 nm for the film deposited at 300°C.

The XRD patterns of the films deposited in the pulsed dc mode indicate a polycrystalline structure over the whole deposition temperature range. In this case, several diffraction peaks which belong to the orthorhombic α-V_2O_5 could be observed. The films deposited at room temperature and 100°C seem to have a preferred (001) orientation while the intensities of the (001) and (110) reflections of the film deposited at 300°C are almost equal. It is worth to mention that the intensity of the peaks from the V_2O_5 phase increases for rising substrate temperatures. Applying the Pseudo-Voight method for the (001) and (110) peaks indicates a decrease in the mean grain size with increasing deposition temperature from 57 to 15 nm for the (001) orientation, and an increase in grain size from 27 to 36 nm along the (110) orientation. In contrast to the amorphous nature of films grown at room temperature by dc sputtering, the polycrystalline growth of the pulsed dc films at room temperature is related to the increased energy and flux of ions bombarding the substrate compared to the dc mode [22]. This is assumed to lead to higher ad-atom mobility [23] and consequently more crystalline V_2O_5 films.

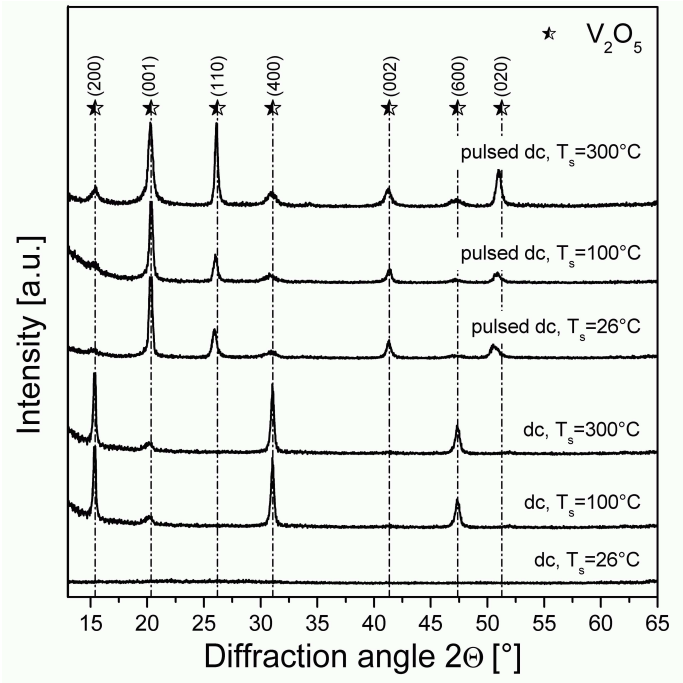

Fig. 1. XRD patterns of V_2O_5 films deposited by dc and pulsed dc sputtering at different substrate temperatures.

Fig. 2 shows Raman spectra of the films deposited by dc and pulsed dc magnetron sputtering at different temperatures which confirm the XRD results. The dc sputtered film

grown at room temperature shows no sharp peaks confirming its amorphous character. With increasing deposition temperature, the spectra exhibit sharp crystalline peaks which are in good agreement with the standard Raman peaks of α-V_2O_5. The intense peak at 145 cm^{-1} is related to vibrations of V-O-V chains and its presence indicates the layer-like structure of the V_2O_5 phase. The Raman band located at 995 cm^{-1} corresponds to the terminal oxygen (V=O) stretching mode and gives information about structural quality and stoichiometry of the film [5,6,15,16].

The spectra of the films deposited by pulsed dc sputtering verify the polycrystalline character of the α-V_2O_5 phase over the whole deposition temperature range (see Fig. 2). However, a broadening of the Raman peaks compared to those deposited in dc mode could be observed which may be due to structural disorder and non-stoichiometry of the pulsed dc V_2O_5 films.

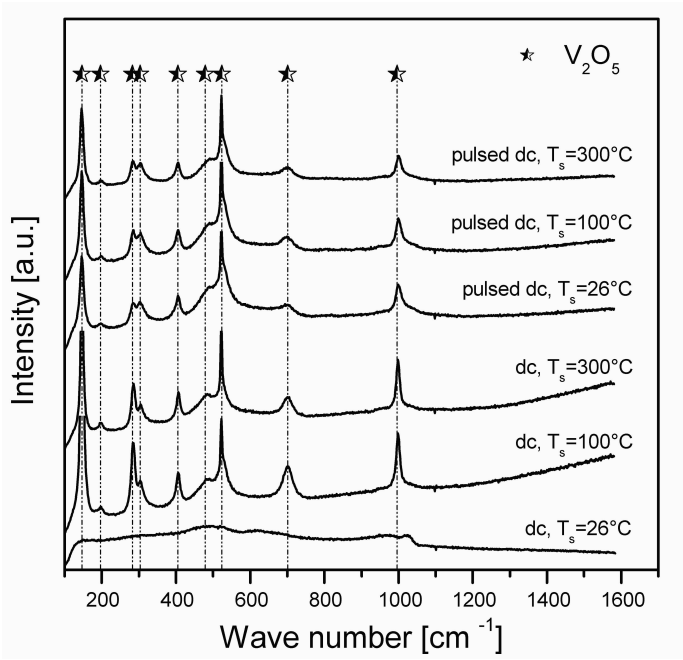

Fig. 2. Raman scattering spectra of dc and pulsed dc V_2O_5 films deposited at different substrate temperatures.

Raman spectra of the films deposited by dc and pulsed dc sputtering at 300°C after annealing in vacuum at 500°C are shown in Fig. 3. Annealing of the dc sputtered film does not lead to any distinct structural changes, confirming its thermal stability of up to 500°C (cf. Fig. 3). On the contrary, the Raman spectrum of the annealed film deposited in pulsed dc mode shows, besides the Raman-active mode for α-V_2O_5, some additional peaks. These peaks

are located at 167, 846, 884 and 937 cm^{-1}, and they agree very well to those obtained by Liu et al. for V_2O_5 nanotubes [24]. Julien et al. [6] reported that the band at 846 cm^{-1} is normally Raman-inactive because of the V_2O_5 symmetry but becomes active due to a structurally disordered film after annealing. This peak might also be assigned to the Raman-active mode of VO_2 [25]. Lee et al. [15] reported that the peak located at 938 cm^{-1} is attributed to V^{4+}=O bonds due to a direct conversion from V^{5+}=O bonds and/or the breaking of the single oxygen bonds involving V^{4+} ions.

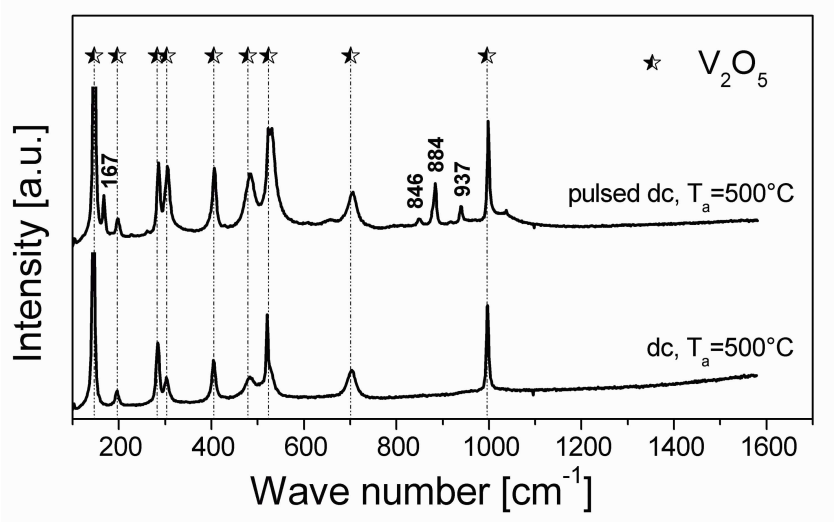

Fig. 3. Raman scattering spectra of dc and pulsed dc V_2O_5 films deposited at 300°C after vacuum annealing at 500°C.

According to cross-sectional SEM analysis, all deposited V_2O_5 films exhibit a dense structure with an average film thickness of approximately 1.2 µm. Top-view SEM images of dc and pulsed dc films prepared at different substrate temperatures (see Fig. 4) show considerable differences in their surface morphology depending on the deposition method and temperature. The dc sputtered film prepared at room temperature (Fig. 4a) has a very smooth surface which might be related to its amorphous nature, and shows a dense structure. On the other hand, the film sputtered in the dc mode at 300°C shows a flake-like structure (Fig. 4b). The pulsed dc sputtered film deposited at room temperature clearly shows a granular surface structure (Fig. 4c). As the deposition temperature increases to 300°C, the granular structure gets finer (Fig. 4d). The differences in surface morphology of the films are in good agreement to XRD and Raman results. They are assumed to be a consequence of the different growth orientation of the films as function of sputtering mode and deposition temperature.

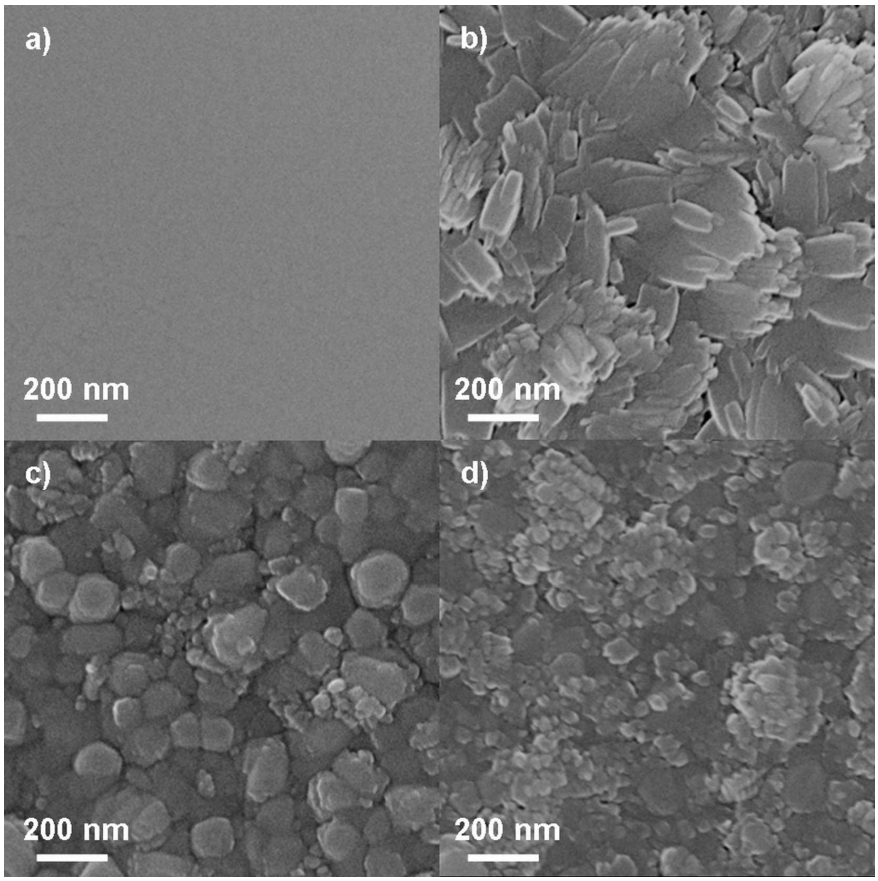

Fig. 4. SEM images of the surface of V_2O_5 films deposited by dc reactive sputtering at substrate temperatures of a) T_s = 26, b) T_s = 300°C and by pulsed dc sputtering at c) T_s = 26 and d) T_s = 300°C.

The average hardness and Young's modulus of dc and pulsed dc sputtered V_2O_5 films as a function of substrate temperature are presented in Figs. 5a and 5b, respectively.

The amorphous film deposited in dc mode at room temperature has a hardness value of 3.2±0.1 GPa and a Young's modulus of 79.4±3.2 GPa. Both hardness and modulus increase with deposition temperature due to the change from amorphous to polycrystalline structure and reach values of 4.8±0.6 and 129.2±6.4 GPa at 300°C, respectively. In the case of the pulsed dc films, the hardness decreases continuously from 7±0.5 GPa at room temperature to 5.3±0.4 GPa at 300°C. This should be attributable to the observed changes in preferred orientation, grain size of the V_2O_5 phase and grain boundary fraction. The Young's modulus of the pulsed dc films deposited at room temperature and 100°C is almost unaffected by the deposition temperature, with an average value of 129.3±6.5 GPa.

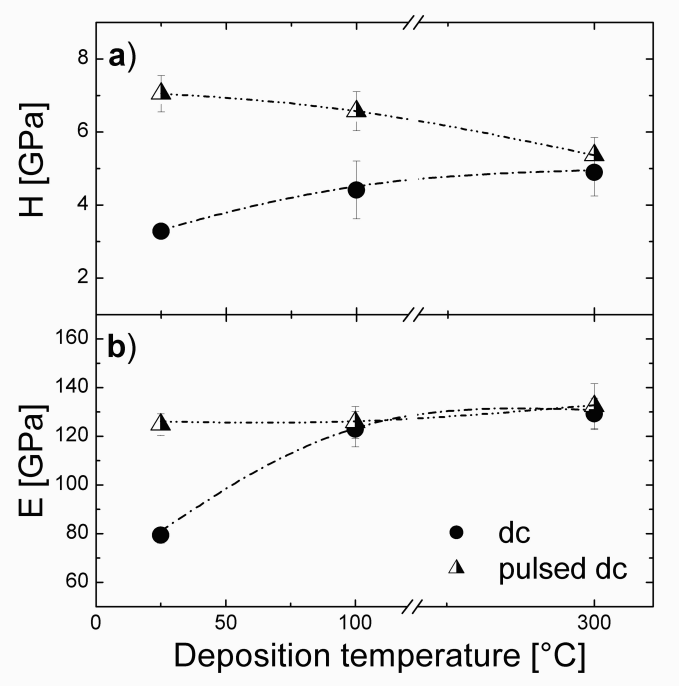

Fig. 5. Averaged hardness and Young's modulus of dc and pulsed dc sputtered V_2O_5 films as a function of substrate temperature.

4. Conclusions

Based on the results presented in this work, it can be concluded that the structural and mechanical properties of V_2O_5 films grown by reactive magnetron sputtering are determined by the sputtering mode and the deposition temperature. Structural investigations using X-ray diffraction and Raman spectroscopy revealed that dc sputtered V_2O_5 films grown at room temperature are amorphous having a very smooth and dense surface. Increasing the deposition temperature favours crystallization of the films due to the increased ad-atom mobility and enhanced diffusion. This leads to a polycrystalline structure at substrate temperatures of 100 and 300°C with (200) preferred orientation and flake-like surface morphology. The transition from amorphous to polycrystalline growth with increasing deposition temperatures yields an increase of hardness and Young's modulus from 3.2±0.1 and 79.4±3.2 GPa at room temperature to 4.8±0.6 and 129.2±6.4 GPa at 300°C, respectively. The V_2O_5 films deposited by pulsed dc reactive magnetron sputtering exhibit a polycrystalline structure over the whole deposition temperature range due to the increased ion bombardment. The surface morphology of the films changes from coarse granular at room temperature to a finer granular structure at 300°C. The films show a continuous decrease of hardness from 7±0.5 GPa at room temperature to 5.3±0.4 GPa at 300°C which is attributed to changes in preferred orientation,

grain size of the V_2O_5 phase and grain boundary fraction. The Young's modulus is almost unaffected by the deposition temperature and reaches values of approximately 129.3±6.5 GPa.

Acknowledgements

This work was supported by the Austrian NANO Initiative via a grant from the Austrian Science Fund FWF within the project "LowFrictionCoatings". The assistance of Rostislav Daniel in nanoindentation and the help of Daniel Kiener for SEM investigations are kindly appreciated.

References

[1] Yurdakoc M K, Haffiner R, Honicke D 1996 *Mater. Chem. Phys.* **44** 276

[2] Nadkarni G S, Shirodkar V S 1983 *Thin Solid Films* **10**5 115

[3] Balog P, Orosel D, Cancarevic Z, Schön S, Jansen M 2007 *J. Alloys Comp.* **429** 87

[4] Enjalbert R, Galy J 1986 *Acta Crystallogr.* A **42** 1467

[5] Ramana C V, Hussain O M, Naidu B S, Reddy P J 1997 *Thin Solid Films* **305** 219

[6] Julien C, Guesdon J P, Gorenstein A, Khelfa A, Ivanov I 1995 *Appl. Surf. Sci.* **90** 389

[7] Lugscheider E, Bärwulf S, Barimani C 1999 *Surf. Coat. Technol.* **120-121** 458

[8] Greenwood N N, Earnshaw A 1997 *Chemistry of the Elements*, 2nd ed., (Oxford: Butterworth-Heinemann)

[9] Gassner G, Mayrhofer P H, Kutschej K, Mitterer C, Kathrein M 2004 *Tribol. Lett.* **17** 751

[10] Fateh N, Gassner G, Fontalvo G A, Mitterer C 2007 *Wear* **262** 1152

[11] Fateh N, Gassner G, Fontalvo G A, Mitterer C 2007 *Tribol. Lett.* **28** 1

[12] Ramana C V, Smith R J, Hussain O M, Julien C M 2004 *J. Vac. Sci. Technol. A* **22** 2453

[13] Ramana C V, Smith R J, Hussain O M, Julien C M 2004 *Mater. Sci. Eng. B* **111** 218

[14] Gies A, Pecquenard B, Benayad A, Martinez H, Gobeau D, Fuess H, Levasseur A 2005 *Solid State Ionics* **176** 1627

[15] Lee S H, Cheong H M, Seong M J, Liu P, Tracy C E, Mascarenhas A, Pitts J R, Deb S K 2003 *Solid State Ionics* **165** 111

[16] Meng L J, Silva R A, Cui H N, Teixeira V, dos Santos M P, Xu Z 2006 *Thin Solid Films* **515** 195

[17] Lim S P, Long J D, Xu S, Ostrikov K 2007 *J. Phys. D: Appl. Phys.* **40** 1085

[18] Fang G J, Liu Z L, Wang Y, Liu Y H, Yao K L 2001 *J. Vac. Sci. Technol. A* **19** 887

[19] Fateh N, Fontalvo G A, Cha L, Klünsner T, Hlawacek G, Teichert C, Mitterer C 2008 *Surf. Coat. Technol.* **202** 1551

[20] Thornton J A 1974 *J. Vac. Sci. Technol.* **11** 666

[21] Dekeijser T H, Langford J I, Mittemeijer E J, Vogels A B P 1982 *J. Appl. Crystallogr.* **15** 308

[22] Bradley J W, Bäcker H, Kelly P J, Arnell R D 2001 *Surf. Coat. Technol.* **135** 221

[23] Kelly P J, Beevers C F, Henderson P S, Arnell R D, Bradley J W, Bäcker H 2003 *Surf. Coat. Technol.* **174-175** 795

[24] Liu X, Huang C, Qiu J, Wang Y 2006 *Appl. Surf. Sci.* **253** 2747

[25] Schilbe P 2002 *Physica B* **316-317** 600

Publication V

Tribological properties of reactive magnetron sputtered V_2O_5 and VN-V_2O_5 coatings

N. Fateh, G. A. Fontalvo, C. Mitterer

Submitted for Publication

Tribological properties of reactive magnetron sputtered V_2O_5 and VN-V_2O_5 coatings

N. Fateh, G. A. Fontalvo, C. Mitterer

Department of Physical Metallurgy and Materials Testing, University of Leoben, Franz-Josef-Strasse 18, A-8700 Leoben, Austria

Abstract

Next generation of advanced hard coatings for tribological applications should combine the advantages of hard wear resistant coatings with low-friction films. Within this work, the tribological behaviour of vanadium pentoxide (V_2O_5) single-layer as well as VN-V_2O_5 bi-layer coatings was investigated in the temperature range between 25 and 600°C. For VN-V_2O_5 bi-layer coatings, V_2O_5 top-layers were deposited by dc and bipolar pulsed dc reactive magnetron sputtering, where the V_2O_5 phase shows preferred growth orientation in (200) and (110), respectively. The V_2O_5 single-layer coatings were prepared by dc reactive magnetron sputtering with a substrate bias of -80 V which leads to a preferred (200) growth orientation. Tribological properties were evaluated using a ball-on-disc configuration in ambient air with alumina balls as counterpart. The structure of the as-deposited films and eventual changes after tribometer testing were identified using X-ray diffraction, Raman spectroscopy and scanning electron microscopy. The friction coefficient of VN-V_2O_5 bi-layer coatings deposited in dc and pulsed dc mode decreases from room temperature to 600°C, while the pulsed dc VN-V_2O_5 coatings have a significantly lower coefficient of friction over the whole testing temperatures, reaching a value of 0.28 at 600°C. Up to 400°C, V_2O_5 single-layer coatings showed almost the same coefficient of friction as pulsed dc VN-V_2O_5 bi-layer coatings, but reached a value of 0.15 at 600°C. It seems that thermal activation of crystallographic slip systems is necessary for V_2O_5 films to show a low-friction effect.

Keywords: V_2O_5 thin films; magnetron sputtering; dry sliding; Friction

1. Introduction

Over the last few years, oxides and their combinations have attracted interest for tribological applications due to their potential as low-friction coatings in the high-temperature range [1-9]. In an earlier study [9], we reported on the beneficial effect of vanadium oxide formation on tribological properties of V and VN coatings. It could also be demonstrated that, to achieve a low-friction effect and at the same time sufficient wear resistance, an oxide layer of overcritical thickness has to be formed on the coating surface, which seems to be stable and efficient after reaching a certain oxidation temperature.

Recently, we have studied in detail the structure and surface morphology of V_2O_5 thin films deposited by reactive magnetron sputtering at different deposition temperatures [10]. Investigations on amorphous and polycrystalline V_2O_5 coatings deposited by dc and bipolar pulsed dc magnetron sputtering showed the role of deposition method as well as substrate temperature on structure, preferential orientation of the V_2O_5 phase and mechanical properties [11]. In literature, several investigations on structural and optical properties of V_2O_5 films prepared by various deposition techniques and under varying deposition conditions can be found [10-18]. However, with the exception of a few investigations [5,19], the tribological properties of V_2O_5 films, particularly at elevated temperatures, have not yet been reported in detail. Therefore, the purpose of the present work was to prepare VN-V_2O_5 bi-layer coatings by dc and bipolar pulsed dc reactive magnetron sputtering with V_2O_5 top-layers having a sufficient thickness and to study their tribological properties. We also characterized the tribological behaviour of V_2O_5 single-layer films during high-temperature tests to verify their suitability as low-friction coatings.

2. Experimental details

The coatings investigated in this work were deposited by means of reactive magnetron sputtering on high-speed steel discs (DIN 1.3343, AISI M2), which were quenched and tempered to a hardness of 65 HRC. After evacuating the vacuum chamber down to a pressure of 8×10^{-4} Pa, the ground and polished substrates were ultrasonically pre-cleaned with acetone and ethanol and ion etched within the deposition chamber prior to deposition. The films were deposited from three V targets (⌀ 50.8×6.35 mm) mounted to a cluster of three unbalanced magnetrons (AJA cluster with A320-XP magnetrons), focused to the substrate holder (AJA SHQ400). Depending on the investigations foreseen, dc and bipolar pulsed dc magnetron

sputtering were applied in a gas mixture of Ar + O_2 or Ar + N_2, respectively. The target current was set to 0.35 A at each magnetron for all experiments. The substrates were positioned parallel to the magnetron cluster in a distance of 7 cm and were rotated at ~ 10 rpm during deposition to obtain uniform films. In all deposition runs, the total gas pressure was kept constant at 0.28 Pa, where for VN and V_2O_5 coatings the N_2 and O_2 partial pressure was 15 % and 21 % of the total pressure, respectively. In case of the VN-V_2O_5 bi-layer coatings, the VN layer was deposited in dc mode at 500°C while the V_2O_5 top-layer was grown in dc and pulsed dc (MKS RPG-50 power supplies, 100 kHz pulsing frequency) modes, respectively, at 300°C and floating potential. These two different modes for depositing V_2O_5 top-layer were used in order to elucidate the dependency between friction coefficient and frequency-stimulated structural differences of the films. The V_2O_5 single-layer was prepared by dc reactive magnetron sputtering at 300°C with a substrate bias potential of -80 V. The average thickness of the VN-V_2O_5 bi-layer coatings was 4 µm (2 µm VN / 2 µm V_2O_5) while the V_2O_5 single-layer coating had an average thickness of 2 µm.

The film structure was determined by X-ray diffraction (XRD) analysis using a Siemens D500 diffractometer in Bragg-Brentano configuration and Cu–Kα radiation. Dry sliding ball-on-disc experiments were conducted using coated high-speed steel discs in ambient air starting from room temperature (RT, ~ 25°C) up to 600°C using alumina balls of 6 mm diameter as counterpart. For all coating systems, the sliding speed was kept constant at 0.1 m/s and the wear track radius at 7 mm while the sliding distance was 50 m. A load of 1 N was used for all experiments. After tribometer testing, the wear tracks on the coatings were characterized using an optical 3D white light profiling system (Wyko NT 1000). Wear tracks and surfaces of the samples were examined using X-ray diffraction, Raman spectroscopy (Horiba Jobin-Yvon LabRAM Raman Microscope, He-Ne laser, λ = 632.8 nm) and scanning electron microscopy (SEM, Zeiss EVO 50) to characterize changes in surface structure and composition after ball-on-disc testing at different temperatures.

3. Results and discussion

Fig. 1 presents XRD patterns of the investigated coatings in the as-deposited state. The patterns are presented in a diffraction angle range between 12-33° to show the preferential orientation of the V_2O_5 phase formed. The XRD pattern of the V_2O_5 single-layer deposited in dc mode at -80 V substrate bias (Fig. 1a) indicates the presence of polycrystalline α-V_2O_5 with a preferred (200) orientation (cf. JCPDS file 01-077-2418). The VN-V_2O_5 bi-layer

coating deposited in dc mode (see Fig. 1b) shows no significant differences in the XRD pattern compared to the V_2O_5 single-layer while the growth orientation of the pulsed dc VN-V_2O_5 coating (Fig. 1c) changes due to its different deposition condition. In this case, the peak at $2\theta = 26.153°$ dominates, indicating that the pulsed dc VN-V_2O_5 coating grows in a preferred (110) orientation.

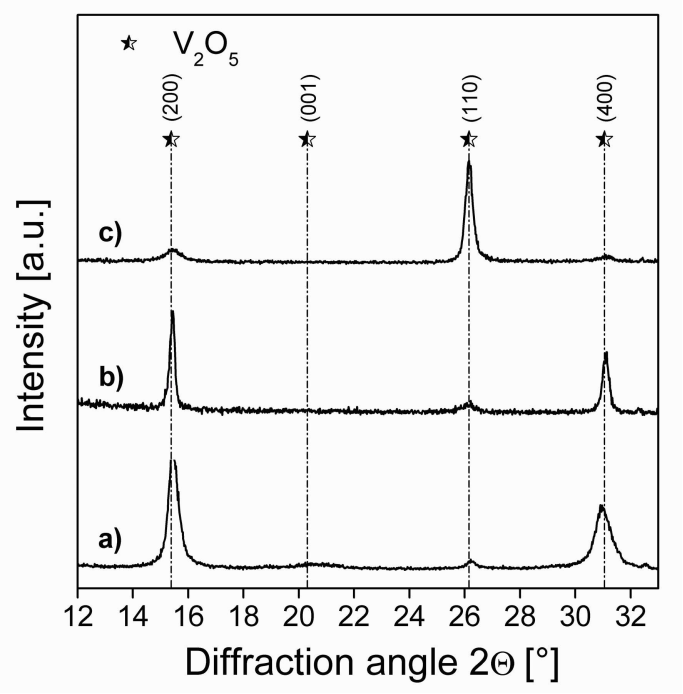

Fig. 1. XRD patterns of a) dc magnetron V_2O_5 single-layer deposited at -80 V substrate bias, b) dc sputtered VN-V_2O_5 bi-layer and c) pulsed dc sputtered VN-V_2O_5 bi-layer film grown at floating potential.

More details on the effect of deposition conditions on structural characteristics of dc and pulsed dc sputtered V_2O5 single-layer films can be found in our previous publication [11]. There, it was shown that V_2O_5 films deposited in pulsed dc mode grow with preferred (110) and (001) orientation. Here, it seems that the VN base-layer favours the growth of the V_2O_5 phase in (110) direction. XRD single-line profile analysis employing the Pseudo–Voight method [20] yields a mean coherently diffracting domain size of the V_2O_5 phase of 21 nm for the V_2O_5 single-layer, 40 nm for the dc sputtered VN-V_2O_5 and 13 nm for the pulsed dc VN-V_2O_5 bi-layer along (200). Applying the Pseudo-Voight method for the (110) orientation indicates a mean domain size of 21 nm for the V_2O_5 single-layer, 15 nm for the dc VN-V_2O_5 and 37 nm for the pulsed dc VN-V_2O_5 bi-layer coatings. Structural investigations by XRD and Raman spectroscopy of the films after tribometer testing up to 600°C reveal no detectable

structural changes compared to the as-deposited state. The results suggest that all single- and bi-layer coatings are stable and remain unchanged also after exposure in ambient air up to 600°C.

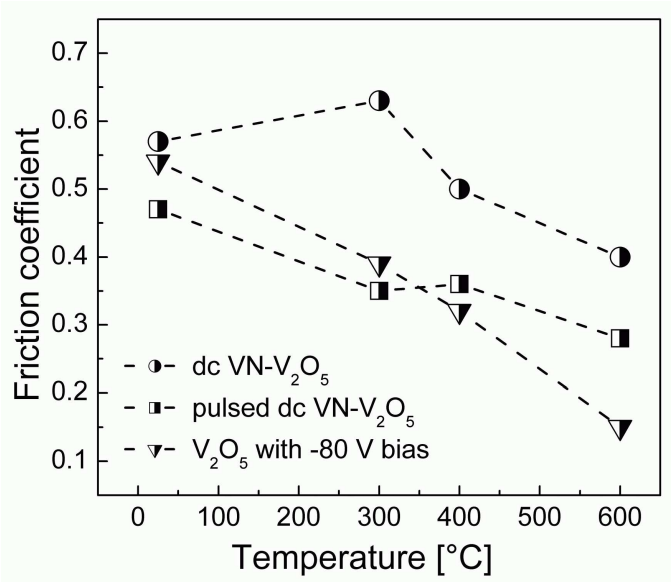

Fig. 2. Friction coefficient of V_2O_5 single-layer and VN-V_2O_5 bi-layer coatings obtained by high-temperature tribometer tests against alumina.

Fig. 2 shows the average friction coefficient investigated by ball-on-disc tests against alumina at different temperatures. It is obvious that the changes in structure and different preferential growth orientation of the coatings depending on the deposition mode influence the value of the friction coefficient. The results show the pulsed dc VN-V_2O_5 coatings to have a significantly lower friction coefficient over the whole temperature range compared to the dc sputtered VN-V_2O_5 coatings. In the case of dc sputtered VN-V_2O_5 coatings, the coefficient of friction increases from ~ 0.57 at RT to ~ 0.63 at 300°C and decreases again with further increase in test temperature. As no significant structural changes could be observed by XRD and Raman measurements after tribometer testing up to 600°C, the increased friction coefficient at 300°C can be attributed to changes occurring at the contacting sliding surfaces, presumably due to the interaction of wear particles with both surfaces in contact. The pulsed dc bi-layer coatings show a continuous decrease of the friction coefficient to a low value of ~0.28 at 600°C (see Fig. 2). The considerable reduction of the friction coefficient to ~ 0.39 at 300°C compared to RT indicates presumably the earlier onset of thermal activation of slip processes along easy shearable crystallographic planes compared to those deposited in dc

mode. This might be related to the (110) preferred growth orientation of the pulsed dc VN-V_2O_5 films. As reported in our previous work, there is a transition from amorphous to polycrystalline growth for V_2O_5 films deposited by dc magnetron sputtering with increasing deposition temperature [10]. In order to illuminate the friction coefficient further, dry sliding tests of the dc sputtered VN-V_2O_5 coatings with an amorphous V_2O_5 top-layer (deposited at RT [10]) were also investigated. It is worth mentioning that no remarkable changes in the friction coefficient compared to dc sputtered VN-V_2O_5 coatings with polycrystalline V_2O_5 top-layer (deposited at 300°C) could be observed. In case of the V_2O_5 single-layer deposited in dc mode, the friction coefficient observed at RT is almost identical to the dc sputtered VN-V_2O_5 bi-layer. However, the friction values of the V_2O_5 single-layer above 300°C are clearly lower compared to the VN-V_2O_5 bi-layer deposited by dc sputtering. As the preferred orientation in both coating systems is (200), the decrease in friction coefficient might be attributed to the different structure of single-layer V_2O_5 films due to the applied substrate bias [21]. The friction coefficient decreases from ~ 0.55 at RT to ~ 0.39 at 300°C and reaches its lowest value of 0.15 at 600°C.

An interpretation of the low friction coefficient appearing at 600°C requires further investigations. According to the XRD patterns of all coatings after testing at 600°C, grain coarsening occurs during the test. Applying the Pseudo-Voight method for the (200) orientation for both dc sputtered films reveals that the mean domain size of the V_2O_5 single-layer increases to 500 nm while that of the bi-layer increases to 262 nm. In case of the pulsed dc sputtered bi-layer film, the mean domain size increases to 211 nm along (110) orientation.

Local melting of the V_2O_5 phase due to high flash temperatures in the sliding contact and thus liquid lubrication could also contribute to the low-friction effect. However, SEM investigations did not give any evidence for the dendritic structure observed on oxidized vanadium containing nitrides [7,8]. We also investigated the surface morphology of the single-layer V_2O_5 and VN-V_2O_5 bi-layer coatings after dry sliding tests at different temperatures by SEM. The results indicate a modification of the surface morphology of all investigated coatings after testing at 600°C. Fig. 3 illustrates the top-view SEM micrographs of V_2O_5 single-layer coatings after dry sliding tests at RT, 300°C and 600°C outside of the wear track. Single-layer V_2O_5 coatings show after testing at 300°C a granular structure similar to the as-deposited state indicated in Fig. 3(a), while the surface morphology of the coating changes to a plate-like structure as the test temperature is increased to 600°C. According to cross-sectional SEM analysis, this phenomenon only occurs on the surface of the coatings and

does not apply for the total coating thickness. The change in the surface morphology might be another reason for the reduction of the friction coefficient for all investigated coatings with increasing testing temperature. However, since the coefficient of friction of the single-layer and bi-layer coatings after the dry sliding tests at 600°C is different, this can obviously not be the only factor determining the resulting friction coefficient.

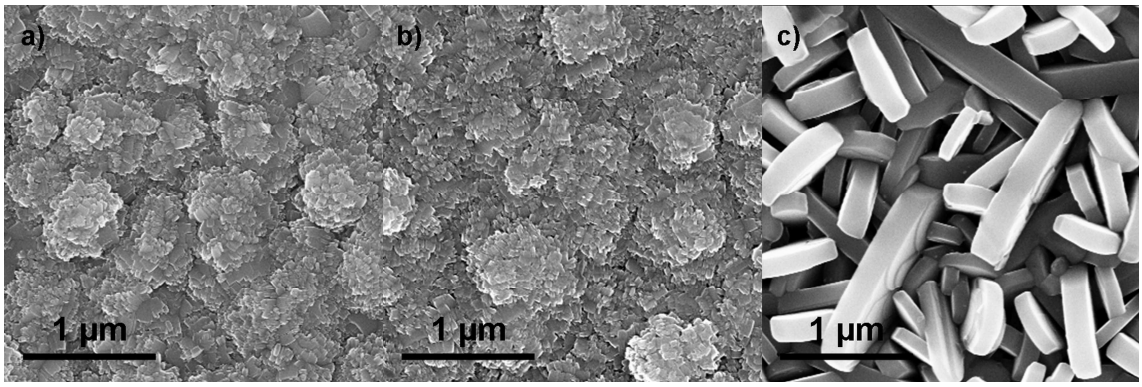

Fig. 3. SEM images of biased V_2O_5 single-layer coatings after dry sliding against alumina at a) RT, b) 300 and c) 600°C outside of the wear track.

It has been mentioned before that grain coarsening takes place at elevated temperatures. Assuming that deformation of the film plays a role in determining the resulting friction coefficient (in accordance with the theory of velocity accommodation of Berthier et al. [22]), it is plausible that a coarsened structure which deforms easier, e.g. by shearing of crystallographic planes, yields a lower friction coefficient. Also the orientation of the films should be related to the deformation mechanism, since the slip systems that might be activated depend on the orientation. Both bi-layer coatings investigated (sputtered in pulsed dc and dc mode, respectively) show comparable grain sizes after thermal exposure to 600°C. The difference in the friction coefficient should thus mainly be related to the different orientation of the films. In case of the V_2O_5 single-layer, the resulting friction coefficient might be determined not only by the orientation (which is similar to the dc sputtered bi-layer film), but also by the coarsened structure of the film. This mechanism might also be effective at lower temperatures since testing at 300°C already represents a homologous temperature of ~ 0.6 for V_2O_5. It is also worth mentioning that, according to XRD single-line profile analysis, the biased single-layer V_2O_5 film shows a more pronounced coarsening than the bi-layer coatings with increasing test temperature. Employing the Pseudo–Voight method revealed an increase in the mean domain size of the single-layer V_2O_5 from 21 nm at RT to ~ 39 nm at

300°C, while the mean domain size in case of the bi-layer coatings changes only slightly. Summing up, grain size, surface morphology and growth orientation might be determinant for the friction coefficient of sputtered V_2O_5 films.

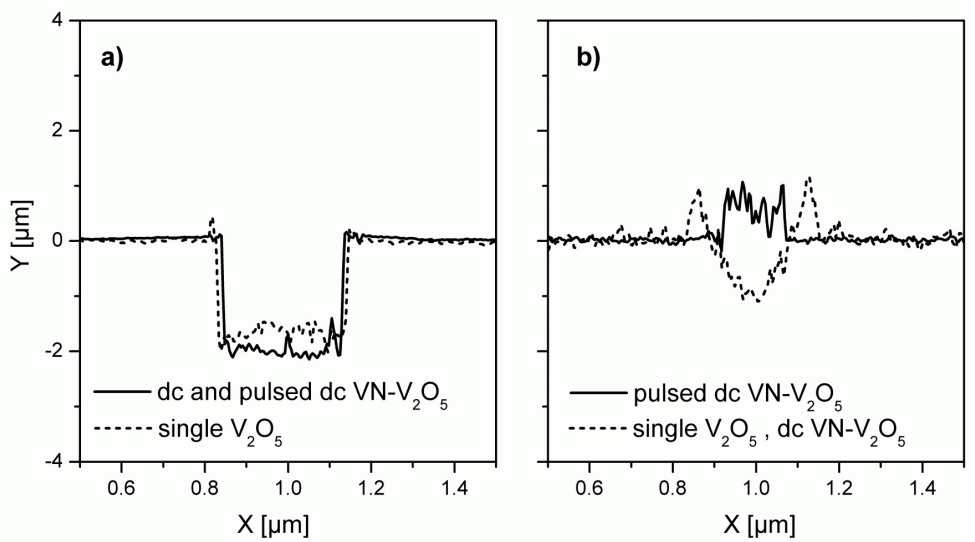

Fig. 4. 2D profiles of the wear tracks of the dc magnetron sputtered V_2O_5 single-layer coatings and the VN-V_2O_5 bi-layers deposited in dc and pulsed dc mode after dry sliding tests at a) RT and b) 600°C.

Two-dimensional surface profiles of the wear tracks of the coatings after tribometer testing at RT and 600°C are shown in Fig. 4. For the dc and pulsed dc sputtered VN-V_2O_5 bi-layers, the predominant wear mechanism at RT is abrasion as evidenced by the deep grooves with a wear track depth of ~ 2.2 µm. In this case, the V_2O_5 layer is completely worn trough while the hard VN layer remains intact after ball-on-disc testing. The V_2O_5 single-layer failed during the test at RT. The wear mechanism in this case is the same, and the depth of the wear track is ~ 2 µm, as shown in Fig. 4a. At a testing temperature of 300°C, all investigated coatings failed. After increasing the temperature to 400°C, most areas of the wear tracks of all investigated coatings show no significant material removal. However, in some small regions grooves with 1.3 - 2.4 µm depth could be observed.

Fig. 5 presents a SEM micrograph of the wear track of the dc sputtered VN-V_2O_5 bi-layer after dry sliding at 400°C as an example for the above mentioned behaviour. Fig. 4b shows the 2D profiles of the wear tracks of the V_2O_5 single-layer and the VN-V_2O_5 bi-layers deposited in dc and pulsed dc mode, respectively, after dry sliding tests at 600°C. This further increase in testing temperature leads to a reduction of the depth of the wear track and to transfer of wear particles, as evidenced by the positive wear shown in Fig. 4b. As clearly

shown in Fig. 4b, the VN-V_2O_5 bi-layer deposited by pulsed dc magnetron sputtering has a better wear performance compared to both, the dc sputtered VN-V_2O_5 bi-layer and V_2O_5 single-layer coatings. It is assumed that the better friction and wear performance of the pulsed dc V_2O_5 coating is attributed to its (110) growth orientation.

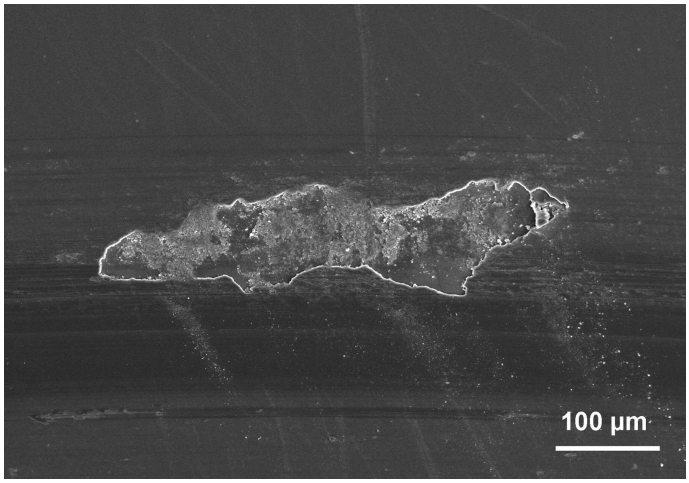

Fig. 5. SEM micrograph of the wear track of a dc sputtered VN-V_2O_5 bi-layer film after dry sliding against alumina at 400°C.

4. Conclusions

VN-V_2O_5 bi-layer coatings grown by dc and pulsed dc reactive magnetron sputtering and V_2O_5 single-layers synthesized by dc reactive magnetron sputtering have been investigated in the temperature range between 25 and 600°C to characterise the influence of sputtering mode, structure and growth orientation of the films on their tribological performance. Structural investigations using X-ray diffraction revealed that the V_2O_5 single-layer and the V_2O_5 top-layer of dc sputtered VN-V_2O_5 coatings have preferred (200) orientation while the V_2O_5 top-layer of pulsed dc VN-V_2O_5 coatings shows preferred (110) growth. According to X-ray diffraction and Raman analysis, all single- and bi-layer coatings investigated in this work are stable and remain unchanged during high-temperature dry sliding tests in ambient air up to 600°C. However, coarsening of the V_2O_5 phase occurs as temperature rises, where the V_2O_5 single-layer shows the most pronounced coarsening. Furthermore, a considerable change in the surface morphology of all investigated coatings from granular to plate-like structure after dry sliding test at 600°C could be observed. Ball-on-disc experiments against alumina show that the friction coefficient of all investigated coatings decreases with increasing temperature, where thermally activated processes seem to be necessary to promote low friction due to easy

shearing of lattice planes. Growth orientation and film structure seem to determine this onset temperature, and both together with surface morphology determine the frictional behaviour. Furthermore, also the wear resistance is improved with increasing testing temperature. Finally, it can be concluded that a combination of a well-adherent VN base-layer with a V_2O_5 top-layer is a promising candidate for coating systems providing low friction with sufficient wear resistance over a wide temperature range.

Acknowledgements

This work was supported by the Austrian NANO Initiative via a grant from the Austrian Science Fund FWF within the project "LowFrictionCoatings". The assistance of Daniel Kiener for SEM investigations is kindly appreciated.

References

[1] Erdemir, A.: A crystal-chemical approach to lubrication by solid oxides. Trib. Lett. 8, 97-102 (2000)

[2] Greenwood, O.D., Moulzolf, S.C., Blau, P.J., Lad, R.J.: The influence of microstructure on tribological properties of WO_3 thin films. Wear 232, 84-90 (1999)

[3] Gardos, M.N.: Magnéli phases of anion-deficient rutile as lubricious oxides. Part I. Tribological behaviour of single-crystal and polycrystalline rutile (Ti_nO_{2n-1}). Trib. Lett. 8, 65-78 (2000)

[4] Lugscheider, E., Knotek, O., Bärwulf, S., Bobzin, K.: Characteristic curves of voltage and current, phase generation and properties of tungsten- and vanadium-oxides deposited by reactive d.c.-MSIP-PVD-process for self-lubricating applications. Surf. Coat. Technol. 142-144, 137-142 (2001)

[5] Lugscheider, E., Knotek, O., Bobzin, K., Bärwulf, S.: Tribological properties, phase generation and high temperature phase stability of tungsten- and vanadium-oxides deposited by reactive MSIP-PVD process for innovative lubrication applications. Surf. Coat. Technol. 133-134, 362-368 (2000)

[6] Gassner, G., Mayrhofer, P.H., Kutschej, K., Mitterer, C., Kathrein, M.: A new low friction concept for high temperatures: Lubricious oxide formation on sputtered VN coatings. Tribol. Lett. 17/4, 751-756 (2004)

[7] Franz, R., Neidhardt, J., Sartory, B., Kaindl, R., Tessadri, R., Polcik, P., Derflinger, V.H., Mitterer, C.: High-temperature low-friction properties of vanadium-alloyed AlCrN coatings. Tribol. Lett. 23/2, 101-107 (2006)

[8] Fateh, N., Fontalvo, G.A., Gassner, G., Mitterer, C.: Influence of high-temperature oxide formation on the tribological behaviour of TiN and VN coatings. Wear 262, 1152-1158 (2007)

[9] Fateh, N., Fontalvo, G.A., Gassner, G., Mitterer, C.: The beneficial effect of high-temperature oxidation on the tribological behaviour of V and VN coatings. Tribol. Lett. 28, 1-7 (2007)

[10] Fateh, N., Fontalvo, G.A., Cha, L., Klünsner, T., Hlawacek, G., Teichert, C., Mitterer, C.: Synthesis-structure relations for reactive magnetron sputtered V_2O_5 films. Surf. Coat. Technol. 202, 1551-1555 (2008)

[11] Fateh, N., Fontalvo, G.A., Mitterer, C.: Structural and mechanical properties of dc and pulsed dc reactive magnetron sputtered V_2O_5 films. J. Phys. D: Appl. Phys. 40, 7716-7719 (2007)

[12] Ramana, C.V., Hussain, O.M., Srinivasulu Naidu, B., Reddy, P.J.: Spectroscopic characterization of electron-beam evaporated V_2O_5 thin films. Thin Solid Films 305, 219-226 (1997)

[13] Julien, C., Guesdon, J.P., Gorenstein, A., Khelfa, A., Ivanov, I.: The influence of substrate material on the growth of V_2O_5 flash-evaporated films. Appl. Surf. Sci. 90, 389-391 (1995)

[14] Gies, A., Pecquenard, B., Benayad, A., Martinez, H., Gobeau, D., Fuess, H., Levasseur, A.: Effect of total gas and oxygen partial pressure during deposition on the properties of sputtered V_2O_5 thin films. Solid State Ionics 176, 1627-1634 (2005)

[15] Lee, S.H., Cheong, H.M., Seong, M.J., Liu, P., Tracy, C.E., Mascarenhas, A., Pitts, J.R., Deb, S.K.: Raman spectroscopic studies of amorphous vanadium oxide thin films. Solid State Ionics 165, 111-116 (2003)

[16] Meng, L.J., Silva, R.A., Cui, H.N., Teixeira, V., dos Santos, M.P., Xu, Z.: Optical and structural properties of vanadium pentoxide films prepared by d.c. reactive magnetron sputtering. Thin Solid Films 515, 195-200 (2006)

[17] Lim, S.P., Long, J.D., Xu, S., Ostrikov, K.: Nanocrystalline vanadium oxide films synthesized by plasma-assisted reactive rf sputtering deposition. J. Phys. D: Appl. Phys. 40, 1085-1090 (2007)

[18] Fang, G.J., Liu, Z.L., Wang, Y., Liu, Y.H., Yao, K.L.: Synthesis and structural, electrochromic characterization of pulsed laser deposited vanadium oxide thin films. J. Vac. Sci. Technol. A 19, 887-892 (2001)

[19] Gulbińnki, W., Suszko, T., Sienicki, W., Warcholiński, B.: Tribological properties of silver-and copper-doped transition metal oxide coatings. Wear 254, 129-135 (2003)

[20] De Keijser, T.H., Langford, J.I., Mittemeijer, E.J., Vogels, A.B.P.: Use of the Voigt function in a single-line method for the analysis of X-ray diffraction line broadening. J. Appl. Crystallogr. 15, 308-314 (1982)

[21] Petrov, I., Barna, P.B., Hultman, L., Greene, J.E.: Microstructural evolution during film growth. J. Vac. Sci. Technol. A 21, 117-128 (2003)

[22] Berthier, Y., Godet, M., Brendle, M.: Velocity Accomodation in friction. Tribol. Trans. 32, 490-496 (1989)